DURBAN UNIVERSITY OF TECHNOLOGY

MODELLING AND PERFORMANCE ANALYSIS OF DOUBLY FED INDUCTION GENERATOR WIND FARM

By

Anuoluwapo Oluwatobiloba Aluko

Student Number: 21752070

A dissertation submitted in fulfilment of the requirements for the degree of Master of Engineering in Electrical Power Engineering

In the Department of Electrical Power Engineering
Faculty of Engineering and Built Environment

Supervisor: Mr. K.T. Akindeji

Co-Supervisor: Prof. D.G. Dorrell

Co-Supervisor: Dr. Sanjeeth Sewchurran

2018

DECLARATION

This dissertation is the student's own work, every cited work or text have been properly referenced. It has not been partially or fully submitted at any other University.

This research was duly supervised by Mr. K.T. Akindeji, Professor D.G. Dorrell and Dr. Sanjeeth Sewchurran, at the Durban University of Technology.

Submitted by:

…… ……

Aluko Anuoluwapo Oluwatobiloba Date

Student Number: 21752070

Approved for Final Submission by:

…… ……

Supervisor: Mr K.T. Akindeji Date

…… …….

Co-Supervisor: Prof D.G. Dorrell Date

…….. …….

Dr. Sanjeeth Sewchurran Date

DEDICATION

This research is dedicated to God who has been my source from the beginning to the end of this work.

ACKNOWLEDGEMENT

The journey so far has been a combination of the highs and lows but in all, this dissertation serves an evidence of triumph which would not have been possible without the academic, emotional, financial, moral, professional, social and spiritual support of the following people:

- My parents
- My siblings and cousins
- My supervisor and co-supervisors
- My colleagues in the department of electrical power engineering here in Durban University of Technology, University of KwaZulu-Natal, University of Capetown and other universities outside South Africa.
- My friends in Nigeria, South Africa and beyond Africa
- Staff in the department of electrical power engineering in Durban University of Technology
- Durban University of Technology
- National Research Foundation
- Eskom Power Plant Engineering Institute.

SIYABONGA ZONKE!

ABSTRACT

Power generation from renewable sources like wind and sun have increased substantially owing to various challenges such as government regulations, environmental pollution and depletion of non-renewable energy sources over the past few decades. Of all renewable energy sources, wind appears to be the foremost of choice due to economies of scale. Due the intermittent nature of wind, the increase in the penetration of wind power to the grid gives rise to several challenges in which power quality is the most critical. The mitigation of power quality challenges to grid-connected wind energy systems and other renewable energy plants led to the development of the renewable energy grid code. This research focuses on voltage quality as one of the power quality issues affecting connection of renewable energy plants to the grid.

This research models and performs analysis of a grid-connected doubly fed induction generator (DFIG) wind farm. Using the IEEE 9 bus system as a base case for the study, the modelled wind farm is then integrated into the base case. Steady state performance and performance during faults are analyzed using load flow study and transient stability studies respectively. The load flow study is carried out to comparatively evaluate the steady state stability of the base case and the wind farm integrated network with respect to the NRS 048 South Africa standard. The transient stability study is carried out on the wind farm integrated network with compliance to the South Africa renewable energy grid code (SAREGC) which allows the wind farm to reduce active power production during a continuous low voltage event below 85% at the point of common coupling. This work compensates the wind farm with a static synchronous compensator (STATCOM) to keep the voltage at the point of common coupling above the set point, thereby keeping the wind farm connected to the grid and supplying maximum active power during a low voltage event. The results show that the static synchronous compensator allows the wind farm ride through a low voltage event without disconnection and reduction in active power supply and the wind farm increases the transient stability of the network.

Table of Contents

LIST of FIGURES

LIST of TABLES

LIST of ACRONYMS and SYMBOLS

AC	Alternating current
BESS	Battery Energy Storage System
CSP	Concentrated Solar Plant
DC	Direct Current
DFIG	Doubly Fed Induction Generator
DigSiLENT	Digital Simulation and Electrical Network Calculation Program
DoE	Department of Energy
FACTS	Flexible Alternating Current Transmission System
FSWT	Fixed Speed Wind Turbine
GSC	Grid Side Converter
HVDC	High Voltage Direct Current
HVRT	High Voltage Ride Through
IEEE	Institute of Electrical and Electronics Engineers
IGBT	Insulated Gate Bipolar Transistor
LVRT	Low Voltage Ride Through
OSIG	Opti Slip Induction Generator
PCC	Point of Common Coupling
PMSG	Permanent Magnet Synchronous Generator
PV	Photo Voltaic
PWM	Pulse Width Modulation
REIPPP	Renewable Energy Independent Power Producers Procurement Programme
RSC	Rotor Side Converter

SAREGC	South Africa Renewable Energy Grid Code
SCIG	Squirrel Cage Induction Generator
SSSC	Static Synchronous Series Compensator
STATCOM	Static Synchronous Compensator
SVC	Static Var Compensator
TCR	Thyristor Controlled Reactor
TCSR	Thyristor Controlled Series Reactor
TSR	Thyristor Switched Reactor
TSC	Thyristor Switched Capacitor
TSSC	Thyristor Switched Series Capacitor
UPFC	Unified Power Flow Controller
VSC	Voltage Source Converter
VSWT	Variable Speed Wind Turbine
WECS	Wind Energy Conversion System
WSCC	Western System Coordinating Council
WRIG	Wound Rotor Induction Generator
WRSG	Wound Rotor Synchronous Generator
ω_s	Angular frequency in stator winding
f_s	Stator frequency
ω_r	Angular frequency in rotor winding
ω_m	Electrical angular frequency in rotor winding
s	Slip
Ω_m	Mechanical speed of rotor
p	Number of pole pairs

A	Area swept by turbine blades
V	Wind speed
ρ	Density of air
C_p	Performance coefficient
λ	Tip speed ratio
β	Pitch angle
R	Radius of turbine blade
v_A, v_B, v_C	Phase voltages of stator
v_a, v_b, v_c	Phase voltages of rotor
r_A, r_B, r_C	Resistance in each phase of stator
r_a, r_b, r_c	Resistance in each phase of rotor
$\varphi_A, \varphi_B, \varphi_C$	Flux linkage in stator windings
$\varphi_a, \varphi_b, \varphi_c$	Flux linkage in rotor windings
i_A, i_B, i_C	Phase current of stator
i_a, i_b, i_c	Phase current of rotor
L_{ss}	Self-inductance of stator winding
L_{rr}	Self-inductance of rotor winding
L_{ms}	Mutual inductance between two stator windings
L_{mr}	Mutual inductance between two rotor windings
L_m	Maximum mutual inductance between phase winding of stator and rotor
$\underline{L}_{rs}$	Stator and rotor mutual inductance matrix
$\underline{V}_{ABC}, \underline{V}_{abc}$	Stator and rotor voltage vectors respectively
$\underline{I}_{ABC}, \underline{I}_{abc}$	Stator and rotor current vectors respectively

$\underline{\varphi_{ABC}}$, $\underline{\varphi_{abc}}$	Stator and rotor flux linkage vectors respectively
$\underline{R_{ss}}$, $\underline{R_{rr}}$	Stator and rotor resistance matrices respectively
$\underline{M_s}$, $\underline{M_r}$	Transformation matrix on the stator and rotor side respectively
$\underline{I_{DQ0}}$, $\underline{I_{dq0}}$	Current of stator and rotor in DQ0 frame of reference
$\underline{V_{DQ0}}$, $\underline{V_{dq0}}$	Voltage of stator and rotor in DQ0 frame of reference
$\underline{\varphi_{DQ0}}$, $\underline{\varphi_{dq0}}$	Flux linkage of stator and rotor in DQ0 frame of reference
$\underline{M_{sro}}$, $\underline{M_{rro}}$	Stator and rotor transformation matrices in DQO-dq0 frame of reference stationary of the rotor
$\underline{M_{sst}}$, $\underline{M_{rst}}$	Stator and rotor transformation matrices in DQO-dq0 frame of reference stationary of the stator
P_m	Mechanical power
T_{em}	Electromechanical torque
i_D, i_Q	Stator currents in DQ0 synchronously rotating frame of reference
i_d, i_q	Rotor currents in dq0 synchronously rotating frame of reference
v_D, v_Q	Stator voltages in DQ0 synchronously rotating frame of reference
v_d, v_q	Rotor voltages in dq0 synchronously rotating frame of reference
φ_D, φ_Q	Stator flux linkages in DQ0 synchronously rotating frame of reference
φ_d, φ_q	Rotor flux linkages in dq0 synchronously rotating frame of reference

P_s	Stator active power
P_r	Rotor active power
Q_s	Stator reactive power
L_S	Leakage inductance in stator
L_R	Leakage inductance in rotor
L_M	Magnetizing inductance
i_{ds}, i_{qs}	Direct axis and quadrature axis of stator current in reduced order model in synchronously rotating frame of reference
i_{dr}, i_{qr}	Direct axis and quadrature axis of rotor current in reduced order model in synchronously rotating frame of reference
v_{ds}, v_{qs}	Direct axis and quadrature axis of stator voltage in reduced order model in synchronously rotating frame of reference
v_{dr}, v_{qr}	Direct axis and quadrature axis of rotor voltage in reduced order model in synchronously rotating frame of reference
φ_{ds}, φ_{qs}	Direct axis and quadrature axis of stator flux linkage in reduced order model in synchronously rotating frame of reference
φ_{dr}, φ_{qr}	Direct axis and quadrature axis of rotor flux linkage in reduced order model in synchronously rotating reference
H	Inertia constant of machine
T_m	Mechanical torque
$e_a(t), e_b(t), e_c(t)$	Three phase voltage of AC side of PWM converter

R_g	Resistance of AC side of PWM converter
L_g	Inductance of AC side of PWM converter
C	DC-link capacitor of PWM converter
R_L	Load resistance of AC side of PWM converter
i_{ag}, i_{bg}, i_{cg}	Three phase current of AC side of PWM converter
i_{dc}	DC-link current of PWM converter
i_L	Load current on AC side of PWM converter
$v_{(a,0)}$, $v_{(b,0)}$, $v_{(c,0)}$	Phase-to-neutral voltage of PWM converter
v_{dc}	DC-link voltage of PWM converter
S_a, S_b, S_c	Switch in the three phase PWM converter

CHAPTER ONE: INTRODUCTION

1.1 Background

With increasing demand in electricity, it is a challenge to supply the required electricity considering quality, reliability and sustainability of electricity. Coal is the most widely used source of fuel contributing about 36 percent of total fuel consumption for production of electricity worldwide and 77 percent of electrical power production in South Africa comes from coal [1, 2]. Owing to environmental pollution, new government regulations and predicted energy crisis, the renewable energy sector has experienced an exponential growth in the last decade. In South Africa, the production of energy from renewable sources has reduced the emission of Carbon Dioxide by 4.4 million tonnes. Of all renewable energy sources available, wind appears to be the foremost of choice because it is clean, cheap and has low operating cost [2].

In 2016, there was an annual installation of 54,110 MW of wind power in the global wind industry thereby increasing global total of wind energy in 2016 to 486,790 MW as shown in Figure 1.1. Asia is the largest producer of wind energy with 203,685 MW with China contributing over 70%, Europe producing 161,330 MW of wind energy, 97,611 MW produced by North America, Latin America and the Caribbean producing 15,296 MW, the Pacific region with 4,963 MW and Africa together with the Middle East is given in Table 1 [3].

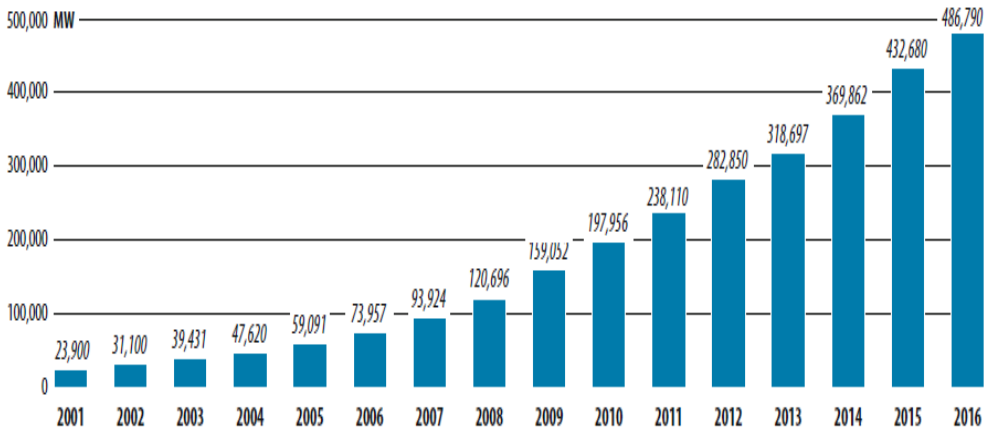

Figure 1.1: Total amount of wind energy installed (2001 – 2016) [3].

Table 1: Wind power production in Africa and Middle East as at end of 2016 [4].

	End of 2016 (MW)	New 2016	End of 2016 (MW)
South Africa	1,053	418	1,471
Egypt	810	----------	810
Morocco	787	----------	787
Ethiopia	324	----------	324
Tunisia	245	----------	245
Jordan	119	----------	119
[1]Others	150	----------	150
Total	3,488	418	3,906

In South Africa, wind energy industry is experiencing tremendous growth due to lower cost of energy as shown in Figure 1.2 and, its water saving benefit because for every kWh of wind that substitutes fossil fuel in the national grid, 1.2 litres of water will be saved. Till date, the Department of Energy (DoE) have procured 3,365 MW of wind energy through the Renewable Energy Independent Power Producers Procurement Programme (REIPPPP) with 36 different wind farms selected [2]. As at time of writing, there are nineteen wind farms in operation with over six hundred units of wind energy conversion systems (WECSs) supplying 1,471 MW of wind energy to the grid. It is suffice to know that there are 55 renewable energy plants currently in operation contributing a total of 2942 MW of energy to the national grid, they are [5]:

- 19 wind farms contributing 1471 MW,
- 31 Solar photovoltaic (PV) plants contributing 1344 MW,
- 3 concentrated solar plants (CSPs) contributing 200 MW
- 2 hydroelectric power plants contributing 14.3 MW

[1] Others include: Algeria, Cape Verde, Iran, Israel, Kenya, Libya and Nigeria.

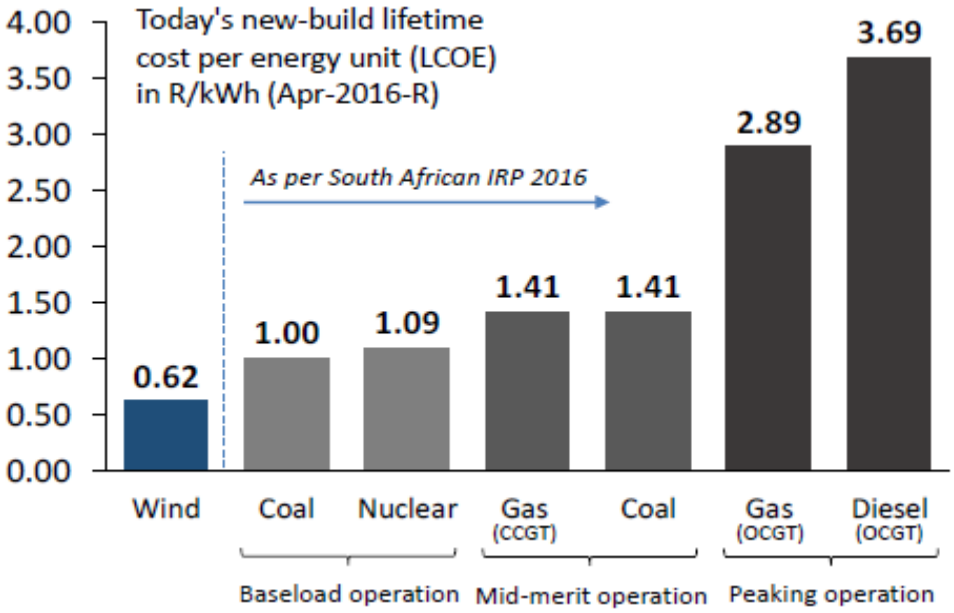

Figure 1.2 Cost per energy unit of different energy sources [6]

1.2 Problem Statement

Due to the intermittent nature of wind, the integration of wind power to the grid presents technical challenges such as reactive power requirement for voltage support, starting and synchronizing of wind farm onto the grid, short-circuit protection, efficiency of grid, sub-synchronous resonance as a result of the electric network and wind turbine interaction, power quality problems, design and optimization of power electronics, cost and reliability, and inadequate transmission lines to accommodate new power systems. Of all these challenges, power quality has gained relevant attention in research because it is directly linked with other challenges.

Power quality of an electrical system at any given point is the characteristics of electrical power at that point. Several problems that affect the power quality of a system are: voltage sag/dip, voltage swell/rise, flicker, harmonics and, short interruptions. Voltage sag or low voltage event is the most dominant problem in a wind energy conversion system. Wind power producers prefer to disconnect the WECS from the grid during faults that lead to low voltage conditions at the point of common coupling to prevent damage to the WECS components especially the power electronic converters. This disconnection from the grid leads to imbalance in active power and can consequently cause partial or total blackout. This is a

challenge if the penetration level of wind power in the grid is increased. To prevent this disconnection, it is necessary to regulate the voltage at the point of common coupling during fault to keep the wind farm in operation. This motivates the investigation of the effect of STATCOM in a DFIG-based wind farm and the use of permanent magnet synchronous generator (PMSG) in place of the DFIG for the 17 wind farms yet to be developed in South Africa.

1.3 Aim and Objectives

The research aims to analyze the effect of STATCOM in providing dynamic reactive power compensation during a low voltage ride-through event in a DFIG-based wind farm. The objectives of this research is as follows:

- Modelling of an 85 MW wind farm made up of 2.5 MW doubly fed induction generator-based wind turbines.
- Investigating the voltage ride through characteristics of the doubly fed induction generator based wind farm when integrated with a base case (IEEE 9 bus system) to represent an energy mix.
- Investigating the performance of STATCOM in the integrated network during low voltage events with respect to the South Africa renewable energy grid code requirements.

The software used for modeling, simulation and analysis is DigSILENT PowerFactory 2017. Mathematical modelling of the doubly fed induction generator is derived and simulated to achieve the first objective. Load flow study is carried out in the wind farm-integrated network to analyze the performance of the network during steady state operation to achieve the second objective. Finally, transient stability study is carried out in the integrated network with and without STATCOM to analyze the performance of the network during fault conditions.

1.4 List of Research Outputs

1. A.O Aluko, K.T. Akindeji, D.G. Dorrell and S. Sewuchurran, “Analysis of generator configuration for grid-connected wind energy systems”.

Eskom Power Plant Engineering Institute Conference, Midrand, South Africa, 14-15 August 2018.

2. A.O. Aluko and K.T. Akindeji, “Mitigation of Low Voltage Contingency of Doubly Fed Induction Generator Wind Farm using Static Synchronous Compensator”. Proceedings of IEEE PES-IAS PowerAfrica Conference, Capetown, South Africa, 26-29 June 2018, pp 75-80.
3. A.O. Aluko and K.T. Akindeji, “Performance Analysis of Grid Connected SCIG and DFIG based wind farm”. Proceedings of Southern Africa Universities Power Engineering Conference (SAUPEC), Johannesburg, South Africa, 24-27 January 2018, pp 20–25.
4. WindAc Africa “Academic Hour for Wind Power” CTICC, Capetown, South Africa. 14th and 15th November, 2017 (Attended)
5. WindAc Africa Student Workshop, South Africa Renewable Energy Technology Centre (SARETEC), Capetown, South Africa. 13th November, 2017 (Attended)

1.5 Dissertation Structure

The subsequent chapters of the dissertation are structured as follows:

- Chapter two presents the literature reviewed in this research with respect to renewable energy, wind energy, doubly fed induction generator, FACTS devices with emphasis on STATCOM.
- Chapter three presents the detailed mathematical modelling of a doubly fed induction generator in different frames of reference for simplicity and easy simulation, and modelling of power electronics converters used in DFIG and STATCOM.
- Chapter four presents and discusses the results of the simulated models with load flow analysis and transient stability studies.
- Chapter five is the concluding chapter with recommendation inclusive.

CHAPTER TWO: LITERATURE REVIEW

2.1 Renewable Energy and Wind Power

Electrical power generation from renewable sources has been on the increase over the past few years and contribute substantially to the overall power generation globally. Due to low penetration level of wind farms in the past, their impact on the grid was considered negligible. There is an increase in the quantity and size of wind farms installed globally, creating a rapid expansion of wind energy industry [7]. Wind energy conversion system (WECS) maybe operated in stand-alone mode where they supply electrical power to local areas or grid-connected where they contribute to the overall power supplied by the distribution network. The grid-connected WECS however need to meet certain standards or codes before being integrated into the grid, these standards are presented in this work. Due to the continuous growth of grid-connected wind farms, it becomes necessary to study the behavior of the wind farm with respect to other power plants and the network in general. A wind farm can be defined as a collection of WECS (tens to hundreds) connected together to produce a single output, it is generally agreed that the output of the wind farm is smoother as compared to the output of a single WECS. The percentage of power contributed by the wind farm to the total power in the grid is defined as the penetration level or ratio of the wind farm [7].

2.2 Wind Power Generation

A basic wind energy conversion system majorly consists of a turbine rotor, gear box, generator, power electronic converter and a transformer. Wind power is captured by the blades of the turbine and converted to mechanical power. The turbine blades are mechanically designed to control power transfer during high wind speed. The mechanical power is transferred through the gearbox to the generator where it is converted to electrical power. The gearbox synchronizes the low speed of the turbine rotor and the high speed of the generator. Depending on the design, the gearbox maybe three-stage or four-stage design. The generated electrical power is transferred to local loads or grid. The generator is usually an asynchronous

generator/induction generator or permanent magnet synchronous generator. The typical block diagram of a WECS is shown in Figure 2.1. Practical WECS consists of auxiliary components such as coolers for generator and gearbox, wind sensor, brakes, pitch drives and gearbox support. The effect of soft-coupling in the shaft (gearbox) between the turbine and generator is to reduce large wind farms consisting of several small WECS to a single equivalent machine was presented in [8], it argued that due to the large area of the wind farm, irregularity in the distributed wind is of significant effect in the each WECS and also presented the “park effect” and “wake effect” as other factors that limit the aggregation of WECS.

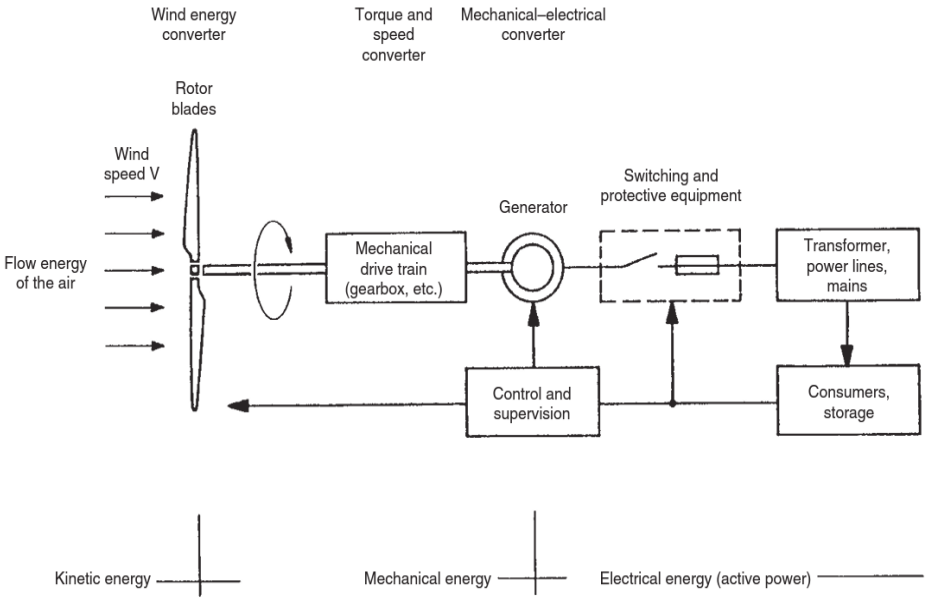

Figure 2.1 Block diagram of a WECS [9]

In [10], wind turbines were categorized into (i) fixed-speed and variable-speed wind turbine (ii) fixed-pitch and variable-pitch wind turbine (iii) wind turbine with no-load compensated induction generators, wind turbine with doubly-fed induction generators and wind turbine with multiple synchronous generator (iv) wind turbine directly connected to ac grids and wind turbines connected to ac grids through frequency converters.

Fixed-Speed Wind Turbine: the speed of the wind turbine is constant regardless of the wind speed. The speed of the turbine depends on the grid frequency, design of the generator and the gearbox ratio. It is usually

coupled with induction generator mostly SCIG and connected directly to the grid, it contains capacitor banks and soft starters for control of reactive power absorption and injection. It attains maximum efficiency at a rated speed and is therefore simple and reliable. It however cannot actively control its reactive power absorption because the capacitor banks only provide static compensation, it has poor power quality and fluctuations in wind speed are transferred to the grid through the fluctuating mechanical torque [7], [11]. It uses stall control to regulate power extraction from the wind because at high wind speed, the rotor reduces its efficiency. The mechanical system affects the performance of the fixed-speed wind turbines leading to costly mechanical construction to achieve high output power [12].

Variable-Speed Wind Turbine: It operates over a broad range of speeds. With varying speed, it is possible to optimize the characteristics of the turbine while the maintaining the generator torque. The varying wind speed are transferred to the rotor of the generator allowing it to rotate at above and below synchronous speed. It may be coupled with an induction generator or synchronous generator which is connected to the grid through an intermediate connection of power electronic converter that regulates the generator speed consequently adjusting the generator frequency and voltage at the grid [10, 13]. The reason for varying speed is for power optimization. It produces better power quality and reduces the mechanical stress because the varying wind speeds are regulated at the generator side. It can actively control the reactive power. It is expensive, complex and associated with increased losses because of the addition of power converters [14].

Wind turbines are designed with power control to regulate the impact of the aerodynamic force on the rotor of the turbine thereby regulating the power at high wind speed to prevent damage of the turbine system. Wind turbines are modelled to generate power at cheap rate, therefore, they are modelled to generate optimum output power at an average wind speed of 15m/s because of economies of scale. Both FSWT and VSWT use either of the following concepts for power control [11, 15, 16]:

Stall Control: In this concept, the turbine blades are connected to the turbine hub at a fixed angle. Stalling is obtained by increasing the angle of attack at which the wind hits the blades of the turbine, it reduces the aerodynamic drag on the turbine blades. At high wind speed, the rotor of the turbine stalls due to the aerodynamic characteristics of the rotor. There is low power fluctuation because of gradual stall of the turbine blades but it presents complexity in aerodynamic design [17, 18].

Pitch Control: In this concept, the blades of the turbine are turned away at high wind speed and turned in at low wind speed using hydraulics or electric motors. A controller is normally installed in the turbine to periodically measure the power output of the turbine and it high power output, it alerts the blade mechanism to pitch the blade away from the wind. It has better power control because even at high wind speed, the average power output of the turbine is within the rated power of the generator [19, 20].

Active-stall Control: In this concept, the turbine blades are actively stalled by rotating the turbine blades about an angle. At low wind speed, the blades of the turbine are rotated similarly to pitch-control to obtain optimum efficiency. At high wind speed, the turbine blades are deeply stalled by rotating the blades at an angle opposite the direction of the wind. This way, the angle of rotation is less compared to pitch control [21, 22]. The power output characteristics from the different control strategies is shown in the Figure 2.2 below.

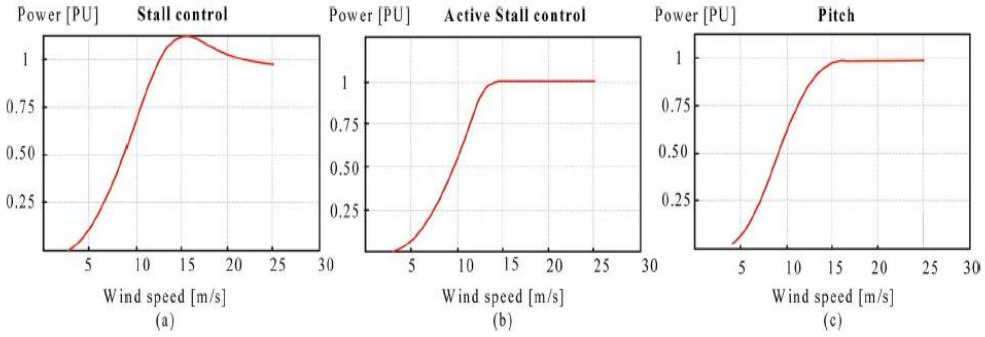

Figure 2.2 Power characteristics of wind turbine (a) stall control (b) active stall control (c) pitch control [23]

Since all of these control concepts are mainly used for power output optimization from the wind, they are not responsive during faults in the power systems and lack of system protection that can cause turbine over-speeding. A control loop in the blade control system can be implemented that acts during faults in the power systems to protect the turbine system against over-speeding [24]. At extremely high wind speeds, the wind turbine is totally disconnected to prevent damage.

Power electronics has found a very useful application in wind power system because they are used to synchronize the characteristics of the wind turbine with the grid connection requirements such as voltage, frequency, harmonics, active and reactive power [25, 26]. They find applications in variable wind turbine allowing it to achieve high efficiency and improve its overall performance [27]. A basic power electronic converter consists of a rectifier (transforms ac to dc), a capacitor (energy storage) and an inverter (transforms dc to ac). The rectifier is a diode and the inverter is majorly an insulated gate bipolar transistor (IGBT). The difference in power output characteristics of the FSWT generating system and VSWT generating system is due to the power electronic converters present in the later [28]. In FSWT generating system, there is no energy isolation therefore fluctuation in wind speed is reflected in the output power while in VSWT generating system, the rotor acts as energy isolator because the output power is regulated by the power electronics converters according to the speed of the rotor [29]. A wind farm with power electronic converters can regulate active and reactive power flow. The use of power system blockset (PSB) in MATLAB/Simulink to analyze power electronics systems was studied in [30], it listed the characteristics of the PSB and simulation of shunt compensated and series compensated power systems were used as examples, the results were compared with the results of EMTP and PSpice simulation and concluded that Simulink provides a faster development and analysis of the power electronic devices used in power systems.

Wind turbine are coupled with three phase generators to convert the mechanical power into electrical power. The following generator configurations are adopted in the wind turbine system:

2.3 Synchronous Generators

The synchronous generator do not require reactive magnetizing current, the magnetic field of the synchronous generator can be generated using a permanent magnet or field windings. It is suitable for total power control because it uses the power electronic converter to transfer power to the grid but its cost implication and mechanical complexity makes the Induction generators preferable [31]. The synchronous generator used in wind turbine can be wound-rotor synchronous generator (WRSG) or permanent magnet synchronous generator (PMSG).

The WRSG consists of stator directly connected to the grid and a rotor excited by direct current from slip rings and brushes. In the rotor winding, the flow of direct current generates an excitatin field that rotates at synchronous speed. The synchronous speed is determined by the frequency of the rotating field and number of poles [32].

The PMSG employs full power conversion from the converters to modify the voltage and frequency generated to match the voltage and frequency of the grid or load. [33, 34]. The stator of the PMSG is usually wound and the rotor has a permanent magnet pole system. The excitation needed is provided without energy dissipation as compared to induction generators [35].

2.4 Asynchronous or Induction Generators

It is the most widely used generator in the wind turbines because it is mechanically simple, cheap, low maintenance, life span (over 50 years) and reduced power to weight ratio than conventional synchronous generators [36]. Induction generator produces power by mechanically rotating the rotor above synchronous speed. It does not use permanent magnet and therefore need excitation from an external source thereby consuming reactive power [37]. The generator’s magnetization is generated when connected to the grid, the needed reactive power is supplied by the grid or a power electronic converter [38]. Its major drawback is the reactive magnetizing current needed by the stator. Induction generators are squirrel-caged or wound-rotor based. The system performance of fixed-speed induction generators was studied in [39] and mentioned that torque-slip curve and reactive

power-slip curve can be used to study the stability of fixed-speed induction generators.

2.4.1 Squirrel Cage Induction Generator (SCIG)

The SCIG found its application in the early technology wind turbine system, it is coupled to the turbine by a gear box (differential speed between speed of turbine rotor and generator rotor), the stator is connected directly to the grid with a transformer in between as shown in Figure 2.3 [40]. The rotor of SCIG rotates at speed directly proportional to the grid frequency. SCIG finds application in FSWT which implies that the fluctuations in wind speed result in varying output power transferred to the grid. The rotor can run at 'two' fixed speed when the pole pairs in the stator winding is changed [41]. At high wind speed, active power generation increases leading to uncontrolled and increased reactive power absorption from the grid, this could cause grid instability. It has a very low full load power factor due the absorption of magnetizing current from the grid during startup. During fault, SCIG without external reactive power compensation causes voltage instability, when the fault is cleared, more reactive power is absorbed from the grid for startup which results to decrease in terminal voltage. As presented, reactive power consumption is the major drawback of SCIG therefore it is mostly coupled with soft-starters and capacitor banks [42]. The soft starter basically comprises of thyristors that are short-circuited by a contactor when magnetization takes place, they are used to lower the in-rush current during startup to reduce grid disturbance. Capacitor banks provide reactive power needed by the generator to reduce reactive power absorption from the grid. The pitch angle is controlled using active-stall control to permit soft-starting without power electronic converters [43]. SCIG also a have the problem of voltage instability as a result of self-excitation when the reactive power absorption from the grid is lost.

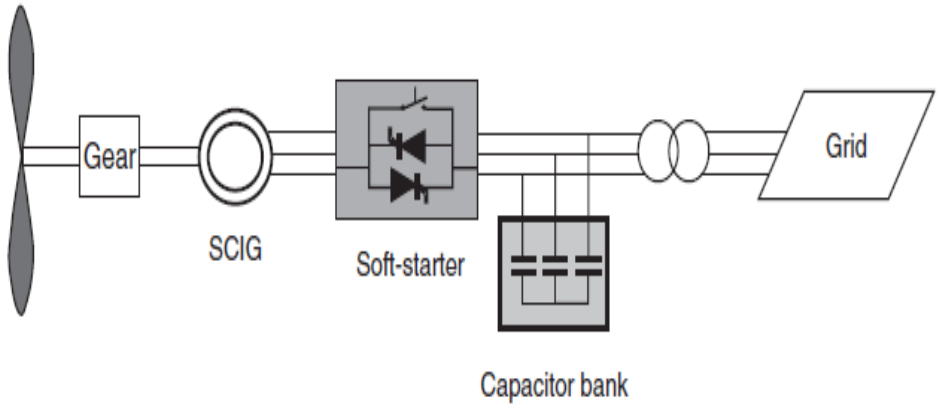

Figure 2.3: Grid-connected SCIG [11]

2.4.2 Wound Rotor Induction Generator (WRIG)

This configuration of induction generator differs from the SCIG because the rotor and the stator can be excited independently but it is expensive compared to the SCIG. The rotor can be excited from an external source such as power electronic converter. It finds application in variable-speed wind turbines. The WRIG can be variable resistance induction generator also known as OptiSlip induction generator (OSIG) or doubly fed induction generator (DFIG) [32]. The OSIG has a variable resistor coupled in the rotor circuit. The slip is varied by adjusting the resistance of the rotor. It does not use slip rings because the converters are controller optically. The stator is directly connected to the grid. The OSIG is simple, has less mechanical stress, reduced power fluctuations when compared to the SCIG. Its drawbacks are that the speed range is proportional to the size of the variable rotor resistance which is cost ineffective, ineffective control of reactive power and losses as a result of slip power in the variable resistor. The DFIG which finds application in this work will be reviewed extensively in this chapter and its model will be presented in the next chapter.

2.4.3 Doubly Fed Induction Generator (DFIG)

In the DFIG, the stator is connected directly to the grid and the rotor is connected via power electronic converters to the grid as shown in Figure 2.4, the power electronic converter is mostly a voltage-source converter (VSC) that uses the on insulated gate bipolar transistor (IGBT) scheme [44]. The grid supplies the stator voltage and the converter supplies the rotor

voltage. The converter supplies the rotor with current of variable frequency to compensate for the difference in the frequency of the turbine and frequency of the grid. The power converters are known as rotor-side converter (RSC) which regulates the active and reactive power flow and grid-side converter (GSC) which maintains the dc-link voltage to ensure unity power factor operation of the converter. A DC-link capacitor is connected across both converters. The DFIG is able to generate power to the grid from the stator at super-synchronous and sub-synchronous speeds. At super-synchronous speed, the rotor supplies power to the grid through the converter while at sub-synchronous speed, power flows from the grid to the rotor. The DFIG is based on the variable-speed wind turbine with the advantages of reduced cost, improved power quality, improved system efficiency and better implementation when compared with fixed-speed wind turbines with SCIG, the RSC also uses maximum power point tracking (MPPT) algorithm to regulate the turbine speed to obtain maximum power without exceeding the turbines nominal power at high wind speed, references [23, 45-47] summarized various methods to carry out MPPT control such as hill climbing searching (HCS) control, tip speed ratio (TSC) control and power signal feedback (PSF) control.

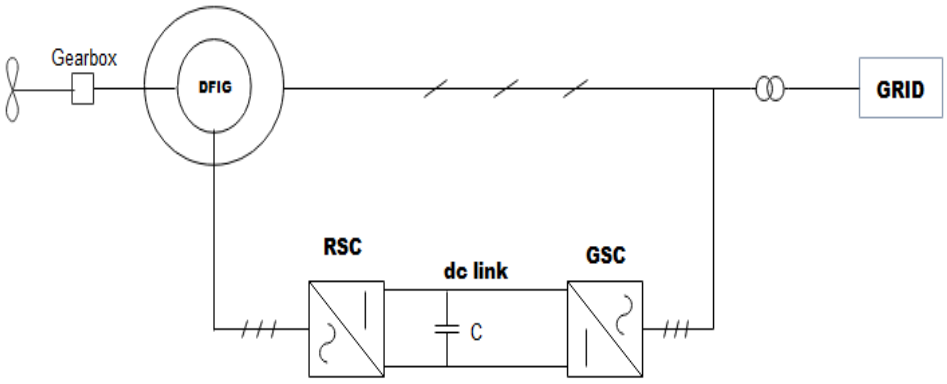

Figure 2.4: Grid-connected DFIG

The control of reactive power by the RSC is used to maintain the stator voltage when the DFIG is connected to a weak grid with inadequate reactive power compensation [48]. The DFIG is able to control the power from the wind turbine to regulate the operating point, reduce the power during high

wind speeds and control the reactive power flow between generator and the grid because of the converter. By means of rotor current injection, the RSC is controls the rotor speed to attain optimum power capture, uphold a steady frequency of the stator voltages and control the stator voltages at set values [49]. The DFIG can control active and reactive power by controlling the excitation current in the rotor independently, generate reactive power to be transmitted to the stator by the GSC. Theoretically, this is absence of reactive power flow at the stator because the GSC operates at unity factor. A major benefit of the DFIG which has made it widely used is the fact that power electronic converters in the rotor circuit handle about one-quarter of the rated power which implies reduced losses and cost in comparison to wind turbines that uses full-power converters. To generate power at constant frequency and voltage, bi-directional flow of power between the rotor and the grid should be controlled in magnitude and direction. A comparison of energy capture between DFIG wind turbine system and other types of wind turbine systems was done in [50] and it was found that the DFIG wind turbine can provide more units of power than the wind turbine using full-power converters, the power capture of the DFIG wind turbine is nearly equal to a fixed-speed wind turbine with active-stall control. The major drawback of the DFIG is the need for slip rings as compared to the OSIG. Modern models of DFIG comprises of rotor speed and pitch angle controllers. Since the control of power with respect to speed characteristics poises some challenges because if the rotor speed reduces from marginally beyond cut-in speed to marginally below cut-in speed, there is a large variation in generated power, rotor speed controller is used to regulate the electromechanical torque and not the power because the torque is affected by the q-axis rotor current that controls the output power as will be shown in chapter three of this work. However, because the control of the electromechanical torque at high wind speeds (super-synchronous speed) causes excessive loading of the power electronic converter and stator, the pitch angle controller becomes operational to increase the rotor blade pitch angle and control the output power. Duing low wind speeds (sub-synchronous speed) the pitch angle controller is locked [51, 52].

Review of DFIG Control Schemes

A major challenge of grid-connected DFIG is low voltage ride-through during faults and techniques such as blocking the RSC with the use of crowbar to short circuit the rotor circuit to prevent it from overcurrent, use of a fuzzy and nonlinear controller to enhance the control scheme of the RSC and use of FACTS technology for fast reactive power compensation as solutions to reduce the effect of this challenge was highlighted in [53]. Parameters that limit power supply to the grid in DFIG were analyzed in [54] and presented a more realistic representation of the DFIG operation with the use of an optimization algorithm to model a wind farm that factors the reactive power supply from the DFIG and the GSC when executing the algorithm, the objective was to achieve a coordinated reactive power management. Authors of [52] compared the DFIG-based wind farm with conventional synchronous generators in terms of stability analysis using the IEEE 14-bus system as a base case, the methodology in this paper used PV curves and modal analysis to show that the DFIG-based wind farm provided improved oscillatory capabilities when replaced with the synchronous generator in the base case. Owing to the fact that DFIG wind turbine systems have low system inertia when compared to fixed-speed induction generators because they decouple the turbine system (mechanical) and generator system (electrical) [55], this decoupling effect makes them irresponsive to variations in systems frequency which is undesirable for large wind farms with several DFIG wind turbine systems, an extra control loop was introduced in [56] to the controller of the DFIG to increase its inertia response during frequency variation. Due to the operational features (constant active power supply) of hydro and nuclear power plants, low penetration level of fossil-powered plants, DFIG-based wind farm has been used for frequency control of power system during periods of low power demand [57], models of DFIG for short-term analysis and long-term analysis were also presented in this paper. Reference [58] stresses that various researches concentrated on the rotor current limits in the DFIG and explained how the reactive power capability of the GSC considerably affects the operation of the DFIG, it used the unified DFIG i.e. DFIG with 3 converters (1 RSC and 2 GSCs) proposed in

[50] to analyze and compare its reactive power capability to conventional DFIG, the effect of varying the firing angle of the RSC and modulation of the GSCs was also discussed. Authors of [59] developed a new DFIG power control scheme that can exclusively control both active and reactive power, the control scheme is applied in the rotating reference frame fixed in the gap flux (M-T frame) where the M-axis and T-axis are fixed in the gap flux and fixed in quadrature with the M-axis respectively. The investigation of several methods for rotor current control were made in [50] with the aim of expelling the effect of back EMF on the rotor current, the method with the best stability characteristics, robustness and best suppression of the back EMF on the rotor current was presented. Rupak Sharma and Amit Manocha reviewed various control techniques such as crowbar method, DC chopper, nonlinear control, series dynamic braking resistor, current feedback technique, tuned damping controller, internal mode control, super capacitor storage, flux linkage tracking and FACTS devices for control of DFIG WECS [2, 60]. Based on participation factor analysis (PFA) of a DFIG-based wind farm, it has been shown that the controllers of the GSC (current controller and dc voltage controller) do not have a major contribution in system stability. However, the variation of parameters of the RSC controllers was studied and its effect on power system stability [61]. A controller was designed in [55] to allow a DFIG-based wind farm assist in voltage support during faults, provide power system stabilizer capability, frequency support on short-term basis and provide compatibility with conventional power stations, the controller is designed such that it can control the rotor flux vector of the DFIG in terms of magnitude and position to make it identical to the control of a synchronous generator for active voltage control and network damping. A direct power control (DPC) of active and reactive power control of a DFIG-based wind farm was developed in [62], the DPC was achieved by using only stator flux for the estimation of the voltage vectors in the rotor circuit. It presented the analysis of the DFIG using the rotor reference frame, the DPC was used solve the difficulty caused by direct torque control which is the control of generator torque by using stator flux and torque information for estimating suitable voltage vectors leading to deterioration in performance

during startup and low wind speed. A study in [63] discussed various characteristics of a DFIG-based wind farm in a network under various conditions, it used the grid voltage control method through the RSC and GSC to study these characteristics. A different control strategy using a state space regulator with the concept of an observer-based controller (OBC) to combine with the regulator using the pole placement theory was presented in [64], the results of this new controller was compared with the PI controller with respect to strength, power reference tracking and sensibility to disturbances. A vector control strategy to remotely control the GSC as a shunt filter to assist the grid with power factor correction, harmonic compensation and to support the power quality at definition points far from the wind farm was proposed in [65]. It was studied in [66] that a DFIG wind farm and wind farm with cage-rotor induction generator coupled with STATCOM can be used to achieve power system stability during grid faults as a result of power electronics converter present in both configurations and it was concluded that the former is advantageous in terms of reduced cost, size and complexity .

To investigate the impacts of transient conditions of WECS on power systems, it is necessary to represent the models of the WECS with accurate dynamic simulation models. The model presented in this work represents the behavior of DFIG under steady state and transient conditions. LVRT is an integral characteristics for WECS to meet the requirements specified by the grid codes. DFIG is easily affected by variations in grid voltage therefore adequate control must be implemented to ensure protection of the power electronics converters from tripping when variations in grid voltage occurs.

For power system analysis, large wind farms can be represented by the aggregation of each wind turbine model, transformers that connect each wind turbine generator to the wind farm substation and a detailed representation of the internal network of the wind farm [67]. In [68], the aggregated model was achieved by using a reduced model of single wind turbine to determine the mechanical torque of each wind turbine and the aggregated mechanical torque is applied to an equivalent DFIG with resized power rating, the degree of efficiency of the aggregated model was

compared with the complete individual models and the simulation results showed that the aggregated model has a faster computation time of about 92%. The aggregated model of a wind farm has the advantage of less computational time because it excludes the necessity for modelling of large number of individual wind turbine generating system.

2.5 Integration of Wind Power into Grid

Due to the growing penetration of wind power, it is pertinent to study its characteristics when connected to the grid and also their interaction with other generating systems. The integration of wind power into the grid presents technical challenges due to the intermittent nature of wind. Some of the challenges include: reactive power requirement for voltage support, starting and synchronizing of wind farm into the grid, short-circuit protection, efficiency of grid, sub-synchronous resonance as a result of electric network and wind turbine interaction, power quality issues, design and optimization of power electronics, cost and reliability, inadequate transmission lines to accommodate new power systems [69, 70]. Production, investment, maintenance and reliability are factors to be considered when wind power is to be integrated into the grid. Large wind farms are expected to execute frequency, voltage, active and reactive power control, perform rapid response during transient and dynamic conditions. When the active power generated changes due to fluctuations in wind speed from the turbine, the reactive power and terminal voltage of the induction generator also change. In [10], the question of what happens in the power with high penetration of wind power when a three-phase short-circuit fault occurs was answered. It presented some ride-through features. As the penetration level of wind energy increases, its integration requires similar requirements to conventional plants [71].

The integration of DFIG WECS into the grid was demonstrated [49] with the IEEE 10-machine39-bus system, it was observed that the DFIG provided a better transient performance and elimination of angular stability problem when compared to conventional synchronous generators, the converters of the DFIG provided a faster control and better ride-through during faults, it

presented the benefits if the continuous operation of the WTG during grid faults as continuous injection of active power to the grid, maintenance of grid frequency during transients and fast recovery of the WTG to full operation after a short-term blocking of the RSC, the simulations were carried out with PSCAD/EMTDC. During grid faults, most wind farms disconnect and reconnect to the grid after the fault is cleared to avoid destruction of the WTG [72]. However, during and after grid fault, DFIG is able to support the network by providing enough reactive power comparable to conventional generators if the proportional gain of the voltage controller is increased beyond as certain level as presented in [73]. An argument was presented in [74] about the distributed generation of electricity, experienced researchers presented that the introduction of uncontrollable sources of power into the distribution network will make the power system more complex while emerging researchers countered that introduction of renewable energy into the distribution network is necessary to reduces CO_2 emission and reduce dependency on conventional sources. The analysis from the research in [75] showed that the integration of wind power into a distribution network increases the overall reliability of the system and considerably reduces the power loss in the network. It also analyzed that installation of WECS at different points in the distribution system reduce dependence on transmission lines leading to reduced power loss in the system.

2.6 Power Quality Issues

Power quality as defined by [76] is the “characteristics of electricity at a given point on an electrical system, evaluated against a set of reference parameters”. The performance of wind turbine systems in terms of power quality are determined based on the standard and measurement with respect to the guidelines specified by the International Electro-technical Commission (IEC), the IEC 61400-21 defines the process for measuring the power quality of a grid-connected wind turbine system [77]. It specifies seven parameters that actively affect the power quality of a wind turbine namely: flickers, harmonics, voltage sag/dip/drop, active power, reactive power, grid protection and reconnection time. An ideal power quality implies

that the voltage is continuously sinusoidal with a steady amplitude and frequency. Depending on the level of penetration, wind farms have notable effect on the power quality and stability of the grid [78]. The reduction of power quality problems involves may involve the use of FACTS devices as specified in [79].

Amongst the parameters specified, voltage sag is a major parameter that affects the power quality of grid-connected wind turbines because of the characteristics of the induction generator. Voltage variations in induction generators have a proportional relationship with reactive power variation which this work aims to analyze. Voltage sag/dip is a random event in power systems majorly caused by faults in the grid, it is denoted with its amplitude and variations. When a short-circuit fault occurs in the area connected to the wind turbine generator, the short-circuit current may cause voltage dip at the wind turbine generator terminal as a result of torque imbalance between the generator and the turbine, when the fault is cleared and the voltage of the power system is restored, reactive power is needed by the induction generator to recover its terminal voltage. The absorption of reactive power causes a high inrush current to be drawn by the induction generator which causes a voltage drop in the line connecting the wind turbine generator and the grid. The resulting voltage drop can cause slow recovery of the generator terminal voltage causing the generator to increase its acceleration leading to an increased reactive power consumption. If the generator fails to recover, it is disconnected from the system thereby leading to significant effect on the stability of the system. The IEC 61400-21 defines six voltage drops with the specification of magnitude and period of the voltage drop [80] as shown in table 2:

Table 2: Specification of test of voltage drops [80]

Voltage drop case	Magnitude of phase-phase voltage (pu)	Magnitude of positive sequence voltage (pu)	Period (s)
VD1[1]	0.90 ± 0.05	0.90 ± 0.05	0.5 ± 0.02
VD2[1]	0.5 ± 0.05	0.5 ± 0.05	0.5 ± 0.02
VD3[1]	0.2 ± 0.05	0.2 ± 0.05	0.2 ± 0.02
VD4[2]	0.90 ± 0.05	0.95 ± 0.05	0.5 ± 0.02
VD5[2]	0.5 ± 0.05	0.75 ± 0.05	0.5 ± 0.02
VD6[2]	0.2 ± 0.05	0.60 ± 0.05	0.2 ± 0.02

[1] 3-phase voltage drop [2] 2-phase voltage drop

Voltage sag is normally expressed as a relative percentage change in voltage of the wind turbine system is given by:

$$d = k_u \frac{S_n}{S_k} \tag{2.1}$$

Where d is relative change in voltage, k_u is voltage reduction factor, S_n is apparent power (rated) and S_k is apparent power (short circuit).

Voltage rise is the increase in the voltage from 1.0pu to about 1.8pu in a period of 0.5 cycles to 1 minute which can be caused by switching-off of large loads, increase in voltage in unfaulty lines during single line-ground fault and excitement of capacitor banks [81].

Another important power quality parameter that is worthy of mention is “flicker” which is caused by fluctuation. The fluctuation in voltage is a major concern when connecting wind turbine system to the grid, it is caused by changes in the wind speed. Voltage fluctuations have direct effect on the active and reactive power in the system. The degree of the voltage fluctuation depend on the strength of the grid, impedance of the network and characteristics of the wind turbine. Flickers are caused by fluctuations in system voltage which is visible from electric light. The magnitude of the flicker is dependent on the degree of fluctuation. It affects the voltage quality

of the grid if not controlled from the generating station. Flickers mostly do not affect VSWT system because the output active power is relatively constant. The fluctuation in voltage and flicker emission for wind turbines connected to the grid is related to factors such as [82]:

1. Average wind speed
2. Turbulence intensity
3. Short-circuit ratio (SCR)

The reactive power of the wind turbine can be controlled to vary the active power thereby making the difference between the grid impedance angle and power factor angle tend to 90 degrees and as a result reducing the flicker level. The flickermeter as specified by the IEC 61000-4-15 is used to measure flicker emission [83]. The IEC flickermeter operate on the principle of simulation of the "transfer function" of the set "voltage-lamp-eye-brain" and gives a corresponding output of the disturbance level known as "Instantaneous flicker sensation" (Sf), the instantaneous flicker is then analysed statistically to generate an output every 10 minutes corresponding to the flicker severity level [79].

Another parameter that compromises the power quality of grid-connected wind turbine system is harmonics, harmonics arises as a result of the presence of power electronic converters mostly found in VSWT coupled with DFIG. The harmonic current and voltage transferred to the grid at the PCC should be limited as specified by the IEC 614400-36 guideline, the total harmonic distortion (THD) of voltage at the PCC is given by [84]:

$$V_{THD} = \sqrt{\sum_{n=2}^{40} \frac{V_n^2}{V_1}} 100 \tag{2.2}$$

Where V_{THD} is total harmonic distortion of voltage, V_1 is voltage at fundamental frequency and V_n is nth harmonic voltage. The THD for a connection to a 132kV grid should be less than 3%.

As a result of the increase in penetration of WECS which will cause an increase in unpredictability of the power quality of the system, it became necessary to impose some level of technical criteria that WECS should meet before they can be connected to the grid. These technical requirements are compiled to form “grid code” which now serves as standard thatt wind farms should meet before successful connection to the grid.

2.7 Grid Code

The fluctuating nature of wind power has brought about the formation of interconnection standards and grid codes to maintain the power quality of the grid during such fluctuations. In the past, wind turbines are permitted to disconnect from the grid in cases of grid faults to prevent damage of the wind turbines [81]. The major challenges in the growth of wind power are associated with grid reliability and intermittency. For good power quality to be achieved, it is important that the grid code be maintained. Grid codes require that wind farms must operate like conventional power generators, that is, they must be able to provide active power and also inject and absorb reactive power to and from the grid during steady-state and fault conditions [85]. Grid codes are the least technical requirements that must be followed during the setup and operation of renewable energy systems to be connected to the grid. The new grid codes establish the low-voltage ride through capability of wind farms to improve transient stability of power system and reactive power capability to provide voltage support for the power system, wind farms operate as an active power compensator during faults [81]. The objective of renewable energy grid code is to improve and regulate the behavior of wind power systems while decreasing the losses of wind power and providing wind power operators with operational characteristics close to those of conventional power plants. The tripping and disconnection of wind turbine systems from the grid during faults is prohibited in the new grid codes. Grid codes are established in different countries to allow wind farm provide certain level of support to the grid during faults [86]. Grid code handles voltage control, reactive power control, flickers, harmonics, active power control and fault ride-through capability issues [87]. The common parameters for local and international renewable

energy grid code include continuous operation parameters, low voltage ride through capability, high voltage ride through capability, active power regulation, reactive power regulation, visibility and control of RPPs [88-90].

The South Africa renewable energy grid code (SAREGC) provides the minimum technical requirements that renewable power plants (RPPs) connected to or seeking connection to the South Africa electrical transmission system or distribution system, it categorizes minimum technical requirements by size of the RPPs (biogas, wind, photovoltaic, landfill gas and concentrated solar power):

1) Category A: 0 – 1MVA (LV connected RPPs) – this category is subdivided into 3:
    a. Category A1: 0 – 13.8kVA
    b. Category A2: 13.8kVA – 100kVA
    c. Category A3: 100kVA – 1MVA
2) Category B: 1MVA – 20MVA
3) Category C: 20MVA or higher

The current version (version 2.9) of the SAREGC released November 2016 specifies the requirements for industrial standardization, network integrity and non-discriminatory access to the grid by RPPs. Due to complexity of the SAREGC, detailed explanation and practical methods to test the compliance of the RPPs to the grid code have been done in [87, 91-93].

The SA grid code allows the renewable power plants (RPPs) to maintain connection to the grid in areas A, B and D, withstand voltage sag up to zero at the PCC for a period of 150ms without disconnecting as shown in Figure 2.5. During symmetrical faults, wind farms greater than 20MVA must provide voltage support to the grid by supplying controlled reactive current to enhance voltage stability to the grid, active power production must be maintained during voltage drop but for voltage drop below 85%, active power production can be reduced.

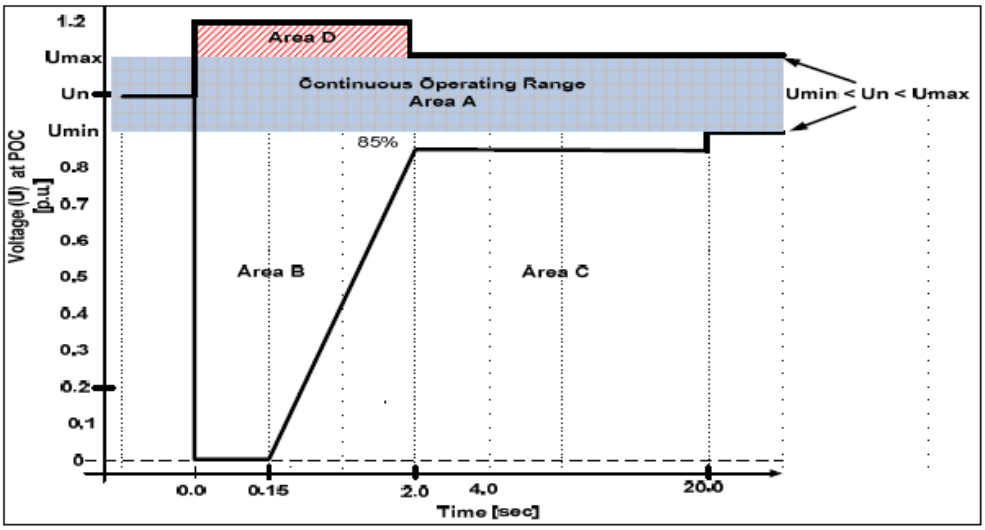

Figure 2.5 Required voltage ride through capability of category C RPPs [94]

The increase in active power demand causes reduction in grid frequency and vice versa, RPPs are required to maintain production of active power at a frequency of 50Hz and also respond to grid frequency changes by regulating active power production within its set-points. P_{Delta} is the amount of active power reserved from the available active power (Pavailable) from the wind farm for gird frequency stability which is usually not less than 3% of Pavailable as seen in Figure 2.6. The frequencies f4, f5, f6, fmin, fmax are provided in Table 3 while frequencies f1, f2, f3 are agreed between the service operator (SO) and the RPP.

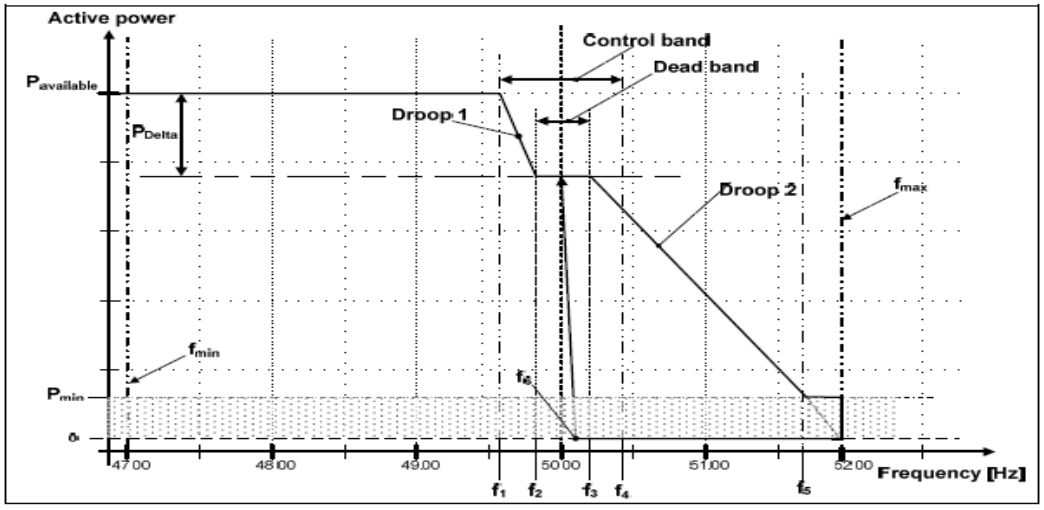

Figure 2.6: Active power response to variation in grid frequency for category C RPPs [94]

Table 3: Frequency settings for RPPs [94]

Frequency	Magnitude (Hz.)
fmin	47
fmax	52
f1	Agreed with SO
f2	Agreed with SO
f3	Agreed with SO
f4	50.5
f5	51.5
f6	50.2

A comprehensive review of grid codes of America, Australia, Europe (Germany, Sweden, Denmark, Spain, Ireland, Belgium and Italy) and UK have been discussed in [95] with respect to fault ride-through requirements.

2.8 Reactive Power Compensation

In a three-phase system, several problems such as reactive power imbalance, voltage control at varying load conditions, stability problems, varying frequencies of different systems and short-circuit power are observed, these problems can be solved with the use of HVDC technology and FACTS technology [96]. Compensation in power systems can either be done in series or parallel/shunt.

Series compensation is used to decrease the effective reactance in the line and thereby increasing the power transfer capability of the line. It also used to reduce transmission angle, voltage drops, improve system stability and control load flow. Parallel compensation is used to improve the power factor and thereby increasing the voltage regulation and reducing losses in power transmission. It is also used for stead-state and transient voltage control, active power oscillation damping, control of reactive power and improve the overall system stability [96].

Reactive power control is necessary to reduce the voltage fluctuations as a result of varying loads and to reduce transmission losses [79].

An induction generator is known to consume reactive power, which is drawn from the grid. It is therefore necessary to provide an alternative source of reactive power to reduce the impact on the reactive power consumption from the grid. Reactive power compensation are traditionally provided by capacitor banks or Load Tap Changers (LTC) but latest developments in the power electronics has adopted the use of FACTS devices for reactive power compensation.

2.9 FACTS Devices

The problem of power system stability when wind farms are connected to the grid cannot be overemphasized. Improved reliability and reduced cost are the major implication of transmission interconnection. However, there is a reduction in the transmission and distribution reliability if one or more transmission parameters such as voltage, frequency, phase angle deviates from its rated value or setoff values. The flexibility of an electrical power system is its ability to maintain steady-state condition during varying operating conditions. FACTS devices have been developed to enhance the transmission reliability by maintaining the system parameters at rated values. FACTS devices are power electronics devices with other static controllers that improve the power transmission capability of electrical power systems [97] with respect to reduced cost, environmental impact and eliminate the necessity of adding new transmission lines to the network. FACTS technology helps to maximize the use of existing transmission systems because it helps to increase the performance of power systems [81]. FACTS devices provide rapid response to maintain the desired voltage level and system stability [79]. The literature reviewed in [72] highlighted the efficiency of FACTS devices in improving the power quality of renewable energy farms. They are able to rapidly compensate for active and reactive power, provide voltage support, and improve transient stability and power damping oscillation [98]. They make generation of electrical power more economical while being environmental friendly. It emphasizes the strategic

positioning of FACTS devices as been instrumental for improving the voltage profile and reducing power losses in power systems. It presented generic algorithm (GA) as an efficient method to determine the optimal location to place FACTS devices because of its robustness. It concluded by pointing the shortcoming of absence of sufficient researches to focus on ride-through of wind energy with optimization methods and the essence of dynamic modelling of wind farms (which this research aims to achieve) to increase the penetration level of wind power. Authors in [99] presented FACTS as effective means of downplaying inadequate power flow and excessive reactive power. FACTS devices can be classified into the following:

1. Shunt-connected controllers:
2. Series-connected controllers
3. Combined series-shunt controllers
4. Combined series-series controllers.

Within the four classifications itemized above, shunt-connected controller which is applicable in this work is reviewed extensively.

2.9.1 Shunt connected Controller: the shunt connected controller has the capability to absorb or inject current in to the line which is an effective way to control the voltage at the point of connection. The various shunt connected controllers are:

2.9.1.a Static Var Compensator (SVC)

According to IEEE, "*a static var generator or absorber whose output is adjusted to exchange capacitive or inductive current so as to maintain or control specific parameter of the electrical power system*" [97]. The SVC is a thyristor-based device without a gate turn-off capability. It comprises the thyristor-controlled reactor (TCR) or thyristor-switched reactor (TSR) for absorbing reactive power and Thyristor-Switched Capacitor (TSC) for injecting reactive power as shown in Figure 2.7. The TCR is "*a thyristor-controller inductor whose effective reactance is varied in a continuous manner by partial induction control of the thyristor valve*", the TSR is "*a thyristor-switched inductor whose effective reactance is varied in a step*

wise manner by full or zero conduction operation of the thyristor valve" and a TSC is "*a thyristor-switched capacitor whose effective reactance is varied in a step wise manner by full or zero conduction operation of the thyristor valve*" [97].

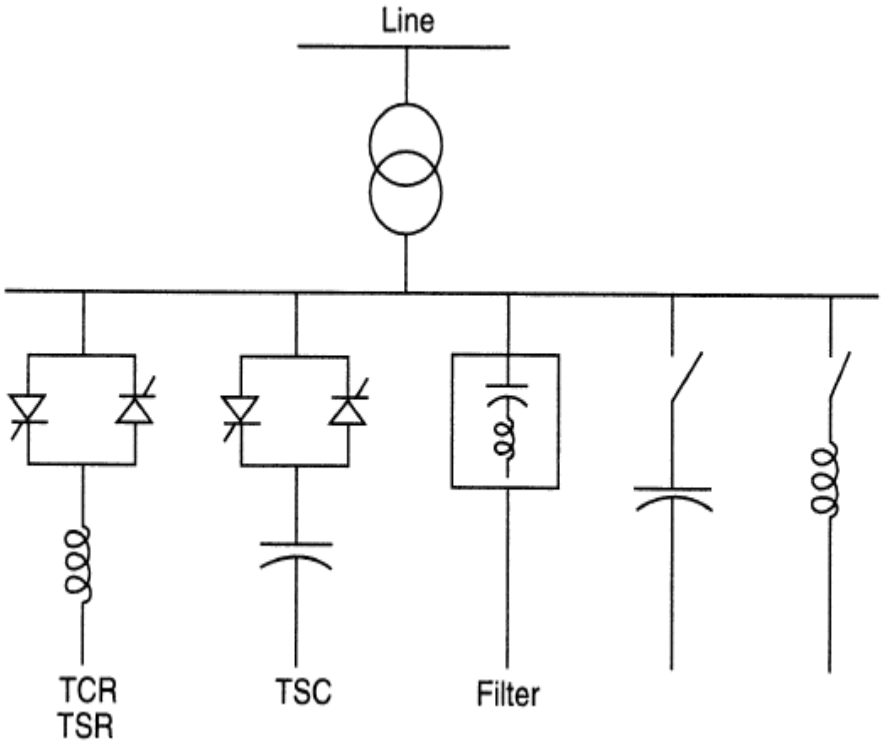

Figure 2.7: Basic configuration of SVC [97]

The TSC of the SVC is a number of capacitor banks in series with a damping reactor and thyristor valves. The thyristor switch is used to connect and disconnect the capacitor bank for a number of half-cycles of the applied voltage, the switching of the capacitor happens when the thyristor voltage is zero [23]. The TSC is harmonic free because it is not phase controlled. The TCR comprises of the induction and static switch which is made up of two antiparallel-connected thyristors, the power is regulated by changing the current flow through the inductor by the switch. The purpose of the SVC control is to determine the susceptance required at the point of connection to the grid to maintain the voltage at its desired value, this is achieved by comparing the grid voltage with the desired voltage, and the controller adjusts the susceptance till the equilibrium voltage is attained. The susceptance of the SVC is a total of the susceptances of the harmonic

filters, TSC and TCR [100]. SVC is also used in alleviation of flicker issues. SVCs are generally connected to the point of common coupling (PCC) for power factor and voltage control. It was presented that the voltage sag during fault with the use of SVC was lower compared to use of capacitor banks in [101]. The ability of SVC to provide voltage control and reactive power control was mentioned in [39] and also suggested that increasing the rating of the SVC increases its performance in the system. The proposed optimization methodology in [54] focused on the use of SVC, it argued that the representation of SVC as a variable reactance that takes into consideration reactive power and voltage limit at the PCC by various researchers is not totally correct. In [102], SVC was mentioned as compensators for reactive power but also give rise to harmonic currents. SVC the oldest and most widely use FACTS device owing to its rapid response, precision and accessibility to provide better steady-state and dynamic voltage control when compared to traditional compensators; in South Africa, the KwaZulu-Natal axis of the Eskom grid supplies Durban and Richard's bay, when the system was loaded to almost its stability limit, there was lack of base load generation in the area, 3 units of SVCs were installed at different load centers to improve the voltage control performance; the reason for choosing SVC was due to reduced cost, reduced environmental impact and minimization of voltages reductions due to fault. SVC's application in Australia, Brazil, Indonesia and USA was also presented in this paper [103]. In developed countries where electric arc furnaces (EAFs) are widely used, they are compensated with SVCs to reduce the amount of reactive power the EAF consume from the supply network, [104] presented the use of a 330 Mvar SVC to compensate a EAF-250 metallurgical plant in Turkey. A reduction of dynamic reactive compensation with SVC from 100Mvar to about 25Mvar was achieved in [24] by optimization of mechanical and electrical parameters of the wind turbine such as reduction in stator resistance, magnetizing reactance and increase of the rotor resistance.

2.9.1.b Static Synchronous Compensator (STATCOM)

As defined by IEEE, "*a static synchronous generator operated as a shunt-connected static var compensator whose capacitive or inductive output current can be controlled independent of the ac system voltage*" [97]. It is normally based on a voltage-sourced or current-sourced converter. STATCOM also known as SVC Light or GTO (gate turn-off type thyristor) based SVC is a VSC-based controller used to generate and absorb reactive power.

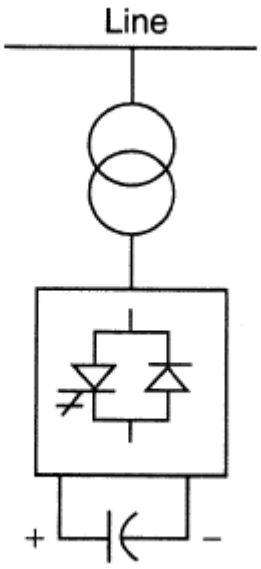

Figure 2.8: STATCOM configuration [97]

The VSC is connected to the grid through a coupling transformer for reactive power injection and absorption. STATCOM behaves as a capacitor by injecting reactive power into the system if its terminal voltage is higher than the system voltage and behaves as an inductor by absorbing reactive power if its terminal voltage is less than the system voltage [81]. STATCOMs do not require huge size of capacitive or inductive device to supply capacitive or inductive reactive power [103, 105]. It provides faster response and better performance during steady-state and transient conditions when compared to SVC. The STATCOM is used to reduce the reactive power demand from the load and induction generator on the grid. BESS-based STATCOM compensation was presented in [38], the BESS is used for regulate the active power during wind fluctuations. A control technique with multi-pulse

STATCOM used to control flicker voltage oscillation in arc furnaces was presented in [79], the reactive power of the multi-pulse STATCOM is varied by the dc capacitor with the conclusion that increasing the size of dc capacitor reduces the flicker level at the disadvantage of cost. The different application of power electronics to increase the overall performance of wind power system to meet the grid connection requirements were discussed in [23], it presented the use of STATCOM and crowbar for fault ride-through of DFIG. The use of robust control theory to design the control scheme of STATCOM to improve the operation of the wind farm was presented in [101] and was concluded that STATCOM can be used to achieve rapid steady-state and transient control of voltage. The preference of thyristor-based STATCOM over self-commutated STATCOM was presented in [99], it gave complexity and cost as a disadvantage of self-commutated STATCOM. The high-voltage-ride-through (HVRT) of type D WECS during voltage rise with STATCOM was shown in [81] to prevent the disconnection of the wind farm from the grid with grid code compliance of USA and Spain. The results presented in [48] showed that STATCOM provides static reactive power compensation to the wind farm and an INC can be added to coordinate the reactive power control between the STATCOM and the GSC of the DFIG wind farm. The use of STATCOM in transmission system for reactive power control and voltage support and in distribution system for power factor correction and voltage control was discussed in [102], it pointed STATCOM as a static synchronous generator that its active energy source is substituted with a dc capacitor and it also mentioned phase angle control, constant dc link voltage scheme, direct current control with instantaneous pq theory, and indirect current control with instantaneous pq theory as control techniques in STATCOM. A steady-state detailed and reduced model of STATCOM is presented in [106], it stated that STATCOM can operate as SSSC if the voltage-source converter is connected in series with the transmission line through a transformer. Bang bang current control scheme where the controller bounds the control variables of STATCOM to the hysteresis area to provide accurate switching signal needed by STATCOM was implemented in [38]. Studies presented in [107] show the

ability of STATCOM to provide reactive power in a wind farm under varying conditions, it states that STATCOM is able to improve the steady state stability of power system. The use of STATCOM to improve the transient stability of wind farms have presented in [108-116].

2.10 Series connected Controller: the series connected controller affects the voltage thereby impacting the current and power flow in the line. The various series connected controllers are static synchronous series compensator (SSSC), thyristor controlled series capacitor (TCSC), thyristor switched series capacitor (TSSC), thyristor controlled series reactor (TCSR).

2.11 Combined Series-Shunt connected Controllers: they are combination of series and shunt controllers whereby the series controller supplies voltage in series with the line and the shunt controller injects current into the line. The various types of combined series-shunt controllers are unified power flow controllers (UPFC), thyristor controlled phase shifting transformer (TCPST) and interphase power controller (IPC).

2.12 Combined series-series Controllers: they are combination of different series controllers, they are controlled in an organized manner in which each series controller provide reactive compensation for each line and also supply the real power through the power link. The combined series-series controller present in literature as at time of writing is the interline power flow controller (IPFC).

The placement of FACTS devices in a network is very important, various methods have been proposed by various researchers to determine the strategic position to place FACTS devices for optimal function [72]. Load sensitivity analysis, optimal power flow analysis, continuous power flow analysis, voltage stability analysis and various artificial intelligence algorithms such as generic algorithm, brainstorm optimization algorithm, particle swarm optimization algorithm, crow-search algorithm, cat-swarm optimization algorithms have been presented as techniques to determine the optimal location of FACTS devices [117-123]. Voltage stability analysis method is used in this work to determine the optimal location of STATCOM.

The technical benefits of FACTS devices are provided in Table 4 and the choice of STATCOM in this work is its relative performance in terms of voltage control and transient stability which are the major areas considered in this work.

Table 4: Technical benefits of FACTS devices

FACTS device	Load Flow Control	Voltage Control	Transient Stability	Dynamic Stability
SVC	*	***	*	**
STATCOM	*	***	**	**
TCSC	**	*	***	**
UPFC	***	***	**	**

Where: * denotes Good, ** denotes Better, and *** denotes Best.

CHAPTER 3: MATHEMATICAL MODELLING OF DFIG

In wind energy conversion systems (WECSs), the kinetic energy present in wind is converted to electrical energy by doubly-fed induction generators (DFIGs) and fed to a local load or to the grid. To analyze the interaction of grid-connected WECSs, an appropriate model of the system needs to be developed and this chapter is dedicated to do so.

A brief introduction of the operation of the variable speed WECS is given, the aerodynamic model of the wind turbine is presented, and the dynamic model of the DFIG is developed in two major frames of reference. The first frame of reference is the ABC frame of reference and the second is the DQO-dqo frame of reference which is derived by Park's transformation of the ABC frame of reference. Also, a reduced order model in the synchronously rotating frame of reference is derived for the DFIG model. Lastly, the models of the three phase pulse-width modulated (PWM) converters are also derived in the ABC and DQO-dqo frames of reference.

3.1 Introduction

The variable speed wind energy conversion system uses a wind turbine to capture wind energy through its blades and transfer energy to the DFIG through a gearbox. The DFIG transfers electrical power directly to the grid through the stator windings, and the back-to-back converter from the rotor windings. The back-to-back converter is divided into the rotor-side converter (RSC) and grid-side converter (GSC) connected by a DC-link capacitor. The RSC is used to decouple active and reactive power and achieve independent control of both while the GSC is used to keep the voltage in the DC-link constant.

The DFIG operates at two different frequencies, the stator/grid side frequency and rotor side frequency as depicted in Figure 3.1. The rotation of the DFIG implies that the frequency of the rotor windings is equivalent to the difference between the stator frequency and rotor speed, and active power is shared between the stator and rotor approximately in the ratio of the slip frequency [124].

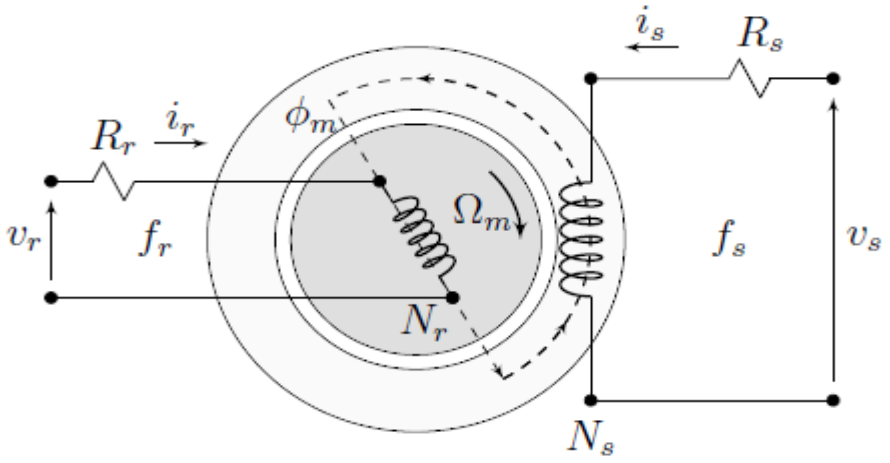

Figure 3.1: Single-phase representation of doubly-fed induction generator [125]

The angular frequency of voltage or current in the stator winding is given as:

$$\omega_s = 2\pi f_s \tag{3.1}$$

where, f_s is the stator or grid frequency. Therefore, the angular frequency of the voltage or current in the rotor winding can be given as:

$$\omega_r = \omega_s - \omega_m \tag{3.2}$$

where, ω_m is the electrical angular frequency of the rotor. The slip, s which describes the relationship between, ω_s and ω_m is given by:

$$s = \frac{\omega_s - \omega_m}{\omega_s} \tag{3.3}$$

The relationship between the electrical angular frequency of the rotor and its mechanical speed can be expressed as:

$$\omega_m = p\Omega_m \tag{3.4}$$

Also, the relationship between the angular frequencies of the rotor and stator windings can be expressed directly as:

$$\omega_r = s\omega_s \tag{3.5}$$

For a negative slip, the DFIG operates at supersynchronous speed which implies the power supplied in the rotor is positive and is transmitted to the grid through the converters. For a positive slip, the DFIG operates at sub-

synchronous speed which implies that the power in the rotor is taken from the grid through the converters.

3.2 Aerodynamic Model

Wind is produced from the differential in temperature and pressure amongst various air areas that are unevenly exposed to the sun, the speed of wind depends on various meteorological events [64]. The kinetic energy in wind with velocity V hitting a surface with area A contains the power given by:

$$P_k = {}^1\!/_2\, \rho A V^3 \tag{3.6}$$

However, only a fraction of P_k can be extracted by the wind turbine blades which is given by:

$$P_w = {}^1\!/_2\, \rho A V^3 C_p \tag{3.7}$$

Given that the blades of the turbine rotates in a circular motion along its radius R and C_p, a dimensionless quantity is a function of the turbine blade tip speed ratio (λ) and pitch angle (β) as shown in Figure 3.2, Equation (3.7) can be written as:

$$P_w = {}^1\!/_2\, \rho \pi R^2 V^3 C_p(\lambda, \beta) \tag{3.8}$$

The blade tip speed ratio λ is defined by:

$$\lambda = \frac{R\Omega_m}{V} \tag{3.9}$$

C_p is known as power coefficient or performance coefficient of the turbine, whose calculation requires the concept of aerodynamics and complex calculations with blade element theory, numerical approximation of C_p cannot exceed 0.59 which is known as Betz limit in theory [9]. This implies that without power losses, only 59% of power can be extracted from the wind by the wind turbine. It can mathematically be expressed as:

$$C_p = 0.73\left(\frac{151}{\lambda_k} - 0.58\beta - 0.002\beta^{2.14} - 13.2\right)e^{-18.5\lambda_k} \tag{3.10}$$

And,

$$\frac{1}{\lambda_k} = \frac{1}{\frac{1}{\lambda - 0.02\beta} - \frac{0.003}{\beta^3 + 1}} \tag{3.11}$$

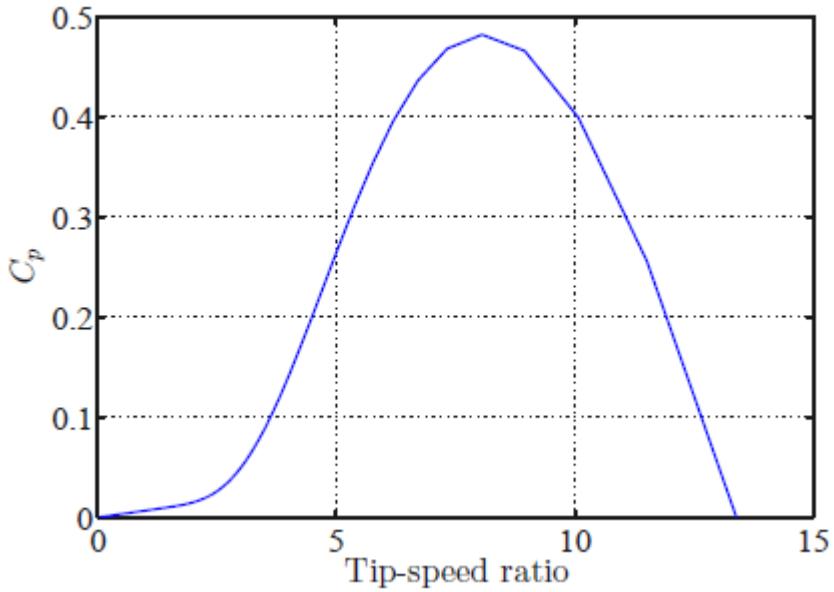

Figure 3.2: Power coefficient curve [126]

3.3 Dynamic Model of the Induction Machine

The dynamic models of the induction machine should provide adequate knowledge for designing the vector control techniques in the WECS. The dynamic model must incorporate steady state and transient characteristics [127]. The model of induction machine developed in this section is valid for random variations of voltage and current with respect to time, and satisfactorily describes the operation of the machine during normal and transient conditions. The model is developed in two frames of reference (ABC frame of reference and other DQ0 frames of reference).

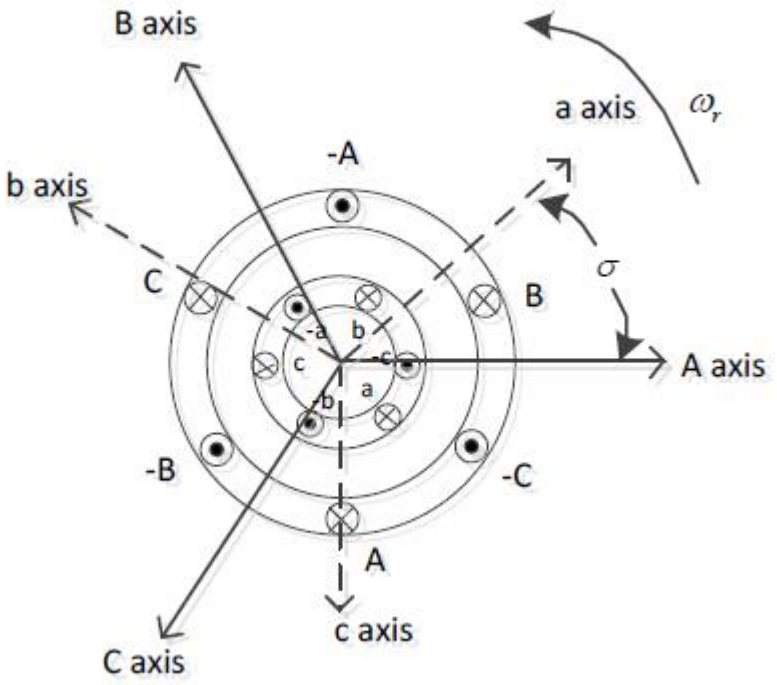

Figure 3.3: Wound rotor induction machine in the ABC frame of reference [125]

Consider a wound rotor induction machine shown in Figure 3.3 with three phase windings on stator and rotor with two symmetrical poles. The stator windings have a displacement of 2π/3 from one another, the rotor windings also have a displacement of 2π/3 from one another. The angle between respective axes of phase windings of stator and rotor is σ. The rotor is moving in an anti-clockwise direction as shown in Figure 3.3 with a speed of:

$$\omega_r = \frac{d\sigma}{dt} \tag{3.12}$$

To satisfactorily model the induction machine in the ABC reference frame, the following assumptions were made [128]:

- The phase winding of the stator and rotor are assumed to be symmetrical in distribution, that is, the inductances (leakage and magnetizing) and resistances are equal in all the three phases.
- Absence of harmonics because of the sinusoidal distribution of the magnetomotive force produced around the stator of the machine.

- The air-gap is assumed constant, meaning that the reluctance of the air-gap around the circle of the mid air-gap is constant. As a result, the mutual inductances between two stator and rotor phase windings are assumed unchanged. However, the mutual inductances between the stator phase winding and rotor phase winding are a function of the angular displacement σ of the rotor.
- The saturation of mutual inductance is assumed negligible.
- Skin effect is assumed negligible. If there in an increase in the frequency of current, skin effect will decrease the leakage inductance and increase the resistance in the stator and rotor of the machine.
- Iron core losses are assumed negligible.
- The cross-coupling between two orthogonal axes, that is, cross-saturation effect is assumed negligible.

The phase voltages,v_A, v_B and v_C of the stator, and v_a, v_b and v_c of the rotor can be expressed from Faraday's law as:

$$v_A = r_A i_A + \rho\varphi_A \quad (3.13)$$

$$v_B = r_B i_B + \rho\varphi_B \quad (3.14)$$

$$v_C = r_C i_C + \rho\varphi_C \quad (3.15)$$

$$v_a = r_a i_a + \rho\varphi_a \quad (3.16)$$

$$v_b = r_b i_b + \rho\varphi_b \quad (3.17)$$

$$v_c = r_c i_c + \rho\varphi_c \quad (3.18)$$

where, r_A, r_B and r_C are the resistances in the phase A, B and C of the stator respectively, r_a, r_b and r_c are the resistances in the phase a, b and c of the rotor respectively, ρ is a Laplace operator given by $\frac{d}{dt}$, φ_A, φ_B and φ_C are the flux linkages in each phase of the stator and φ_a, φ_b and φ_c are the flux linkages in each phase of the rotor which can be expressed as:

$$\varphi_A = L_{AA}i_A + L_{AB}i_B + L_{AC}i_C + L_{Aa}i_a + L_{Ab}i_b + L_{Ac}i_c \quad (3.19)$$

$$\varphi_B = L_{AB}i_A + L_{BB}i_B + L_{BC}i_C + L_{Ba}i_a + L_{Bb}i_b + L_{Bc}i_c \quad (3.20)$$

$$\varphi_C = L_{AC}i_A + L_{BC}i_B + L_{CC}i_C + L_{Ca}i_a + L_{Cb}i_b + L_{Cc}i_c \quad (3.21)$$

$$\varphi_a = L_{Aa}i_A + L_{Ba}i_B + L_{Ca}i_C + L_{aa}i_a + L_{ab}i_b + L_{ac}i_c \quad (3.22)$$

$$\varphi_b = L_{Ab}i_A + L_{Bb}i_B + L_{Cb}i_C + L_{ab}i_a + L_{bb}i_b + L_{bc}i_c \quad (3.23)$$

$$\varphi_c = L_{Ac}i_A + L_{Bc}i_B + L_{Cc}i_C + L_{ac}i_a + L_{cb}i_b + L_{cc}i_c \quad (3.24)$$

From the set of stator flux linkage equations above, it can be deduced that the flux linkage in each phase consists of self-flux linkage term as a result of one phase of stator current, two mutual flux linkages produced by the other stator phase currents in the stator phase windings and three stator-to-rotor flux linkages produced by the rotor currents. Also, from the set of rotor flux linkage equations, it can be deduced that the flux linkage in each phase of the rotor windings consist of self-flux linkage term produced by the rotor phase current, two mutual rotor flux linkages produced by the other two rotor currents of the rotor phase windings and three stator-to-rotor flux linkages produced by the stator currents.

Therefore, Equation (3.13) to (3.18) can be written as:

$$v_A = r_A i_A + \frac{d}{dt}(L_{AA}i_A + L_{AB}i_B + L_{AC}i_C + L_{Aa}i_a + L_{Ab}i_b + L_{Ac}i_c) \quad (3.25)$$

$$v_B = r_B i_B + \frac{d}{dt}(L_{AB}i_A + L_{BB}i_B + L_{BC}i_C + L_{Ba}i_a + L_{Bb}i_b + L_{Bc}i_c) \quad (3.26)$$

$$v_C = r_C i_C + \frac{d}{dt}(L_{AC}i_A + L_{BC}i_B + L_{CC}i_C + L_{Ca}i_a + L_{Cb}i_b + L_{Cc}i_c) \quad (3.27)$$

$$v_a = r_a i_a + \frac{d}{dt}(L_{Aa}i_A + L_{Ba}i_B + L_{Ca}i_C + L_{aa}i_a + L_{ab}i_b + L_{ac}i_c) \quad (3.28)$$

$$v_b = r_b i_b + \frac{d}{dt}(L_{Ab}i_A + L_{Bb}i_B + L_{Cb}i_C + L_{ab}i_a + L_{bb}i_b + L_{bc}i_c) \quad (3.29)$$

$$v_c = r_c i_c + \frac{d}{dt}(L_{Ac}i_A + L_{Bc}i_B + L_{Cc}i_C + L_{ac}i_a + L_{cb}i_b + L_{cc}i_c) \quad (3.30)$$

For a balanced and uniformly distributed three phase winding in the stator and rotor of the machine, the following deductions are made:

- The resistance in each phase of the stator can be written as:

$$r_A = r_B = r_C = r_s \quad (3.31)$$

  where r_s is the stator resistance.

- The resistance in each phase of the rotor can be written as:

$$r_a = r_b = r_c = r_r \quad (3.32)$$

  where r_r is the rotor resistance.

- For identical flux paths in the three phases A, B and C of the stator,

$$L_{AA} = L_{BB} = L_{CC} = L_{ss} \tag{3.33}$$

where L_{ss} denotes self-inductance present in the phase winding of the stator, independent of angular rotor displacement, σ.

- L_{AB}, L_{BC} and L_{AC} have equal magnitudes and are independent of the angular rotor displacement, σ. Therefore,

$$L_{AB} = L_{BC} = L_{AC} = L_{ms} \tag{3.34}$$

where L_{ms} denotes mutual inductance between two stator windings.

- The rotor inductance coefficients can be expressed as:

$$L_{aa} = L_{bb} = L_{cc} = L_{rr} \tag{3.35}$$

where L_{rr} denotes self-inductance of the phase winding of the rotor and independent of angular rotor displacement, σ.

- The mutual inductance between two rotor phase windings can be expressed as:

$$L_{ab} = L_{bc} = L_{ac} = L_{mr} \tag{3.36}$$

where L_{mr} denotes mutual inductance between two rotor windings.

- The other coefficients of inductance L_{Aa}, L_{Ab}, L_{Ac}, L_{Ba}, L_{Bb}, L_{Bc}, L_{Ca}, L_{Cb} and L_{Cc} are dependent on the angular displacement σ between the rotor and stator phase winding, and phase difference which is given by:

$$L_{Aa} = L_{Bb} = L_{Cc} = L_m \cos\sigma \tag{3.37}$$

$$L_{Ab} = L_{Bc} = L_{Ca} = L_m \cos\left(\sigma + {}^{2\pi}/_{3}\right) \tag{3.38}$$

$$L_{Ac} = L_{Ba} = L_{Cb} = L_m \cos\left(\sigma - {}^{2\pi}/_{3}\right) \tag{3.39}$$

where, L_m denotes maximum mutual inductance between stator and rotor phase windings.

- The angular displacement, σ between the respective phase windings of the rotor and stator can be expressed as:

$$\sigma = \int_0^t \omega_r(t) + \sigma_0 \tag{3.40}$$

By substituting the expressions of inductances and resistances into the voltage Equations of the stator and rotor, the expression of the induction machine in the ABC frame of reference can be written as the equation presented in Appendix A.

Equation in Appendix A shows that the inductance matrix in the ABC frame of reference is dependent on the rotor displacement which is a function of time from Equation (3.40). This implies that the calculation of the inductance matrix must be done for every time step, thereby resulting to slower calculation time of the model. It is therefore necessary to express the model of the induction machine in several DQ0 frames of reference because of simplicity, quicker computation time and easy implementation [125].

3.4 Induction Machine Representation in DQ0-dq0 Frame of Reference Stationary on the Rotor

The dynamic model equation of the induction machine expressed in Equation (3.41) can be rewritten as:

$$\underline{V_{ABC}} = \underline{R_{ss}} \cdot \underline{I_{ABC}} + \frac{d}{dt}\left(\underline{\varphi_{ABC}}\right) \tag{3.41}$$

$$\underline{V_{abc}} = \underline{R_{rr}} \cdot \underline{I_{abc}} + \frac{d}{dt}\left(\underline{\varphi_{abc}}\right) \tag{3.42}$$

and,

$$\underline{\varphi_{ABC}} = \underline{L_{ss}} \cdot \underline{I_{ABC}} + \underline{L_{rs}} \cdot \underline{I_{abc}} \tag{3.43}$$

$$\underline{\varphi_{abc}} = \underline{L^t_{rs}} \cdot \underline{I_{ABC}} + \underline{L_{rr}} \cdot \underline{I_{abc}} \tag{3.44}$$

where, $\underline{V_{ABC}}$ and $\underline{V_{abc}}$ are stator and rotor voltage vectors respectively, $\underline{I_{ABC}}$ and $\underline{I_{abc}}$ are stator and rotor current vectors respectively, $\underline{\varphi_{ABC}}$ and $\underline{\varphi_{abc}}$ are stator and rotor flux linkage vectors respectively, $\underline{R_{ss}}$ and $\underline{R_{rr}}$ are stator and rotor resistance matrices, $\underline{L_{ss}}$ and $\underline{L_{rr}}$ are stator and rotor

–self and mutual- inductance matrices, and $\underline{L_{rs}}$ is the stator and rotor mutual inductance matrix.

Considering the transformation on the stator side, such that:

$$\underline{I_{DQ0}} = \underline{M_s} \cdot \underline{I_{ABC}} \tag{3.45}$$

$$\underline{V_{DQ0}} = \underline{M_s} \cdot \underline{V_{ABC}} \tag{3.46}$$

$$\underline{\varphi_{DQ0}} = \underline{M_s} \cdot \underline{\varphi_{ABC}} \tag{3.47}$$

where, $\underline{M_s}$ is a nonsingular transformation matrix on the stator side

Also considering the transformation on the rotor side, it follows that:

$$\underline{I_{dq0}} = \underline{M_r} \cdot \underline{I_{abc}} \tag{3.48}$$

$$\underline{V_{dq0}} = \underline{M_r} \cdot \underline{V_{abc}} \tag{3.49}$$

$$\underline{\varphi_{dq0}} = \underline{M_r} \cdot \underline{\varphi_{abc}} \tag{3.50}$$

where, $\underline{M_r}$ is a nonsingular transformation matrix on the rotor side

Substituting Equations (3.45) to (3.50) into Equations (3.41) to (3.44), the expression of the transformed DQ0 model in the DQ0-dq0 arbitrary frame of reference is given by:

$$\begin{bmatrix} \underline{V_{DQ0}} \\ \underline{V_{dq0}} \end{bmatrix} = \begin{bmatrix} \underline{M_s} \bullet \underline{R_{ss}} \bullet \underline{M_s^{-1}} & 0 \\ 0 & \underline{M_r} \bullet \underline{R_{rr}} \bullet \underline{M_r^{-1}} \end{bmatrix} \begin{bmatrix} I_{DQ0} \\ I_{dq0} \end{bmatrix} +$$

$$\frac{d}{dt}\left\{ \begin{bmatrix} \underline{M_s} \bullet \underline{L_{ss}} \bullet \underline{M_s^{-1}} & \underline{M_s} \bullet \underline{L_{rs}} \bullet \underline{M_r^{-1}} \\ \underline{M_r} \bullet \underline{L_{rs}^t} \bullet \underline{M_s^{-1}} & \underline{M_r} \bullet \underline{L_{rr}} \bullet \underline{M_r^{-1}} \end{bmatrix} \begin{bmatrix} I_{DQ0} \\ I_{dq0} \end{bmatrix} \right\} - \begin{bmatrix} \dot{\underline{M}}_s \bullet \underline{L_{ss}} \bullet \underline{M_s^{-1}} & \dot{\underline{M}}_s \bullet \underline{L_{rs}} \bullet \underline{M_r^{-1}} \\ \dot{\underline{M}}_r \bullet \underline{L_{rs}^t} \bullet \underline{M_s^{-1}} & \dot{\underline{M}}_r \bullet \underline{L_{rr}} \bullet \underline{M_r^{-1}} \end{bmatrix} \begin{bmatrix} I_{DQ0} \\ I_{dq0} \end{bmatrix}$$

(3.51)

To express the DQO-dqo frame of reference stationary on the rotor, the Figure (3.4) is considered:

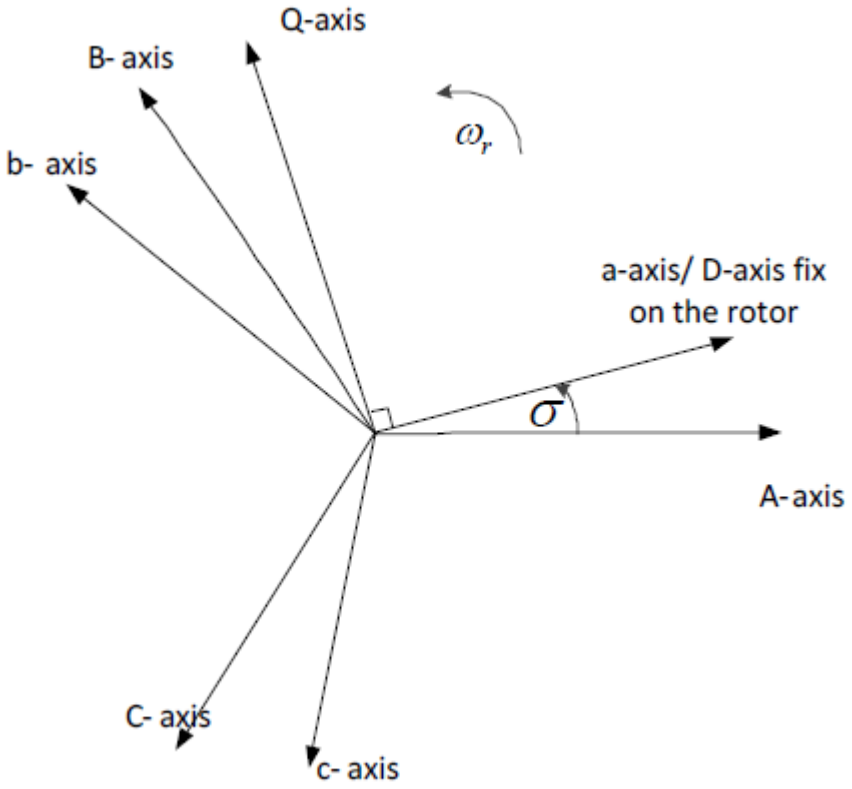

Figure 3.4: Transformation from ABC to DQO-dq0 frame of reference stationary on the rotor [127]

From Figure 3.4, the stator transformation matrix, $\underline{M}_{sro}$ and rotor transformation matrix, $\underline{M}_{rro}$ is deduced by projecting variables of the rotor and stator in the D-axis and Q-axis stationary on the rotor. $\underline{M}_{sro}$ and $\underline{M}_{rro}$ can be written as:

$$\underline{M}_{sro} = \frac{2}{3}\begin{bmatrix} \cos(\sigma) & \cos(\sigma - {}^{2\pi}/_{3}) & \cos(\sigma - {}^{4\pi}/_{3}) \\ -\sin(\sigma) & -\sin(\sigma - {}^{2\pi}/_{3}) & -\sin(\sigma - {}^{4\pi}/_{3}) \\ {}^{1}/_{2} & {}^{1}/_{2} & {}^{1}/_{2} \end{bmatrix} \tag{3.52}$$

$$\underline{M}_{rro} = \frac{2}{3}\begin{bmatrix} 1 & -{}^{1}/_{2} & -{}^{1}/_{2} \\ 0 & {}^{\sqrt{3}}/_{2} & -{}^{\sqrt{3}}/_{2} \\ {}^{1}/_{2} & {}^{1}/_{2} & {}^{1}/_{2} \end{bmatrix} \tag{3.53}$$

Therefore, substituting Equations (3.52) and (3.53) into Equation (3.51), we have:

$$\begin{bmatrix} \underline{V_{DQ0}} \\ \underline{V_{dq0}} \end{bmatrix} = \begin{bmatrix} \underline{M_{sro}} \bullet \underline{R_{ss}} \bullet \underline{M_{sro}^{-1}} & 0 \\ 0 & \underline{M_{rro}} \bullet \underline{R_{rr}} \bullet \underline{M_{rro}^{-1}} \end{bmatrix} \begin{bmatrix} I_{DQ0} \\ I_{dq0} \end{bmatrix} +$$

$$\frac{d}{dt}\left\{ \begin{bmatrix} \underline{M_{sro}} \bullet \underline{L_{ss}} \bullet \underline{M_{sro}^{-1}} & \underline{M_{sro}} \bullet \underline{L_{rs}} \bullet \underline{M_{rro}^{-1}} \\ \underline{M_{rro}} \bullet \underline{L_{rs}^{t}} \bullet \underline{M_{sro}^{-1}} & \underline{M_{rro}} \bullet \underline{L_{rr}} \bullet \underline{M_{rro}^{-1}} \end{bmatrix} \begin{bmatrix} I_{DQ0} \\ I_{dq0} \end{bmatrix} \right\} - \begin{bmatrix} \dot{\underline{M}}_{sro} \bullet \underline{L_{ss}} \bullet \underline{M_{sro}^{-1}} & \dot{\underline{M}}_{sro} \bullet \underline{L_{rs}} \bullet \underline{M_{rro}^{-1}} \\ \dot{\underline{M}}_{rro} \bullet \underline{L_{rs}^{t}} \bullet \underline{M_{sro}^{-1}} & \dot{\underline{M}}_{rro} \bullet \underline{L_{rr}} \bullet \underline{M_{rro}^{-1}} \end{bmatrix} \begin{bmatrix} I_{DQ0} \\ I_{dq0} \end{bmatrix}$$

(3.54)

The expression of the dynamic model of the induction machine in the DQO-dq0 frame of reference stationary on the rotor can therefore be written as the equation presented in Appendix B

3.5 Induction Machine Representation in DQ0-dq0 Frame of Reference Stationary on the Stator

The dynamic model of the induction machine in the DQO-dqo frame of reference can also be fixed on the stator. Figure 3.5 shows the transformation from the ABC to DQO-dqo stationary on the stator.

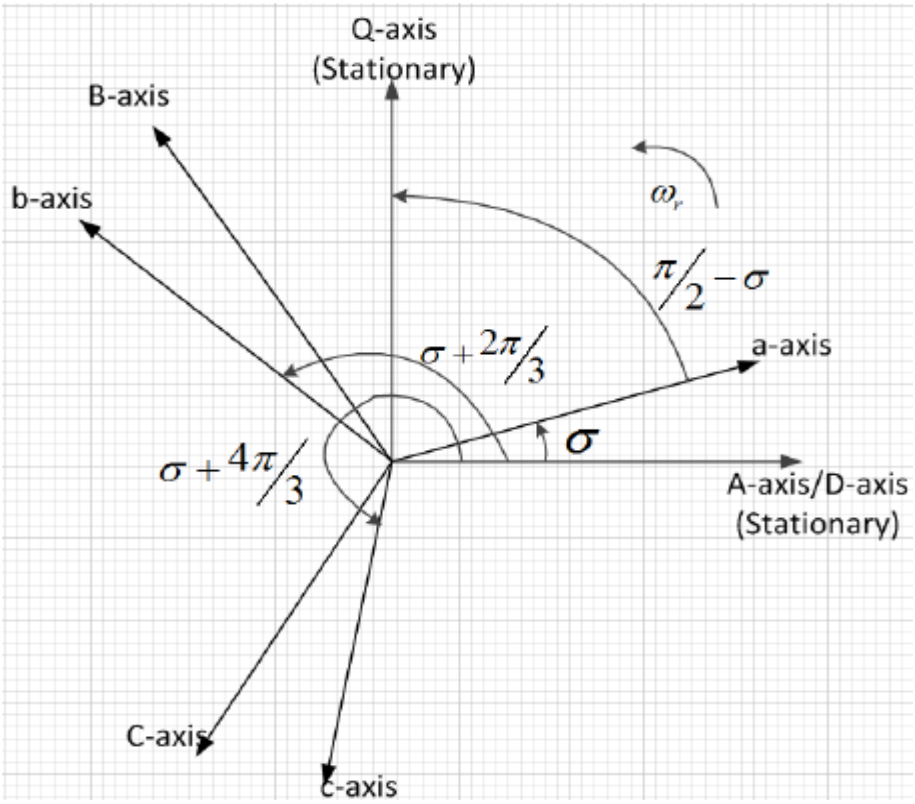

Figure 3.5: Transformation from ABC to DQO-dq0 frame of reference stationary on the stator [127]

Projecting the rotor and stator variables in the D-axis and Q-axis stationary on the stator, the stator transformation matrix, $\underline{M}_{sst}$ and rotor transformation matrix, $\underline{M}_{rst}$ is given as:

$$\underline{M}_{sst} = \frac{2}{3}\begin{bmatrix} 1 & -1/2 & -1/2 \\ 0 & \sqrt{3}/2 & -\sqrt{3}/2 \\ 1/2 & 1/2 & 1/2 \end{bmatrix} \tag{3.55}$$

$$\underline{M}_{rst} = \frac{2}{3}\begin{bmatrix} \cos(\sigma) & \cos(\sigma + 2\pi/3) & \cos(\sigma + 4\pi/3) \\ \sin(\sigma) & \sin(\sigma + 2\pi/3) & \sin(\sigma + 2\pi/3) \\ 1/2 & 1/2 & 1/2 \end{bmatrix} \tag{3.56}$$

By substituting Equation (3.55) and (3.56) into Equation (3.51), the matrix form of the induction machine represented by the DQO-dqo frame of reference can be written as:

$$\begin{bmatrix} V_{DQ0} \\ \underline{V_{dq0}} \end{bmatrix} = \begin{bmatrix} \underline{M_{sst}} \bullet \underline{R_{ss}} \bullet \underline{M_{sst}^{-1}} & 0 \\ 0 & \underline{M_{rst}} \bullet \underline{R_{rr}} \bullet \underline{M_{rst}^{-1}} \end{bmatrix} \begin{bmatrix} I_{DQ0} \\ I_{dq0} \end{bmatrix} +$$

$$\frac{d}{dt}\left\{ \begin{bmatrix} \underline{M_{sst}} \bullet \underline{L_{ss}} \bullet \underline{M_{sst}^{-1}} & \underline{M_{sst}} \bullet \underline{L_{rs}} \bullet \underline{M_{rst}^{-1}} \\ \underline{M_{rst}} \bullet \underline{L_{rs}^{t}} \bullet \underline{M_{sst}^{-1}} & \underline{M_{rst}} \bullet \underline{L_{ee}} \bullet \underline{M_{rst}^{-1}} \end{bmatrix} \begin{bmatrix} I_{DQ0} \\ I_{dq0} \end{bmatrix} \right\} - \begin{bmatrix} \dot{\underline{M}}_{sst} \bullet \underline{L_{ss}} \bullet \underline{M_{sst}^{-1}} & \dot{\underline{M}}_{sst} \bullet \underline{L_{rs}} \bullet \underline{M_{rst}^{-1}} \\ \dot{\underline{M}}_{rst} \bullet \underline{L_{rs}^{t}} \bullet \underline{M_{sst}^{-1}} & \dot{\underline{M}}_{rst} \bullet \underline{L_{rr}} \bullet \underline{M_{rst}^{-1}} \end{bmatrix} \begin{bmatrix} I_{DQ0} \\ I_{dq0} \end{bmatrix}$$

(3.57)

The expression of the dynamic model of the induction machine in the DQO-dq0 frame of reference stationary on the stator can therefore be written as the equation presented in Appendix C.

3.6 Induction Machine Representation in DQ0-dq0 Synchronously Rotating Frame of Reference

Rather than keeping the direct-axis stationary on the rotor or stator, the direct-axis in the induction machine represented in the synchronously rotating frame of reference rotates at the synchronous speed. Expression of the dynamic model of the induction machine in the synchronously rotating frame of reference makes the time-dependent variables such as rotor

currents and voltages, stator current voltages, constant. This is essential for formulation and implementation of the control system on a computer. This dissertation adopts this frame of reference for ease of implementation.

Consider the Figure 3.6 below that shows the transformation of ABC frame of reference to DQO-dqo synchronously rotating frame of reference.

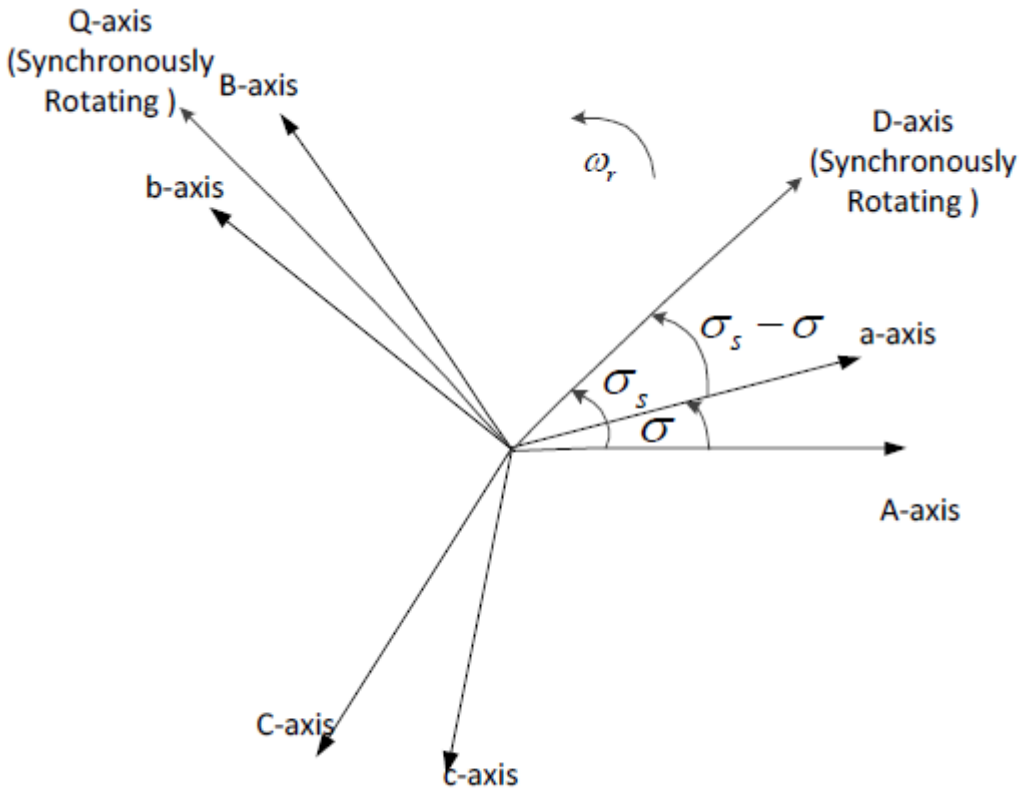

Figure 3.6: Transformation from ABC to DQO-dq0 synchronously rotating frame of reference [127]

Where, σ_s, is the angular displacement between the stator's phase A and the direct-axis rotating at synchronous speed ω_s, and is mathematically expressed as:

$$\sigma_s = \int_0^t \omega_t(t)dt + \sigma_{so} \tag{3.58}$$

By using similar approach of the DQO-dqo frames of reference fixed at the rotor and stator in the previous cases, the stator transformation matrix, $\underline{M_s}$ and rotor transformation matrix, $\underline{M_r}$, is written as:

$$\underline{M_s} = \frac{2}{3}\begin{bmatrix} \cos(\sigma_s) & \cos(\sigma_s - {}^{2\pi}/_{3}) & \cos(\sigma_s - {}^{4\pi}/_{3}) \\ -\sin(\sigma_s) & -\sin(\sigma_s - {}^{2\pi}/_{3}) & -\sin(\sigma_s - {}^{4\pi}/_{3}) \\ {}^{1}/_{2} & {}^{1}/_{2} & {}^{1}/_{2} \end{bmatrix} \tag{3.59}$$

$$\underline{M_r} = \frac{2}{3}\begin{bmatrix} \cos(\sigma_s - \sigma) & \cos((\sigma_s - \sigma) - {}^{2\pi}/_{3}) & \cos((\sigma_s - \sigma) - {}^{4\pi}/_{3}) \\ -\sin(\sigma_s - \sigma) & -\sin((\sigma_s - \sigma) - {}^{2\pi}/_{3}) & -\sin((\sigma_s - \sigma) - {}^{4\pi}/_{3}) \\ {}^{1}/_{2} & {}^{1}/_{2} & {}^{1}/_{2} \end{bmatrix} \tag{3.60}$$

The dynamic model of the induction machine in the DQO-dqo synchronously rotating frame of reference is deduced as the equation presented in Appendix D.

The torque developed from synchronously rotating frame of reference is deduced from the input wind power, P_i which can be derived as follows [125]:

$$P_i = \underline{I}_{ABC}^{t} \cdot \underline{V}_{ABC} + \underline{I}_{abc}^{t} \cdot \underline{V}_{abc} \tag{3.61}$$

Similarly, the mechanical power, P_m is given as:

$$P_m = P_i - \underline{I}_{ABC}^{t} \cdot \underline{R}_{ss} \cdot \underline{I}_{ABC} - \underline{I}_{abc}^{t} \cdot \underline{R}_{rr} \cdot \underline{I}_{abc} \tag{3.62}$$

From Equations (3.42) and (3.43), P_m can be written as:

$$P_m = \underline{I}_{ABC}^{t} \cdot \left(\frac{d}{dt}\underline{\varphi}_{ABC}\right) + \underline{I}_{abc}^{t} \cdot \left(\frac{d}{dt}\underline{\varphi}_{abc}\right) \tag{3.63}$$

To express the mechanical power in the DQO-dqo arbitrary frame of reference, substitute Equation (3.45) to Equation (3.50) into Equation (3.63), given as:

$$P_m = \left(\underline{M}_s^{-1} \cdot \underline{I}_{DQO}\right)^{t} \cdot \left[\frac{d}{dt}\left(\underline{M}_s^{-1} \cdot \underline{\varphi}_{DQO}\right)\right] + \left(\underline{M}_r^{-1} \cdot \underline{I}_{dqo}\right)^{t} \cdot \left[\frac{d}{dt}\left(\underline{M}_r^{-1} \cdot \frac{d}{dt}\underline{\varphi}_{dqo}\right)\right] \tag{3.64}$$

$$P_m = \underline{I}_{DQO}^{t} \cdot \left(\underline{M}_s^{-1}\right)^{t} \cdot \left(\underline{M}_s^{-1} \cdot \frac{d}{dt}\underline{\varphi}_{DQO} - \underline{M}_s^{-1} \cdot \dot{\underline{M}}_s \cdot \underline{M}_s^{-1} \cdot \underline{\varphi}_{DQO}\right)$$

$$+\underline{I}_{dqo}^{t} \cdot \left(\underline{M}_r^{-1}\right)^{t} \cdot \left(\underline{M}_r^{-1} \cdot \frac{d}{dt}\underline{\varphi}_{dqo} - \underline{M}_r^{-1} \cdot \dot{\underline{M}}_r \cdot \underline{M}_r^{-1} \cdot \underline{\varphi}_{dqo}\right) \tag{3.65}$$

To develop the mechanical power in the synchronously rotating frame of reference, the transformation matrices, $\underline{M_s}$ and $\underline{M_r}$ must be substituted into Equation (3.65). The inverse of, $\underline{M_s}$ and $\underline{M_r}$ is given as:

$$\underline{M_s}^{-1} = \begin{bmatrix} \cos(\sigma_s) & \sin(\sigma_s) & 1 \\ \cos(\sigma_s - {}^{2\pi}/_{3}) & -\sin(\sigma_s - {}^{2\pi}/_{3}) & 1 \\ \cos(\sigma_s - {}^{4\pi}/_{3}) & -\sin(\sigma_s - {}^{4\pi}/_{3}) & 1 \end{bmatrix} \tag{3.66}$$

$$\underline{M_r}^{-1} = \begin{bmatrix} \cos(\sigma_s - \sigma) & \sin(\sigma_s - \sigma) & 1 \\ \cos((\sigma_s - \sigma) - {}^{2\pi}/_{3}) & -\sin((\sigma_s - \sigma) - {}^{2\pi}/_{3}) & 1 \\ \cos((\sigma_s - \sigma) - {}^{4\pi}/_{3}) & -\sin((\sigma_s - \sigma) - {}^{4\pi}/_{3}) & 1 \end{bmatrix} \tag{3.67}$$

Also,

$$\left(\underline{M_r}^{-1}\right)^t \cdot \underline{M_r}^{-1} = \begin{bmatrix} {}^{3}/_{2} & 0 & 0 \\ 0 & {}^{3}/_{2} & 0 \\ 0 & 0 & 3 \end{bmatrix} = K_r \underline{C_r} \tag{3.68}$$

Where, $K_s = K_r = {}^{3}/_{2}$ and $\underline{C_s} = \underline{C_r} = \begin{bmatrix} 1 & 0 & 0 \\ 0 & 1 & 0 \\ 0 & 0 & 2 \end{bmatrix}$ (3.69)

Therefore, Equation (3.65) now becomes:

$$P_m = K_s \cdot \underline{I_{DQO}^t} \cdot \underline{C_s} \cdot \frac{d}{dt}\underline{\varphi_{DQO}} - K_s \cdot \underline{I_{DQO}^t} \cdot C_s \cdot \left(\underline{\dot{M}_s} \cdot \underline{M_s}^{-1}\right) \cdot \underline{\varphi_{DQO}}$$

$$+K_r \cdot \underline{I_{dqo}^t} \cdot \underline{C_r} \cdot \frac{d}{dt}\underline{\varphi_{dqo}} - K_r \cdot \underline{I_{dqo}^t} \cdot C_r \cdot \left(\underline{\dot{M}_r} \cdot \underline{M_r}^{-1}\right) \cdot \underline{\varphi_{dqo}} \tag{3.70}$$

Equation (3.70) can be further reduced by neglecting the transformer voltage terms which becomes [125]:

$$P_m = -K_s \cdot \underline{I_{DQO}^t} \cdot C_s \cdot \left(\underline{\dot{M}_s} \cdot \underline{M_s}^{-1}\right) \cdot \underline{\varphi_{DQO}} - K_r \cdot \underline{I_{dqo}^t} \cdot C_r \cdot \left(\underline{\dot{M}_r} \cdot \underline{M_r}^{-1}\right) \cdot \underline{\varphi_{dqo}} \tag{3.71}$$

Where,

$$\underline{\dot{M}_s} = \frac{2}{3}\omega_s \begin{bmatrix} -\sin(\sigma_s) & -\sin(\sigma_s - {}^{2\pi}/_{3}) & -\sin(\sigma_s - {}^{4\pi}/_{3}) \\ -\cos(\sigma_s) & -\cos(\sigma_s - {}^{2\pi}/_{3}) & -\cos(\sigma_s - {}^{4\pi}/_{3}) \\ 0 & 0 & 0 \end{bmatrix} \tag{3.72}$$

$$\dot{\underline{M}}_r = \frac{2}{3}(\omega_s - \omega_s)\begin{bmatrix} -\sin(\sigma_s - \sigma) & -\sin((\sigma_s - \sigma) - 2\pi/3) & -\sin((\sigma_s - \sigma) - 4\pi/3) \\ -\cos(\sigma_s - \sigma) & -\cos((\sigma_s - \sigma) - 2\pi/3) & -\cos((\sigma_s - \sigma) - 4\pi/3) \\ 0 & 0 & 0 \end{bmatrix} \tag{3.73}$$

The electromechanical torque can therefore be expressed as:

$$T_{em} = \frac{P_m}{\Omega_m} = -\frac{K_s}{\Omega_m} \cdot \underline{I}_{DQO}^t \cdot C_s \cdot \left(\dot{\underline{M}}_s \cdot \underline{M}_s^{-1}\right) \cdot \underline{\varphi}_{DQO} - \frac{K_r}{\Omega_m} \cdot \underline{I}_{dqo}^t \cdot C_r \cdot \left(\dot{\underline{M}}_r \cdot \underline{M}_r^{-1}\right) \cdot \underline{\varphi}_{dqo} \tag{3.74}$$

From Equation in Appendix A, the flux linkage of the stator and rotor can be expressed as:

$$\underline{\varphi}_{DQO} = \begin{bmatrix} \varphi_D \\ \varphi_Q \\ \varphi_O \end{bmatrix} = \begin{bmatrix} L_{ss} - L_{sm} & 0 & 0 \\ 0 & L_{ss} - L_{sm} & 0 \\ 0 & 0 & L_{ss} + 2L_{sm} \end{bmatrix} \begin{bmatrix} i_D \\ i_Q \\ i_O \end{bmatrix} + \begin{bmatrix} \frac{3}{2}L_m & 0 & 0 \\ 0 & \frac{3}{2}L_m & 0 \\ 0 & & 0 \end{bmatrix} \begin{bmatrix} i_d \\ i_q \\ i_o \end{bmatrix} \tag{3.75}$$

$$\underline{\varphi}_{dqo} = \begin{bmatrix} \varphi_d \\ \varphi_q \\ \varphi_o \end{bmatrix} = \begin{bmatrix} \frac{3}{2}L_m & 0 & 0 \\ 0 & \frac{3}{2}L_m & 0 \\ 0 & & 0 \end{bmatrix} \begin{bmatrix} i_D \\ i_Q \\ i_O \end{bmatrix} + \begin{bmatrix} L_{rr} - L_{sm} & 0 & 0 \\ 0 & L_{rr} - L_{sm} & 0 \\ 0 & 0 & L_{rr} + 2L_{sm} \end{bmatrix} \begin{bmatrix} i_d \\ i_q \\ i_o \end{bmatrix} \tag{3.76}$$

By substituting Equation (3.75) to (3.76) into Equation (3.74), it yields:

$$T_{em} = -\frac{3/2}{\Omega_m}\left[\omega_s\left(i_D\varphi_Q - i_Q\varphi_D\right) + (\omega_s - \omega_r)(i_d\varphi_q - i_q\varphi_d)\right] \tag{3.77}$$

Equation (3.82) can be factorized as:

$$T_{em} = -\frac{3/2}{\Omega_m}\left[\omega_s\left(i_D\varphi_Q - i_Q\varphi_D + i_d\varphi_q - i_q\varphi_d\right) + \omega_r(i_d\varphi_q - i_q\varphi_d)\right] \tag{3.78}$$

From Equations (3.75) and (3.76), it can be deduced that:

$$\omega_s\left(i_D\varphi_Q - i_Q\varphi_D + i_d\varphi_q - i_q\varphi_d\right) = 0 \tag{3.79}$$

Equation (3.78) therefore becomes:

$$T_{em} = \frac{3}{2}p(i_d\varphi_q - i_q\varphi_d) \tag{3.80}$$

Expressing (3.80) in terms of currents only, it yields:

$$T_{em} = \frac{3}{2}p(\frac{3}{2}L_m)(i_Q i_d - i_D i_q) \tag{3.81}$$

Expressing Equation (3.80) in the form of current and flux linkage of the stator:

$$T_{em} = \frac{3}{2}p\left(i_Q\varphi_D - i_D\varphi_Q\right) \tag{3.82}$$

The active and reactive powers of a three phase induction machine at the stator terminals can be derived as:

$$P_s = \frac{3}{2}Re\left(\vec{V}\cdot\vec{I}^*\right) = \frac{3}{2}Re(v_D + jv_Q)\cdot(i_D - ji_Q) \tag{3.83}$$

$$= \frac{3}{2}Re\left[\left(v_D i_D + v_Q i_Q\right) + j\left(v_Q i_D - v_D i_Q\right)\right] = \frac{3}{2}\left(v_D i_D + v_Q i_Q\right) \tag{3.84}$$

$$Q_s = \frac{3}{2}Im\left(\vec{V}\cdot\vec{I}^*\right) = \frac{3}{2}Re(v_D + jv_Q)\cdot(i_D - ji_Q) \tag{3.85}$$

$$= \frac{3}{2}Im\left[\left(v_D i_D + v_Q i_Q\right) + j\left(v_Q i_D - v_D i_Q\right)\right] = \frac{3}{2}\left(v_Q i_D - v_D i_Q\right) \tag{3.86}$$

3.7 Reduced Order Model of the Induction Machine in the DQO-dqo Synchronously Rotating Frame of Reference

Due to the symmetry of the stator windings and rotor windings, the zero-sequence components in the DQO-dqo synchronously rotating frame of reference can be neglected and the equation in Appendix D can be easily expanded and written as:

$$v_D = r_s\cdot i_D + (L_{ss} - L_{sm})\cdot i_D + \frac{3}{2}L_m\cdot i_d - \omega_s\cdot(L_{ss} - L_{sm})\cdot i_Q - \frac{3}{2}\omega_s\cdot L_m\cdot i_q \tag{3.87}$$

$$v_Q = r_s \cdot i_Q + (L_{ss} - L_{sm}) \cdot i_Q + \frac{3}{2} L_m \cdot i_q + \omega_s \cdot (L_{ss} - L_{sm}) \cdot i_D + \frac{3}{2} \omega_s \cdot L_m \cdot i_d \quad (3.88)$$

$$v_d = r_r \cdot i_d + \frac{3}{3} L_m \cdot i_D + (L_{rr} - L_{rm}) \cdot i_d - \frac{3}{2} (\omega_s - \omega_r) L_m \cdot i_Q - (\omega_s - \omega_r)(L_{rr} - L_{rm}) \cdot i_q \quad (3.89)$$

$$v_q = r_r \cdot i_q + \frac{3}{3} L_m \cdot i_Q + (L_{rr} - L_{rm}) \cdot i_q + \frac{3}{2} (\omega_s - \omega_r) L_m \cdot i_D + (\omega_s - \omega_r)(L_{rr} - L_{rm}) \cdot i_d \quad (3.90)$$

Reducing the expression of the inductances in Equations (3.87) to (3.90) as:

$$L_S = L_{ss} - L_{sm} \quad (3.91)$$

$$L_R = L_{rr} - L_{rm} \quad (3.92)$$

$$L_M = \frac{3}{2} L_m \quad (3.93)$$

Where, L_S, L_R and L_M are the leakage inductance in stator, leakage inductance in rotor and magnetizing inductance respectively. Equations (3.87) to (3.90) can be rewritten as:

$$v_D = r_s \cdot i_D + L_S \cdot i_D + L_M \cdot i_d - \omega_s \cdot L_S \cdot i_Q - \omega_s \cdot L_M \cdot i_q \quad (3.94)$$

$$v_Q = r_s \cdot i_Q + L_S \cdot i_Q + L_M \cdot i_q + \omega_s \cdot L_S \cdot i_D + \omega_s \cdot L_M \cdot i_d \quad (3.95)$$

$$v_d = r_r \cdot i_d + L_M \cdot i_D + L_R \cdot i_d - (\omega_s - \omega_r) L_M \cdot i_Q - (\omega_s - \omega_r) L_R \cdot i_q \quad (3.96)$$

$$v_q = r_r \cdot i_q + L_M \cdot i_Q + L_R \cdot i_q + (\omega_s - \omega_r) L_M \cdot i_D + (\omega_s - \omega_r) L_R \cdot i_d \quad (3.97)$$

Neglecting the voltage drops across the stator and rotor resistances because they are small, the others terms on the right hand side (RHS) of Equations (3.94) to (3.97) can be termed as flux linkages and its derivative. Therefore, the flux linkage equations can be deduced as:

$$\varphi_D = L_S i_D + L_M i_d \quad (3.98)$$

$$\varphi_Q = L_S i_Q + L_M i_q \quad (3.99)$$

$$\varphi_d = L_R i_d + L_M i_D \quad (3.100)$$

$$\varphi_q = L_R i_q + L_M i_Q \quad (3.101)$$

To differentiate the reduced model and the DQO-dqo model, a new subscript is adopted for the reduced model. The subscripts, ds and dr represent the stator and rotor direct axis components respectively, while qs and qr are the stator and rotor quadrature axes components respectively. Using the currents as an example to show the relationship, it follow as:

$$i_D \equiv i_{ds}, i_Q \equiv i_{qs}, i_d \equiv i_{dr}, i_q \equiv i_{qr} \quad (3.102)$$

This relationship also exists for the voltages and flux linkages. Using the reduced model subscripts and substituting Equations (3.98) to (3.101) into Equations (3.94) to (3.97), the dynamic model of the induction machine can be deduced as:

$$v_{ds} = r_s i_{ds} + \frac{d\varphi_{ds}}{dt} - \omega_s \varphi_{qs} \quad (3.103)$$

$$v_{qs} = r_s i_{qs} + \frac{d\varphi_{qs}}{dt} - \omega_s \varphi_{ds} \quad (3.104)$$

$$v_{dr} = r_r i_{dr} + \frac{d\varphi_{dr}}{dt} - (\omega_s - \omega_r)\varphi_{qr} \quad (3.105)$$

$$v_{qr} = r_r i_{qr} + \frac{d\varphi_{dr}}{dt} - (\omega_s - \omega_r)\varphi_{dr} \quad (3.106)$$

The expressions for flux linkages can also be written as:

$$\varphi_{ds} = L_S i_{ds} + L_M i_{dr} \quad (3.107)$$

$$\varphi_{qs} = L_S i_{qs} + L_M i_{qr} \quad (3.108)$$

$$\varphi_{dr} = L_R i_{dr} + L_M i_{ds} \quad (3.109)$$

$$\varphi_{qr} = L_R i_{qr} + L_M i_{qs} \quad (3.110)$$

The Equations (3.103) to (3.106) make up the full order model of the DFIG that is generally used in WECS studies and it requires complex computations and longer simulation time in transient stability studies of power systems. The reduced order model steady state model of the DFIG can be easily obtained by neglecting the rotor and stator transients, i.e., making the rotor and stator derivative terms equal to zero. Therefore, the steady state equation of the DFIG model which can be easily solved and simulated can be written as:

$$v_{ds} = r_s i_{ds} - \omega_s \varphi_{qs} \tag{3.111}$$

$$v_{qs} = r_s i_{qs} - \omega_s \varphi_{ds} \tag{3.112}$$

$$v_{dr} = r_r i_{dr} - (\omega_s - \omega_r)\varphi_{qr} \tag{3.113}$$

$$v_{qr} = r_r i_{qr} - (\omega_s - \omega_r)\varphi_{dr} \tag{3.114}$$

The reduced order model does not affect the results of short-term transient stability studies presented in this work because the operation of the DFIG is uninterrupted throughout the simulation time. Another observation from the reduced model is the cross-coupling of the d, q axes between the stator voltages and stator currents. The d-axis stator voltage is influenced by the q-axis stator flux (directly affected by the q-axis stator current) while the q-axis stator voltage is influenced by the d-axis stator flux (directly affected by the d-axis stator current).

The torque, active and reactive power of the stator can be rewritten with the new subscripts as:

$$T_{em} = \frac{3}{2} p\left[\varphi_{ds} i_{qs} - \varphi_{qs} i_{ds}\right] \tag{3.115}$$

$$P_s = \frac{3}{2}\left(v_{ds} i_{ds} + v_{qs} i_{qs}\right) \tag{3.116}$$

$$Q_s = \frac{3}{2}\left(v_{qs} i_{ds} + v_{ds} i_{qs}\right) \tag{3.117}$$

Finally, the swing equation of the induction machine using a single mass model representation is given as:

$$\frac{d\Omega_m}{dt} = \frac{1}{2H}(\mathrm{T}_m - T_{em}) \quad (3.118)$$

Where, H is the inertia constant of the machine and T_m is the mechanical torque.

The decoupling of active and reactive power from the grid is achieved by vector control scheme.

3.8 Vector Control Scheme

Using Stator-flux orientation, i.e. aligning the dq reference with stator flux [129],

$$\varphi_{qs} = 0 \quad (3.119)$$

$$0 = -L_S i_{qs} - L_M i_{qr} \quad (3.120)$$

$$i_{ds} = \frac{-1}{L_S}(\varphi_{ds} + L_M i_{dr}) \quad (3.121)$$

$$i_{qs} = \frac{-L_M}{L_S} i_{qr} \quad (3.122)$$

When aligning the d-axis with the stator flux, voltage aligns with the quadrature reference (v_{ds}=0), therefore:

$$P_S = \frac{3}{2} v_{qs} i_{qs} \quad (3.123)$$

$$P_s = \frac{3}{2} v_{qs} \left\{\frac{-L_m}{L_s}\right\} i_{qr} \quad (3.124)$$

$$T_{em} = P_S \omega_s \quad (3.125)$$

$$= v_{qs} i_{qs} \omega_s$$

$$T_e = \frac{3}{2} v_{qs} \left\{\frac{-L_M}{L_S} \omega_s\right\} i_{qr} \quad (3.126)$$

$$Q_s = \frac{3}{2} v_{qs} i_{ds} \quad (3.127)$$

$$Q_s = -\frac{3}{2} \frac{v_{qs}}{L_S} \{\varphi_{ds} + L_M i_{dr}\} \quad (3.128)$$

From Equations (3.124) and (3.128), it is observed that the active power P_s and reactive power Q_s are decoupled by the rotor currents i_{qr} and i_{dr} respectively.

3.9 Model of Three Phase Back-to-Back Converter

The objective of the back-to-back converter –PWM voltage source converter in a DFIG-based WECS is to achieve bi-directional operation of the system, that is, operation in the sub-synchronous and super-synchronous mode. The back-to-back converters is made up of the rotor-side converter (RSC) and grid-side converter (GSC) with a DC-link capacitor between them. The objective of the RSC is to decouple the active and reactive power to permit independent control of both and the objective of the GSC is to keep the voltage of the DC-link capacitor constant irrespective of the magnitude and direction of the power in the rotor. To achieve these objectives, the study of the model of the converter is necessary. This section provides the model of a three phase PWM voltage source converter in the ABC and DQO-dqo synchronously rotating frames of reference. The GSC model is considered which is also applicable to the static synchronous compensator (STATCOM) model.

3.9.1 Model of Three Phase PWM Voltage Source Converter in ABC Frame of Reference

The three phase PWM voltage source converter consists of six insulated-gate bipolar transistors with antiparallel, a DC capacitor, three AC inductors and resistors, and a load resistor as shown in Figure 3.7.

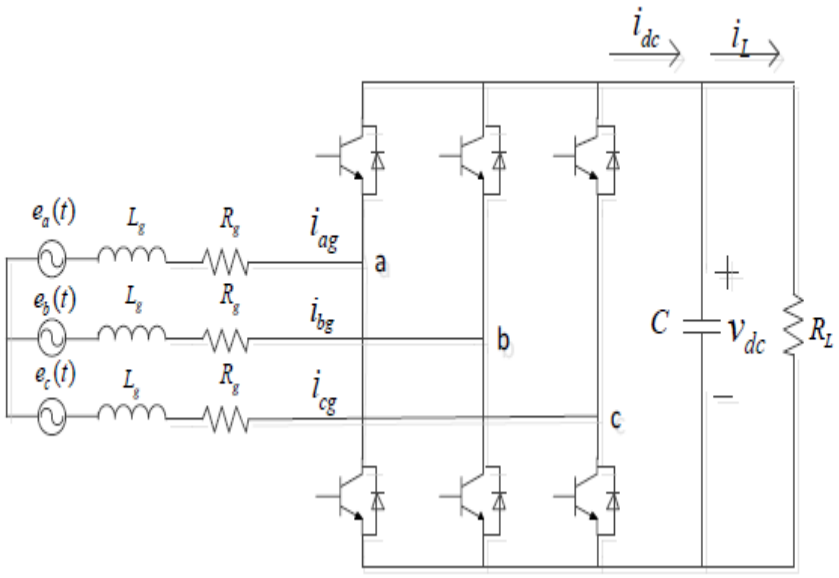

Figure 3.7: Three phase PWM voltage source converter [125]

From Figure 3.7, $e_a(t), e_b(t)\ and\ e_c(t)$, represents the three phase voltage sources from the grid, $R_g\ and\ L_g$ are the AC resistance and inductance respectively, C is the DC-link capacitor, v_{dc} is the DC-link voltage, R_L is the load resistance, $i_{ag}, i_{bg}, i_{cg}, i_{dc}\ and\ i_L$ are the input currents from the source, DC-link current and load current respectively.

Using Kirchhoff's law to analyze Figure 3.7, we obtain the following expressions:

$$\begin{cases} L_g \dfrac{di_{ag}}{dt} = e_a - R_g i_{ag} - v_{(a,0)} \\ L_g \dfrac{di_{bg}}{dt} = e_b - R_g i_{bg} - v_{(b,0)} \\ L_g \dfrac{di_{cg}}{dt} = e_c - R_g i_{cg} - v_{(c,0)} \end{cases} \qquad (3.129)$$

Where, $v_{(a,0)}$, $v_{(b,0)}$ and $v_{(c,0)}$ represent the AC voltages from the phase to the neutral point of the converter , and can be expressed as:

$$\begin{cases} v_{(a,0)} = v_{(a,N)} + v_{(N,0)} \\ v_{(b,0)} = v_{(b,N)} + v_{(N,0)} \\ v_{(c,0)} = v_{(c,N)} + v_{(N,0)} \end{cases} \qquad (3.130)$$

Where, $v_{(N,0)}$ is the voltage from neutral point N to point 0, $v_{(a,N)}$, $v_{(b,N)}$ and $v_{(c,N)}$ are the voltages from the converter to neutral point N.

Taking phase a, as reference, when the switch of the first IGBT is on and the second IGBT is off, it can be deduced that:

$$S_a = 0 \ \ and \ \ v_{(a,N)} = v_{dc} \tag{3.131}$$

Also, when the switch of the second IGBT is on and the first IGBT is off, it can be deduced that:

$$S_a = 0 \ \ and \ \ v_{(a,N)} = 0 \tag{3.132}$$

Therefore, it can be deduced that:

$$v_{(a,N)} = v_{dc} * S_a \tag{3.133}$$

The expressions for $v_{(a,N)}$, $v_{(b,N)}$, $v_{(c,N)}$ and $v_{(N,0)}$ can be written as:

$$\begin{cases} v_{(a,N)} = S_a v_{dc} \\ v_{(b,N)} = S_b v_{dc} \\ v_{(c,N)} = S_c v_{dc} \\ v_{(N,0)} = -\frac{1}{3}(S_a + S_b + S_c) v_{dc} \end{cases} \tag{3.134}$$

By substituting Equations (3.130) and (3.134) into (3.129), the following expressions can be deduced:

$$\begin{cases} L_g \dfrac{di_{ag}}{dt} = e_a - R_g i_{ag} - v_{dc}\left(S_a - \dfrac{1}{3}\sum_{k=a,b,c} S_k\right) \\ L_g \dfrac{di_{bg}}{dt} = e_b - R_g i_{bg} - v_{dc}\left(S_b - \dfrac{1}{3}\sum_{k=a,b,c} S_k\right) \\ L_g \dfrac{di_{cg}}{dt} = e_c - R_g i_{cg} - v_{dc}\left(S_c - \dfrac{1}{3}\sum_{k=a,b,c} S_k\right) \end{cases} \tag{3.135}$$

Assuming a three phase system under balanced condition, the expression between the AC and DC power is given by:

$$\sum_{k=a,b,c} i_{kg}(t) v_{kN}(t) = i_{dc}(t) v_{dc} \tag{3.136}$$

Equation (3.134) and (3.146) can be combined as:

$$i_{dc}(t) = i_{ag}(t)S_a + i_{bg}(t)S_b + i_{cg}(t)S_c \tag{3.137}$$

Also, using Kirchhoff's law at the capacitor positive node, the current expression can be written as:

$$C\frac{dv_{dc}}{dt} = S_a i_{ag} + S_b i_{bg} + S_c i_{cg} - \frac{v_{dc}}{R_L} \tag{3.138}$$

Rewriting the Equations (3.135) and Equation (3.138), the model of the PWM voltage source converter in the ABC frame of reference is given by:

$$\begin{cases} C\dfrac{dv_{dc}}{dt} = \displaystyle\sum_{k=a,b,c} S_k i_{kg} - i_L \\ L_g\dfrac{di_{ag}}{dt} + R_g i_{kg} = e_k - v_{dc}\left(S_k - \dfrac{1}{3}\displaystyle\sum_{j=a,b,c} S_j\right), k = a,b,c \\ \displaystyle\sum_{k=a,b,c} e_k = \sum_{k=a,b,c} i_{kg} = 0 \end{cases} \tag{3.139}$$

3.9.2 Model of Three Phase PWM Voltage Source Converter in the DQO-dqo Synchronously Rotating Frame of Reference

Using the transformation matrix in Equation (3.60), which represents the transformation of the DFIG model to DQO-dqo synchronously rotating frame of reference, the transformation matrix for the PWM converter can be deduced as:

$$M = \frac{2}{3}\begin{bmatrix} cos\theta & \cos(\theta - {}^{2\pi}/_{3}) & \cos(\theta - {}^{4\pi}/_{3}) \\ -sin\theta & -\sin(\theta - {}^{2\pi}/_{3}) & -\sin(\theta - {}^{4\pi}/_{3}) \\ {}^{1}/_{2} & {}^{1}/_{2} & {}^{1}/_{2} \end{bmatrix} \tag{3.140}$$

Where, θ is the angular displacement between the arbitrary frame of reference and synchronous frame of reference, which can be expressed as:

$$\theta = \omega_{gs}t + \theta_0 \tag{3.141}$$

Where, ω_{gs} is the synchronous speed of the AC voltage.

Applying Equation (3.140) to Equation (3.139) and neglecting the zero-sequence component, the model of the PWM voltage source converter in the DQ synchronously rotating frame of reference can be written as:

$$\begin{cases} C\dfrac{dv_{dc}}{dt} = \dfrac{3}{2}\left(i_{dg}s_d + i_{qg}s_q\right) - i_L \\ L_g\dfrac{di_{dg}}{dt} - \omega_{gs}L_g i_{qg} + R_g i_{dg} = e_d - v_d \\ L_g\dfrac{di_{qg}}{dt} - \omega_{gs}L_g i_{dg} + R_g i_{qg} = e_q - v_q \end{cases} \tag{3.142}$$

3.10 Operation of STATCOM

STATCOM is a shunt-connected FACTS device that is capable of injecting and absorbing reactive power in a power system. It consists of DC capacitor connected in parallel with a VSC and a transformer as shown in Figure 3.8 below.

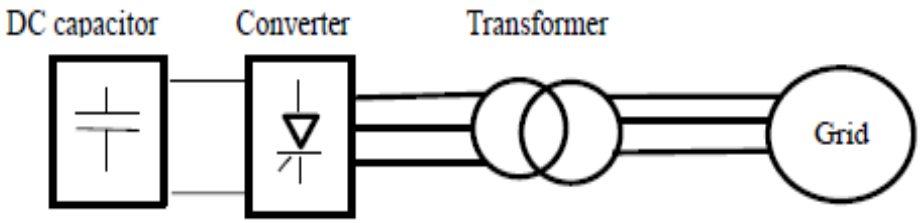

Figure 3.8: Configuration of STATCOM [130]

The operation of STATCOM within a power system can be described as the case of alternating current sources connected through a series reactance as shown in Figure 3.9. If the resistance of the transformer is negligible and the voltage of the converter is controlled such that the power angle is zero, therefore no active power is produced. The reactive power Q transfer between source V1 of the VSC and source V2 of the power system is determined by the voltage magnitude difference between V1 and V2.

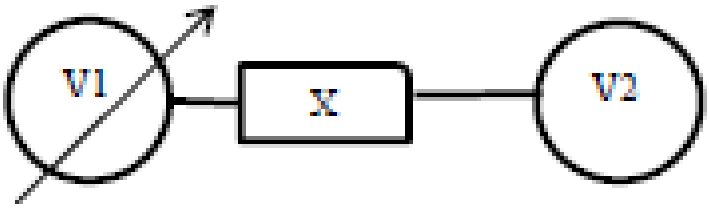

Figure 3.9: Simplified configuration of STATCOM [130]

For the low voltage ride through event considered in this work, the voltage of the VSC is greater than voltage of the power system (voltage at the point of common coupling during fault), therefore STATCOM delivers reactive power to the system as given in Equation (3.143).

$$Q = \frac{V2(V1 - V2)}{X} \tag{3.143}$$

The PowerFactory circuit diagram and block diagram for STATCOM are shown in Figure 3.10 and 3.11 respectively.

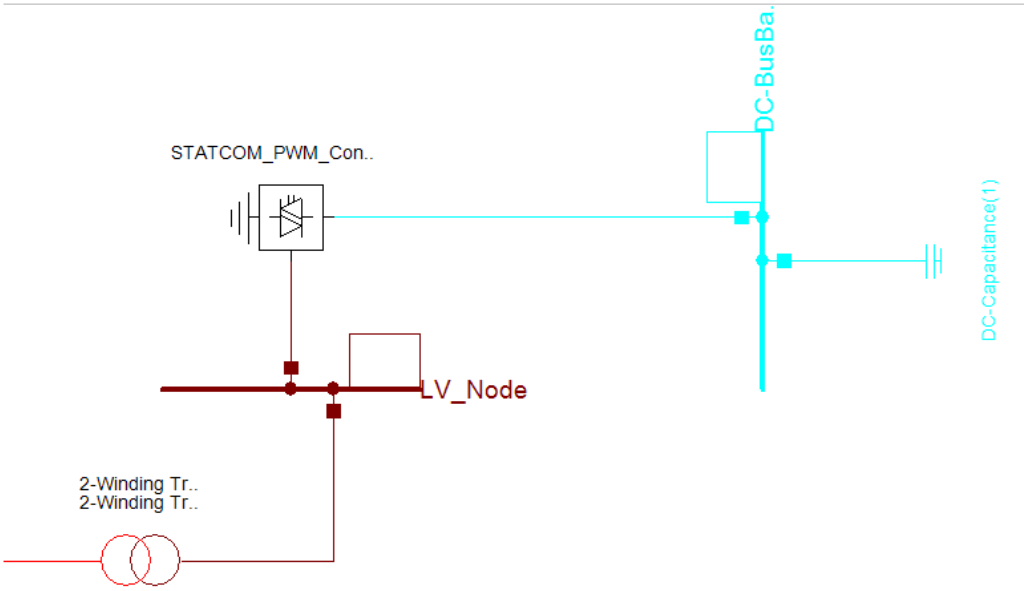

Figure 3.10: Circuit diagram of STATCOM in PowerFactory

Due to the similar circuitry of the GSC of the DFIG machine and STATCOM, the deduced model of the PWM voltage source converter in the DQ synchronously rotating frame of reference as seen Equation 3.142 is used to develop the control scheme for the STATCOM controller. The vector control scheme is used to regulate the reactive power exchange between

the STATCOM and PCC for voltage regulation. The schematic block diagram of the DSL implementation of the STATCOM controller in PowerFactory is given in Appendix E. The control strategy has two current loop controllers. The active current controller is used to adjust the d-axis reference (i_{d_ref}) current depending on the difference between the actual and reference capacitor voltages, the reactive current controller is used to regulate q-axis reference (i_{q_ref}) current according to the difference between the actual and desired PCC bus voltage. The d-axis and q-axis currents are used to generate reference voltages ($v_{d\_ref}\ and\ v_{q\_ref}$) which are then used to generate three phase reference voltages ($v_{a\_ref}, v_{b\_ref}\ and\ v_{c\_ref}$) to control the PWM converter of STATCOM.

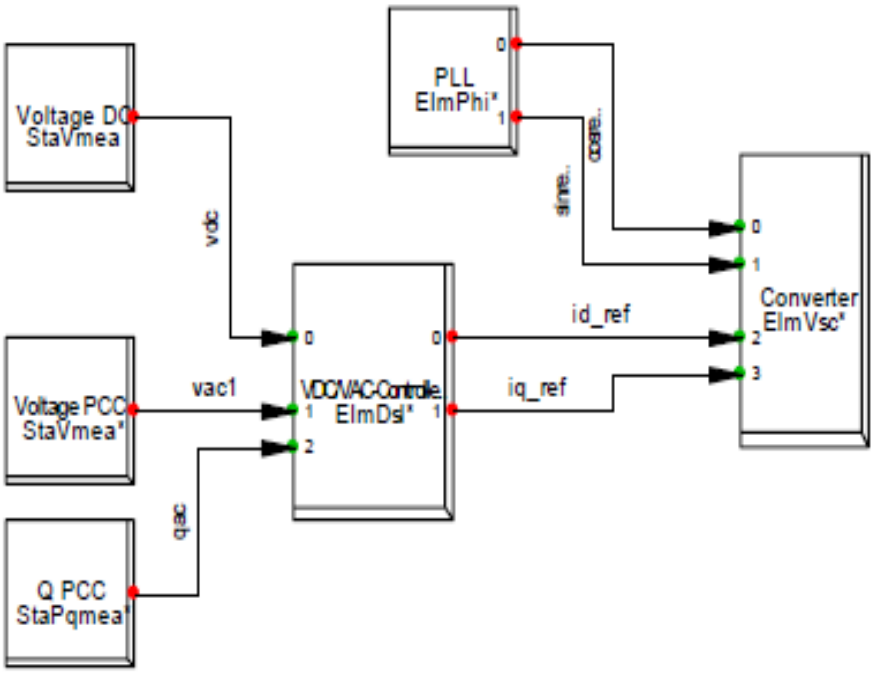

Figure 3.11: Block diagram of STATCOM Controller

CHAPTER FOUR: RESULT AND DISCUSSION

4.1 Load Flow Analysis

The objective of load flow analysis is to determine the load power utilization, active, and reactive power at each bus in an electrical power system. It is necessary in the planning and operation of power systems to analyze the steady state operation of a power system under varying conditions and to consider the effect of variations in the configuration of equipment. The essence of load flow analysis is to determine the following [131]:

- Active and reactive power generated in the network
- Active and reactive power flow in the network
- Active and reactive power consumed in the network
- Active and reactive power losses
- Voltage magnitude at each bus in the network.

To perform load flow studies, the IEEE 9 bus system which represents a simple approximation of the Western System Coordinating Council (WSCC) of an equivalent system with nine buses, three generators, six transmission lines, six transformers and three constant impedance loads is used as a base case. The PowerFactory model of the IEEE 9 bus system is shown in Figure 4.1 [132] and the data is presented in Appendix F.

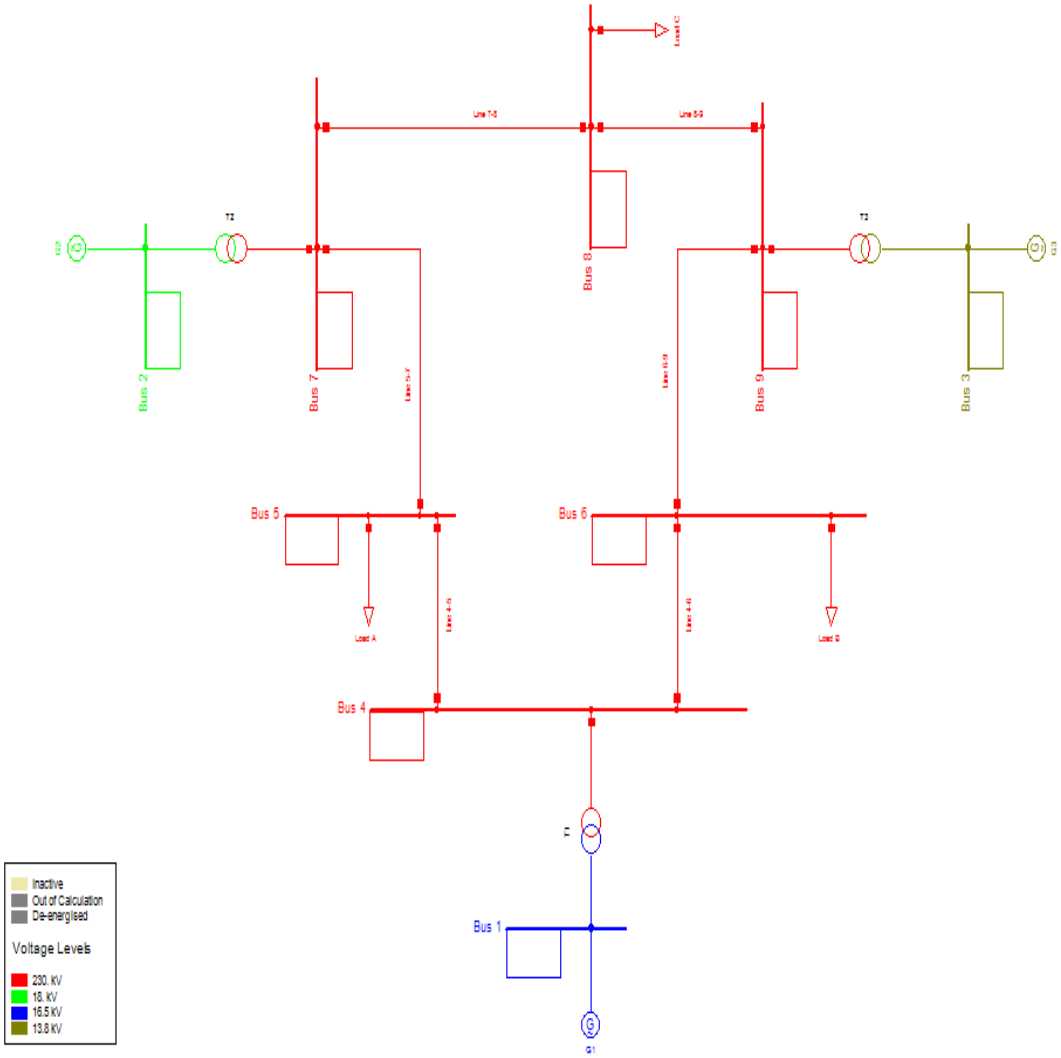

Figure 4.1: IEEE 9 bus system [132]

Two scenarios are defined for load flow studies:

- Base case scenario: IEEE 9 bus system
- With wind farm scenario: Replacement of 85 MW synchronous generator (G3) in base case with an equivalent wind farm (34 units of 2.5 MW DFIG).

The data of the DFIG wind farm is presented in Appendix G.

The two scenarios are subjected to the same operating conditions and continuous power flow analysis is performed to comparatively evaluate and investigate the impact of increased loading on voltage (reactive power) and make deductions for compensation. The minimum and maximum limit of

voltage in p.u for healthy voltage profile (voltage stability) is 0.95 p.u and 1.05 p.u respectively as specified by the research conducted in [131]. Values beyond these limits imply the non-compliance with the NRS 048 [133].

The loading conditions to be considered are λ = 1, 1.1, 1.2(100%, 110%, 120% respectively). λ is the loading factor.

At λ = 1, it is observed from Figure 4.2 that the voltage profile of both scenarios are healthy with all buses operating with the stability limit as a result of adequate supply of reactive power to the system.

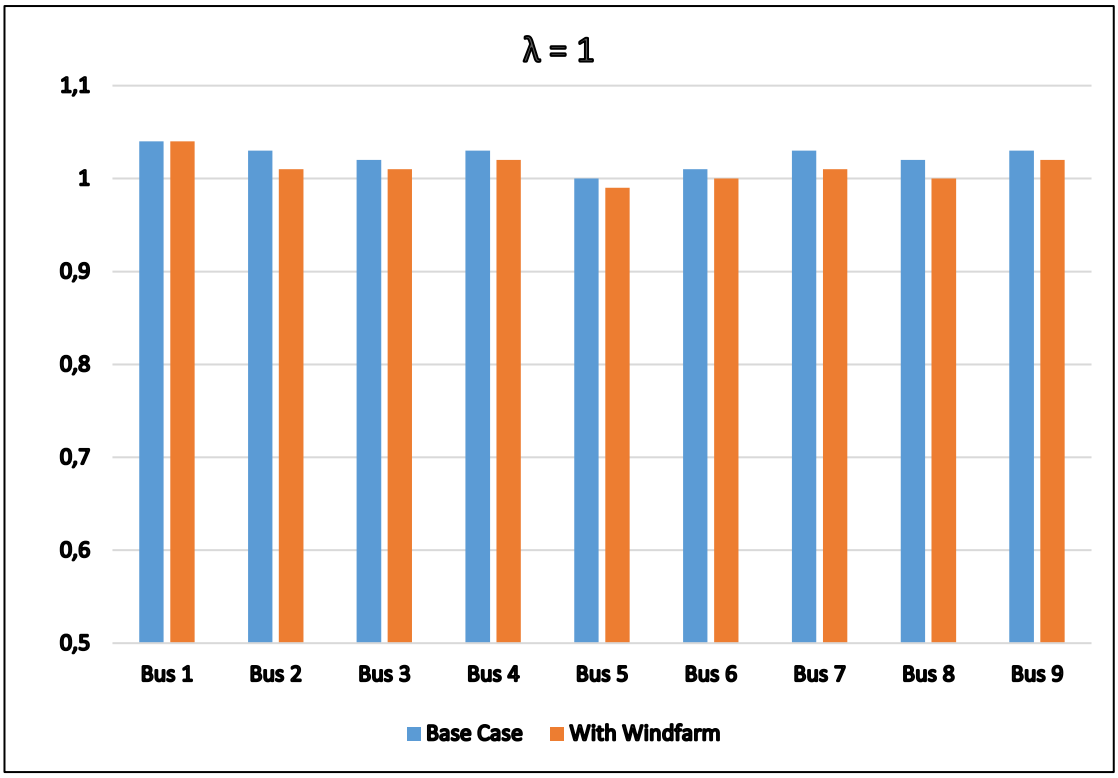

Figure 4.2: Voltage profile at 100% loading

At λ = 1.1, it is observed from Figure 4.3 that the voltage profile of the base case has reduced by a considerable amount with the voltage at bus 5 (0.95pu) reaching the minimum limit for voltage stability requirement while the voltage profile of the system with wind farm is still healthy with the minimum bus voltage at 0.97pu which is above the minimum limit for voltage stability. It is observed that reactive power injected into the system in the

base case is just sufficient to maintain voltage stability at this loading condition.

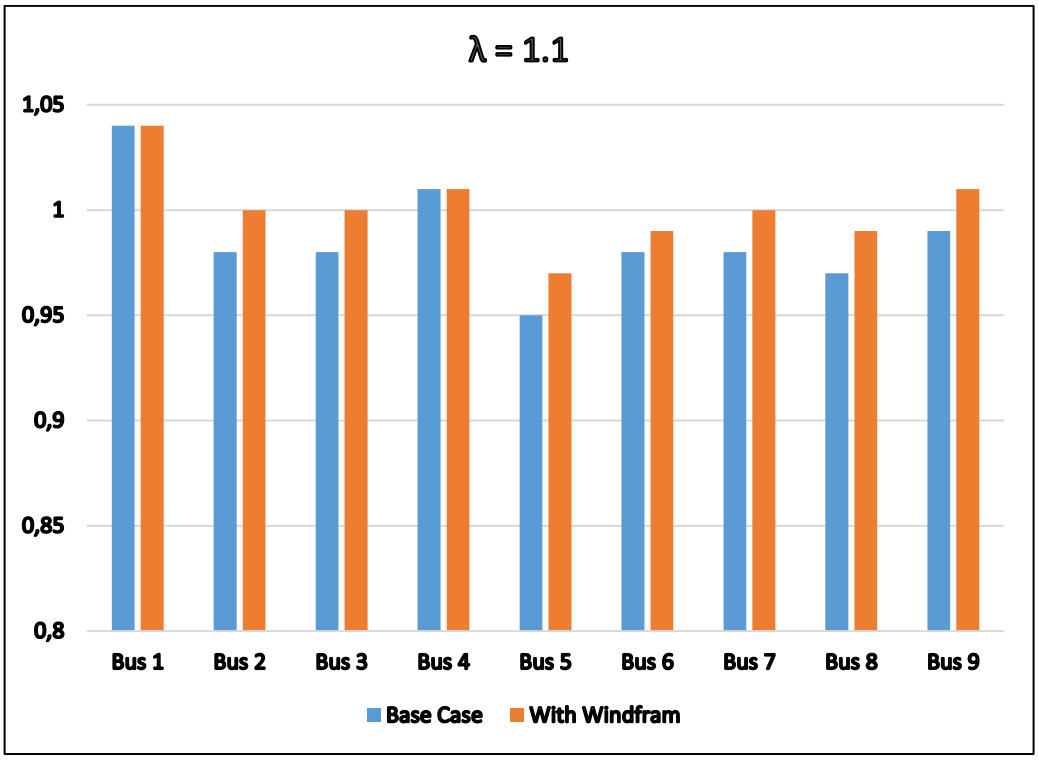

Figure 4.3: Voltage profile at 110% loading

At λ = 1.2, as presented in Figure 4.4, the base case has experienced voltage collapse at all buses excluding the swing bus (bus 1) and bus 6 therefore the overall system is said to be unstable. The system needs reactive power from an external source to compensate for the reactive power shortage and improve the voltage profile to acceptable limit of voltage stability compliance. The system with the wind farm as also shown in Figure 4.4 is still within stability limit with the minimum bus voltage of 0.96pu (bus 5) which is above the minimum limit for voltage stability. Therefore at 120% loading, the system with wind farm remains compliant while the system without wind farm (base case) is non-compliant.

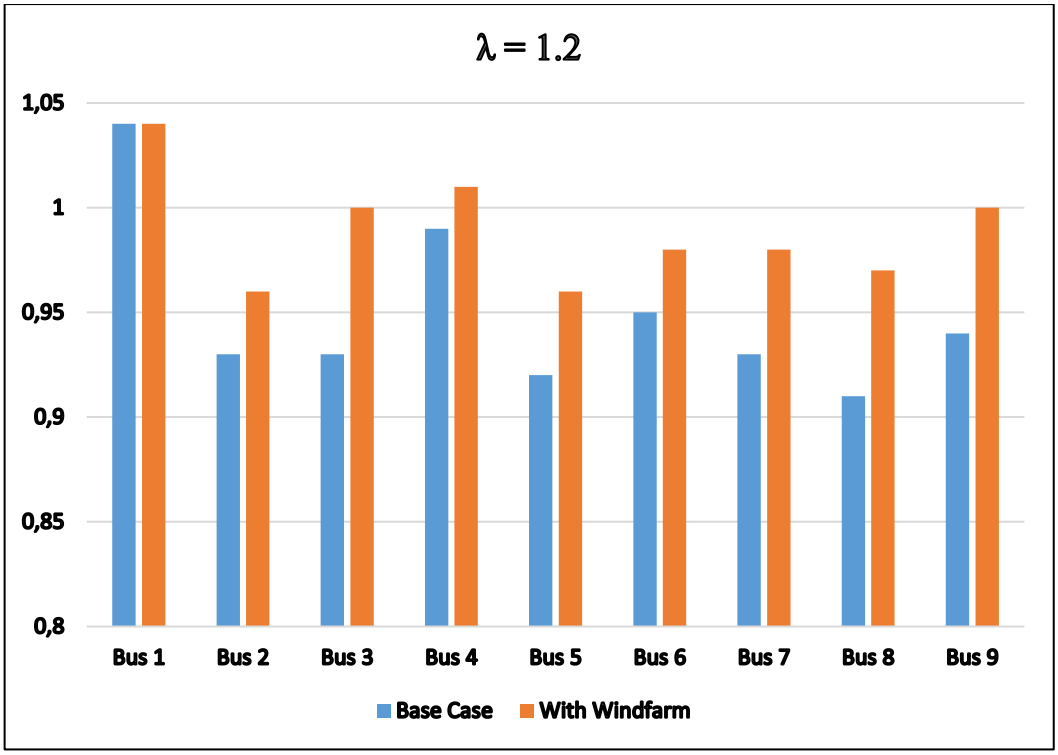

Figure 4.4: Voltage profile at 120% loading

With regards to the South Africa standard NRS 048 referenced in this work, the system with wind farm integration achieves better steady state stability with respect to voltage at maximum loading condition (120%) while the base case requires some form of reactive power compensation to achieve such stability.

4.2 Transient Stability Analysis

Transient or dynamic stability is defined as the stability of a system during and after rapid changes or imbalance such as short-circuit, loss of generator, line tripping etc. in the system.

With the justification of the impacts of wind farm in steady state analysis presented in the load flow studies above, it is also important to study the behavior of wind farms during faults, interaction with other power generation plants and their overall impact in the power system during operation. Transient stability studies is used in this work to present the effect of low voltage ride through (LVRT) in a renewable energy integrated grid.

The results presented below show the impacts of DFIG-based wind farm during a three phase faults at a location outside the PCC. The effect of voltage dip at the PCC, the effect the fault has on the operation of the DFIG, the effect of fault on the stability of other generators connected in the network and the mitigation of these effects are discussed below. STATCOM is connected to the network at the PCC (bus 9) as shown in Figure 4.5.

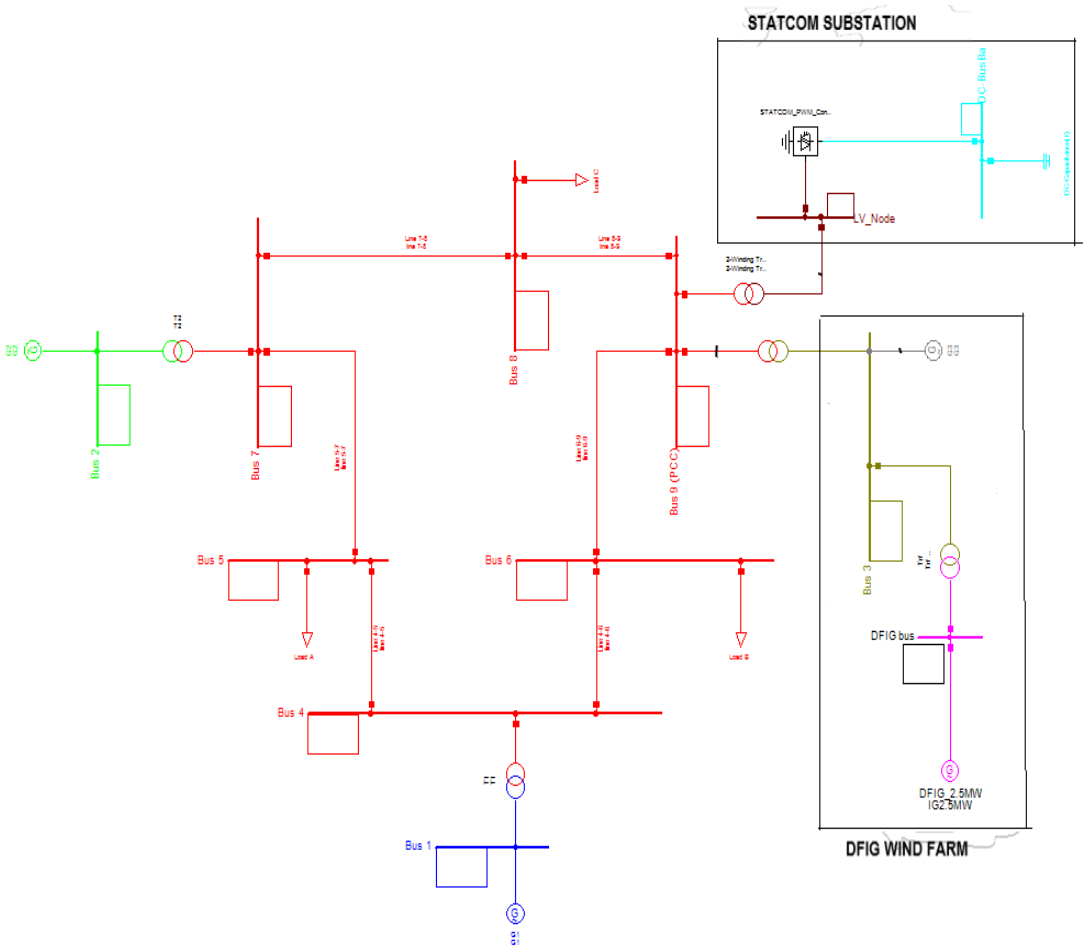

Figure 4.5: IEEE 9 bus system with wind farm and STATCOM station installed

A three phase short-circuit fault is placed at bus 5 (load A bus) at 0.3s and cleared after 100ms (0.4s). The wind farm is permitted to reduced active power production when the voltage at the PCC is below 0.85 p.u as specified in section 5.10 of the SAREGC which states that "*the supply of reactive power has first priority in area B, while the supply of active power has second priority. Active power shall be maintained during voltage drops,*

but a reduction in active power within the RPP's design specifications is required in proportion to voltage drop for voltages below 85%". Due to the increasing penetration level of wind farms, such reduction in active power is undesirable.

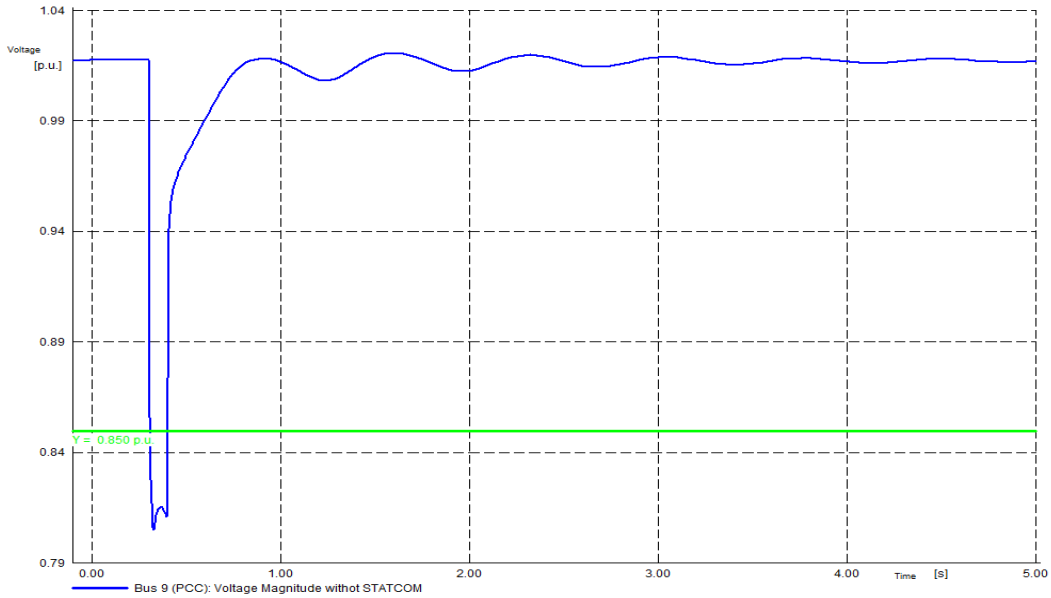

Figure 4.6: Voltage at PCC without STATCOM

During the fault, the voltage at the PCC drops to approximately 0.8pu as shown in Figure 4.6 which means that wind farm reduces active power supplied to the grid. The active power reduction can consequentially lead to active power imbalance in the grid which can cause grid instability. To maintain maximum active power production by the wind farm and maintain stability, the voltage at the PCC must be kept above 0.85pu for voltage ride through of the wind farm during faults.

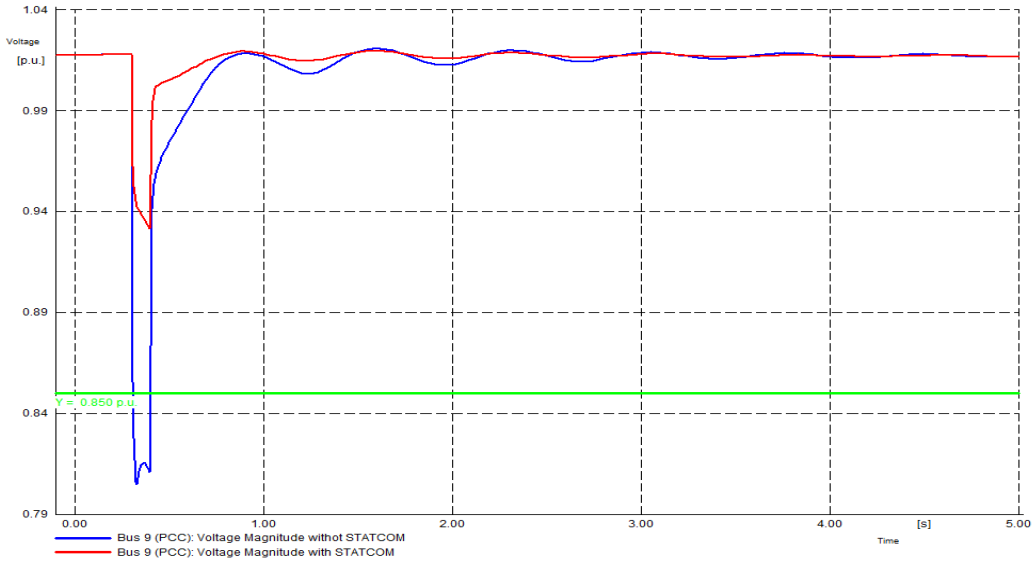

Figure 4.7: Voltage at PCC with and without STATCOM

Figure 4.7 shows the voltage at the PCC with and without the installation of STATCOM. The installation of STATCOM at the PCC keeps the voltage at the PCC above 0.85 p.u therefore allowing the wind farm to ride through the fault condition without reduction in active power as required by the SAREGC for low voltage events. Also, the connection of STATCOM at the PCC improves the settling time of the voltage allowing the system to attain steady state stability faster.

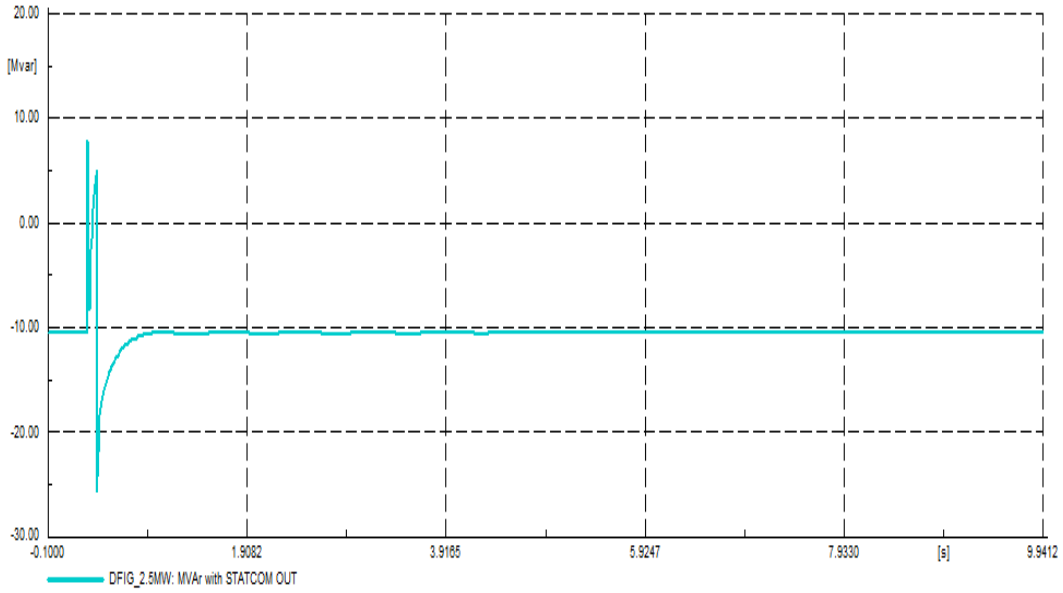

Figure 4.8: Reactive Power of DFIG without STATCOM

Reactive power absorption and injection is key in transient stability studies because it determines the voltage profile of the network. During a fault, reactive power in the DFIG increases rapidly as presented in Figure 4.8 due to increase in reactive current that occurs as a results of voltage dip experienced during the fault. After the fault is cleared, the DFIG draws more reactive power from the system to achieve stability. With the connection of STATCOM at the PCC, the reactive power of the DFIG is controlled during a fault with little reactive current injection and reaches stability twice as fast as without STATCOM as shown in Figure 4.9.

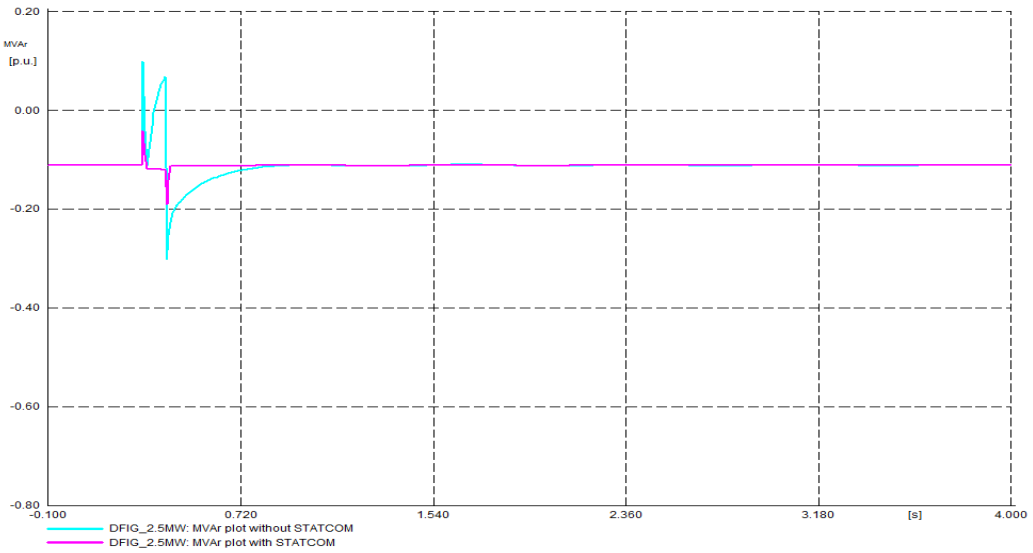

Figure 4.9: Reactive Power of DFIG with and without STATCOM

Figure 4.10 presents the response of the rotor angle of the synchronous generator (G2) when STATCOM is connected at the PCC versus when STATCOM is not connected to the PCC. When STATCOM is not connected during the fault, active power is reduced in the system and the accelerating power of the synchronous generator is increased therefore increasing the rotor angle accelerations as shown in the STATCOM out scenario. When STATCOM is connected at the PCC, the wind farm remains connected in the system as a result of the ride through capability. This consequentially reduces the rotor angle acceleration of the synchronous generator and it settling time. The transient stability of the synchronous generator is improved with the connection of the STATCOM at the PCC.

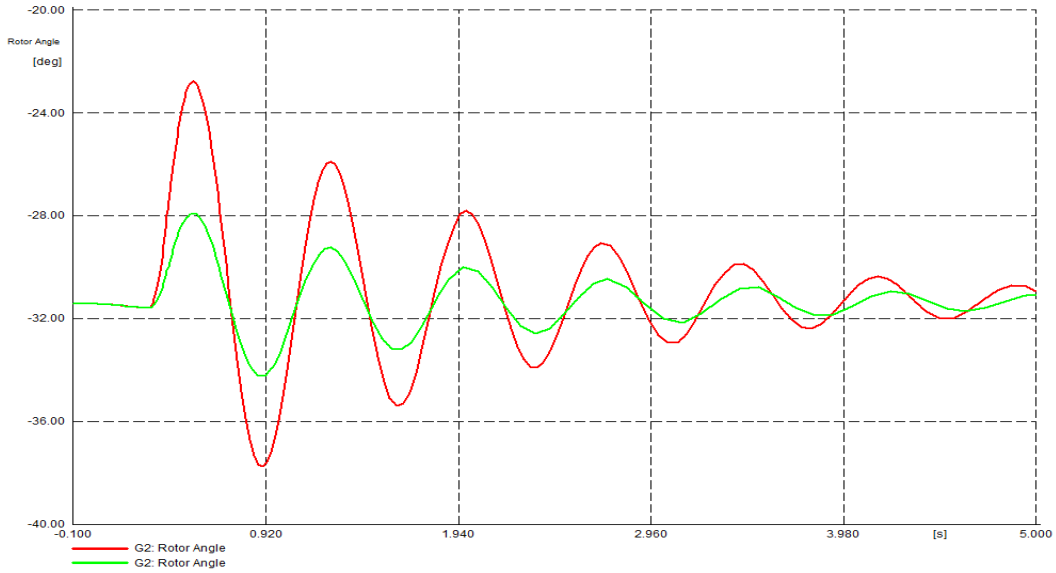

Figure 4.10: Rotor angle of synchronous generator (G2) with and without STATCOM

From Figure 4.11, it is observed that the synchronous machine has settled at different settling angle with and without the wind farm. This is because the wind farm helps in feeding the fault which reduces the active power required by the synchronous generator to feed the fault. Thus the transient stability of the synchronous machine is improved with the installation of the DFIG wind farm.

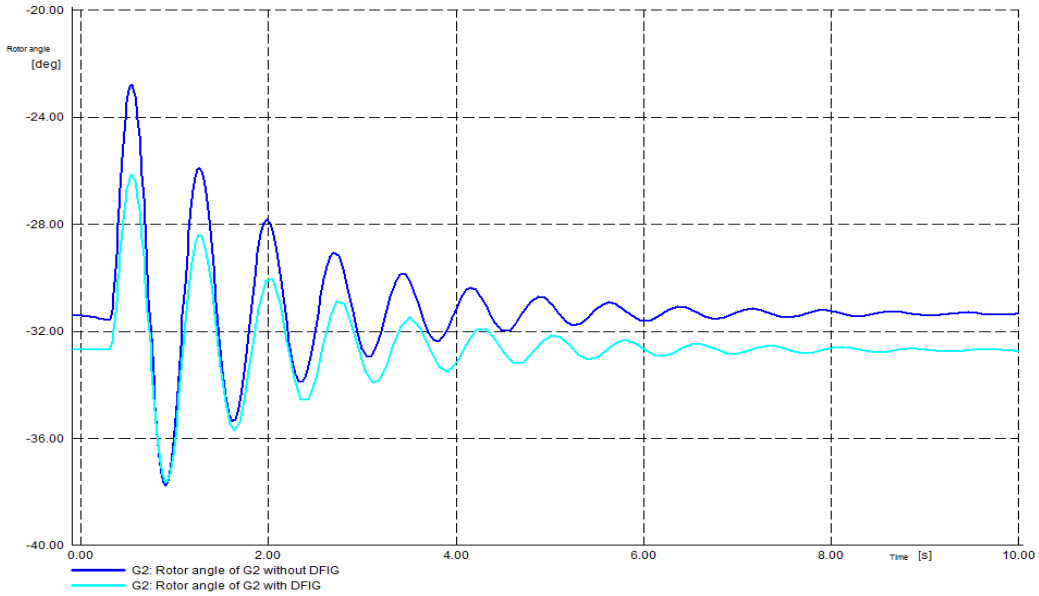

Figure 4.11: Rotor angle of synchronous generator (G2) with and without DFIG wind farm.

From the above results, the DFIG with STATCOM improves the transient stability of the network and better ride through during voltage dip. However, the performance of PMSG under same fault conditions is assessed. During the faults, the network with PMSG connected maintains ride through condition as seen in Figure 4.12. The voltage dip is above 0.85 p.u keeping the wind farm connected to the network without the installation of STATCOM. This is achieved as a result of full control of active and reactive power by the converters. The reactive current injection and stability of the PMSG during fault as shown in Figure 4.13 is similar with the DFIG network with STATCOM installed which makes the PMSG more efficient than DFIG for voltage ride through capability.

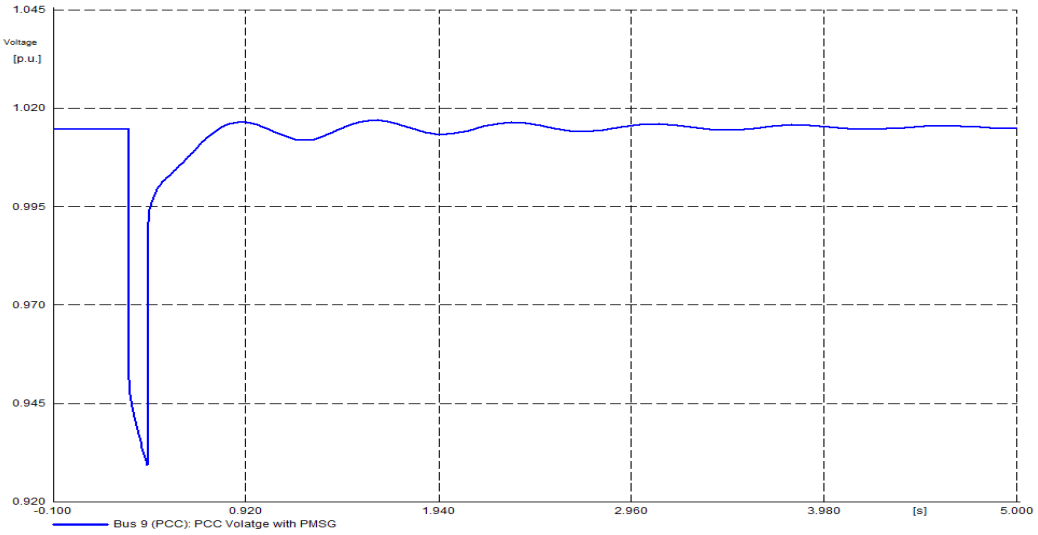

Figure 4.12: Voltage at PCC with PMSG

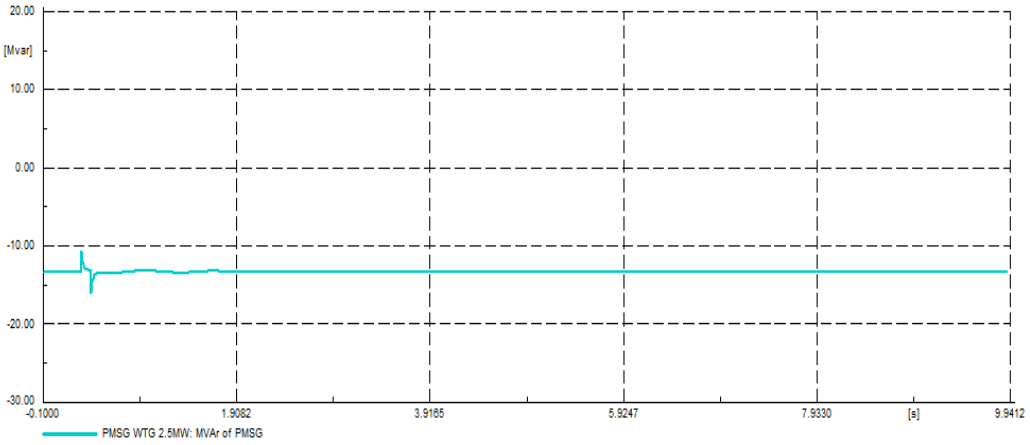

Figure 4.13: MVAr of PMSG

CHAPTER FIVE: CONCLUSION

5.1 Conclusion

The performance of a doubly fed induction generator-based wind farm was analyzed with respect to load flow studies and transient stability analysis. Also, the effect of STATCOM in the system as a device for dynamic reactive power compensation was considered in this work. The analysis on the wind farm was validated using the IEEE 9-bus system.

As a basis for this work, the IEEE 9-bus system was modelled in PowerFactory v2017. The mathematically modelling of the doubly fed induction generator in different frames of reference was presented for understanding of the configuration and working principle of the generator. The ABC frame of reference provides the characteristics of the generator in three phase and time domain which is complex in calculation and take longer simulation time. The DQO-dqo frames of reference presented is the transformation of the ABC frame of reference into two phase with the neglecting of time domain which makes calculation easier and simulation faster.

The IEEE 9 bus system is represented as the base case system in which load flow and transient stability analysis was carried out with and without wind farm. For Load flow studies, it was observed that the base case remains compliant to the NRS 048 standard up to loading of 110% while the integration of the wind farm into the base case maintains the compliance of the system to a loading of 120% because the converters in the wind farm is able to actively decouple and control the active and reactive power to provide necessary compensation within its limits during steady state operation. For instances that affect the steady state operation of the wind farm integrated system such as faults, transient stability analysis was carried out to observe the performance of the system during these conditions. A three phase fault was simulated for a period of 100ms and it was observed that the wind farm could not provide necessary reactive power needed during this transient period thereby causing the voltage at the PCC to drop below the required limit for maximum active power

production as specified by the SA grid code. To provide the needed reactive power, STATCOM is connected at the point of common coupling. The connection of STATCOM aided the ride through of the wind farm during this low voltage event by keeping the voltage at the PCC above 0.85 p.u which prevents reduction in active power transfer.

The results presented in this work validates the facts the DFIG-based wind farm assisted in the steady state characteristics of the system, improves the transient stability of the system and STATCOM improves the low voltage ride through features of the wind farm.

To provide a background for further research, an introductory study on the use of PMSG in place of DFIG was presented, it was observed that the PMSG-based wind farm provided a better LVRT requirement than the DFIG-based wind farm without STATCOM.

5.2 Recommendation

For areas with low penetration of wind power, disconnection of the wind farm during faults do not majorly affect the stability of the system and therefore can be permitted.

The research can be carried out using larger standard test systems such as the IEEE 14-bus and 39-bus systems to verify the impacts of a DFIG wind farm on large networks. The penetration level of the wind farm can also be varied to analyze its effect on the power quality of the grid.

With the increasing penetration of wind farms, the grid code is been reviewed periodically, and thereby becoming more strict of renewable power plants, it is therefore needed for wind farm operators to upgrade the compensation of the generating plant to meet the grid code requirements and for new wind farms, an introductory simulation of PMSG-based wind farm has been done in the chapter four of this work to present the advantage of PMSG over DFIG, however, research in the control of PMSG for LVRT studies is highly recommended.

REFERENCES

[1] D. o. Energy. (2015, 12 December). *Department of Energy*. Available: http://www.energy.gov.za/files/coal_frame.html

[2] A. O. Aluko and K. T. Akindeji, "Mitigation of low voltage contingency in doubly fed induction generator using static synchronous compensator in South Africa," presented at the IEEE PES-IAS, South Afrcia, 2018.

[3] "Global Wind Report," Global Wind Energy Council 2017.

[4] S. Sawyer, "Wind energy report," Global Wind Enegy Council, Brussels2017.

[5] (2017). *South Africa Wind Fact Sheet, 2016*.

[6] SAWEA, "Cost of Wind Energy," in *Wind Fact Series*, ed, 2017.

[7] A. F. Z and M. J, "A Comprehensive Overview on Reactive Power," 2006.

[8] V. Akhmatov and H. Knudsen, "An aggregate model of a grid-connected, large-scale, offshore wind farm for power stability investigations—importance of windmill mechanical system," *International Journal of Electrical Power & Energy Systems,* vol. 24, no. 9, pp. 709-717, 2002.

[9] S. Heier, *Grid integration of wind energy: onshore and offshore conversion systems*. John Wiley & Sons, 2014.

[10] V. Akhmatov, "Analysis of dynamic behaviour of electric power systems with large amount of wind power," Ph.D, Electrical power engineering, Technical University of Denmark, 2003.

[11] T. Ackermann, *Wind power in power systems*. England: John Wiley and Sons Ltd, 2005.

[12] S. Muller, M. Deicke, and R. W. De Doncker, "Doubly fed induction generator systems for wind turbines," *IEEE Industry applications magazine,* vol. 8, no. 3, pp. 26-33, 2002.

[13] J. Slootweg, S. De Haan, H. Polinder, and W. Kling, "Modeling wind turbines in power system dynamics simulations," in *Power Engineering Society Summer Meeting*, 2001, vol. 1, pp. 22-26: IEEE.

[14] J. M. Rodríguez *et al.*, "Incidence on power system dynamics of high penetration of fixed speed and doubly fed wind energy systems: study of the Spanish case," *IEEE Transactions on Power Systems,* vol. 17, no. 4, pp. 1089-1095, 2002.

[15] F. Blaabjerg, Z. Chen, and S. B. Kjaer, "Power electronics as efficient interface in dispersed power generation systems," *IEEE transactions on power electronics,* vol. 19, no. 5, pp. 1184-1194, 2004.

[16] Z. Chen and F. Blaabjerg, "Wind turbines-a cost effective power source," *Przegląd Elektrotechniczny,* vol. 80, no. 5, pp. 464-469, 2004.

[17] E. Muljadi, K. Pierce, and P. Migliore, "Control strategy for variable-speed, stall-regulated wind turbines," in *Proceedings of the American Control Conference*, 1998, vol. 3, pp. 1710-1714: IEEE.

[18] J. Yen and N. A. Ahmed, "Enhancing vertical axis wind turbine by dynamic stall control using synthetic jets," *Journal of Wind Engineering and Industrial Aerodynamics,* vol. 114, pp. 12-17, 2013.

[19] E. Muljadi and C. P. Butterfield, "Pitch-controlled variable-speed wind turbine generation," *IEEE transactions on Industry Applications,* vol. 37, no. 1, pp. 240-246, 2001.

[20] M. Smida and A. Sakly, "Pitch angle control for variable speed wind turbines," *Renewable Energy and Sustainable Development,* vol. 1, no. 1, pp. 81-88, 2015.

[21] H. Polinder, D. Bang, R. Van Rooij, A. McDonald, and M. Mueller, "10 MW wind turbine direct-drive generator design with pitch or active speed stall control," in *International Electric Machines & Drives Conference*, 2007, vol. 2, pp. 1390-1395: IEEE.

[22] L. Mihet-Popa, F. Blaabjerg, and I. Boldea, "Wind turbine generator modeling and simulation where rotational speed is the controlled variable," *IEEE Transactions on Industry Applications,* vol. 40, no. 1, pp. 3-10, 2004.

[23] Z. Chen, J. M. Guerrero, and B. F, "A review of the state of the art of power electronics for wind turbines," *IEEE Transactions on power electronics,* vol. 24, no. 8, pp. 1859-1875, 2009.

[24] V. Akhmatov, H. Knudsen, A. H. Nielsen, J. K. Pedersen, and N. K. Poulsen, "Modelling and transient stability of large wind farms," *International Journal of Electrical Power & Energy Systems,* vol. 25, no. 2, pp. 123-144, 2003.

[25] M. Kaźmierkowski, R. Krishnan, and F. Blaabjerg, *Control in power electronics: selected problems*. Academic press, 2002.

[26] H. Li and Z. Chen, "Overview of generator topologies for wind turbines," *IET Proc. Renewable Power Generation,* vol. 2, no. 2, pp. 123-138, 2008.

[27] Z. Chen, S. A. Gomez, and M. McCormick, "A fuzzy logic controlled power electronic system for variable speed wind energy conversion systems," 2000.

[28] Z. Chen and E. Spooner, "Voltage source inverters for high-power, variable-voltage DC power sources," *IEE Proceedings-Generation, Transmission and Distribution,* vol. 148, no. 5, pp. 439-447, 2001.

[29] J. Slootweg and W. Kling, "Modeling of large wind farms in power system simulations," in *Power Engineering Society Summer Meeting*, 2002, vol. 1, pp. 503-508: IEEE.

[30] G. Sybille and H. Le-Huy, "Digital simulation of power systems and power electronics using the MATLAB/Simulink Power System Blockset," in *Power Engineering Society Winter Meeting*, 2000, vol. 4, pp. 2973-2981: IEEE.

[31] M. Dubois, H. Polinder, and J. Ferreira, "Comparison of generator topologies for direct-drive wind turbines," *Proceedings of NORPIE'00,* pp. 22-26, 2000.

[32] L. Hansen *et al.*, "Conceptual survey of generators and power electronics for wind turbines," 8755027431, 2002.

[33] Z. Chen and E. Spooner, "A modular, permanent-magnet generator for variable speed wind turbines," 1995.

[34] Z. Chen and E. Spooner, "Grid power quality with variable speed wind turbines," *IEEE Transactions on energy conversion,* vol. 16, no. 2, pp. 148-154, 2001.

[35] M. Alatalo, "Permanent magnet machines with air gap windings and integrated teeth windings," Chalmers University of Technology, 1996.

[36] H. El-Helw and S. Tennakoon, "Evaluation of the suitability of a fixed speed wind turbine for large scale wind farms considering the new UK grid code," *Renewable Energy,* vol. 33, no. 1, pp. 1-12, 2008.

[37] T. Hammons, S. Lee, and K. Low, "Analysis of torques in large steam turbine driven induction generator shafts following disturbances on the system supply," *IEEE transactions on energy conversion,* vol. 11, no. 4, pp. 693-700, 1996.

[38] S. W. Mohod and M. V. Aware, "A STATCOM-control scheme for grid connected wind energy system for power quality improvement," *IEEE systems journal,* vol. 4, no. 3, pp. 346-352, 2010.

[39] L. Xu, L. Yao, and C. Sasse, "Comparison of using SVC and STATCOM for wind farm integration," in *International Conference on Power System Technology*, 2006, pp. 1-7: IEEE.

[40] F. Shibata and K. Taka, "A self-cascaded induction generator combined with a separately controlled inverter and a synchronous condenser," in *Conference Record of the Industry Applications Society Annual Meeting*, 1990, pp. 309-317: IEEE.

[41] N. McQuin, "Power system transients on large induction generator installations," in *IEE Colloquium onSafeguarding Industrial Plant During Power System Disturbances*, 1989, pp. 15/1-15/3: IET.

[42] F. Jiang, Z. Bo, and L. Roumei, "Performance of induction generator in parallel with an unbalanced three phase system," in *International Conference on Power System Technology*, 1998, vol. 2, pp. 1193-1197: IEEE.

[43] N. D. Caliao, "Dynamic modelling and control of fully rated converter wind turbines," *Renewable Energy,* vol. 36, no. 8, pp. 2287-2297, 2011.

[44] S. Salman and B. Badrzadeh, "New Approach for modelling Doubly-Fed Induction Generator (DFIG) for grid-connection studies," in

European wind energy conference an exhibition, London, 2004, vol. 1, p. 1.

[45] Q. Wang and L. Chang, "An intelligent maximum power extraction algorithm for inverter-based variable speed wind turbine systems," *IEEE Transactions on power electronics,* vol. 19, no. 5, pp. 1242-1249, 2004.

[46] K. Tan and S. Islam, "Optimum control strategies in energy conversion of PMSG wind turbine system without mechanical sensors," *IEEE transactions on energy conversion,* vol. 19, no. 2, pp. 392-399, 2004.

[47] S. Bhowmik, R. Spee, and J. H. Enslin, "Performance optimization for doubly fed wind power generation systems," *IEEE Transactions on Industry Applications,* vol. 35, no. 4, pp. 949-958, 1999.

[48] W. Qiao, R. G. Harley, and G. K. Venayagamoorthy, "Coordinated reactive power control of a large wind farm and a STATCOM using heuristic dynamic programming," *IEEE Transactions on Energy Conversion,* vol. 24, no. 2, pp. 493-503, 2009.

[49] W. Qiao and R. G. Harley, "Effect of grid-connected DFIG wind turbines on power system transient stability," in *Power and Energy Society General Meeting-Conversion and Delivery of Electrical Energy in the 21st Century*, 2008, pp. 1-7: IEEE.

[50] A. Petersson, *Analysis, modeling and control of doubly-fed induction generators for wind turbines*. Chalmers University of Technology, 2005.

[51] J. Slootweg, H. Polinder, and W. Kling, "Dynamic modelling of a wind turbine with doubly fed induction generator," in *IEEE Power Engineering Society Summer Meeting, 2001*, 2001, vol. 1, pp. 644-649.

[52] J. Muñoz and C. Cañizares, "Comparative stability analysis of DFIG-based wind farms and conventional synchronous generators," in *Power Systems Conference and Exposition (PSCE), 2011 IEEE/PES*, 2011, pp. 1-7: IEEE.

[53] M. G. S and D. N. A, "Rotor side converter control of DFIG based wind energy conversion system," *International Journal of Engineering Research & Technology (IJERT),* vol. 4, no. 8, 2015.

[54] H. Amaris and M. Alonso, "Coordinated reactive power management in power networks with wind turbines and FACTS devices," *Energy Conversion and Management,* vol. 52, no. 7, pp. 2575-2586, 2011.

[55] F. M. Hughes, O. Anaya-Lara, N. Jenkins, and G. Strbac, "Control of DFIG-based wind generation for power network support," *IEEE Transactions on Power Systems,* vol. 20, no. 4, pp. 1958-1966, 2005.

[56] J. Ekanayake and N. Jenkins, "Comparison of the response of doubly fed and fixed-speed induction generator wind turbines to changes in network frequency," *IEEE Transactions on Energy conversion,* vol. 19, no. 4, pp. 800-802, 2004.

[57] M. Fujimitsu, T. Komatsu, K. Koyanagi, K. Hu, and R. Yokoyama, "Modeling of doubly-fed adjustable-speed machine for analytical studies on long-term dynamics of power system," in *International Conference on Power System Technology*, 2000, vol. 1, pp. 25-30: IEEE.

[58] V. Sumitha and R. Gnanadass, "Enhancement of reactive power capability of DFIG using grid side converter," *Asian Power Electronics Journal,* vol. 4, no. 3, 2010.

[59] M. Yamamoto and O. Motoyoshi, "Active and reactive power control for doubly-fed wound rotor induction generator," *IEEE Transactions on Power Electronics,* vol. 6, no. 4, pp. 624-629, 1991.

[60] R. Sharma and A. Manocha, "A literature review of different control techniques for a DFIG wind turbine," *International Journal of Research Review in Engineering Science and Technology,* vol. 5, no. 1, pp. 1-5, 2016.

[61] M. Ghofrani, A. Arabali, and M. Etezadi-Amoli, "Modeling and simulation of a DFIG-based wind-power system for stability analysis," in *IEEE Power and Energy Society General Meeting,*, 2012, pp. 1-8.

[62] L. Xu and P. Cartwright, "Direct active and reactive power control of DFIG for wind energy generation," *IEEE Transactions on energy conversion,* vol. 21, no. 3, pp. 750-758, 2006.

[63] J. Ekanayake, L. Holdsworth, X. Wu, and N. Jenkins, "Dynamic modeling of doubly fed induction generator wind turbines," *IEEE transactions on power systems,* vol. 18, no. 2, pp. 803-809, 2003.

[64] M. Machmoum, F. Poitiers, C. Darengosse, and A. Queric, "Dynamic performances of a doubly-fed induction machine for a variable-speed wind energy generation," in *International Conference on Power System Technology*, 2002, vol. 4, pp. 2431-2436: IEEE.

[65] E. Tremblay, A. Chandra, and P. J. Lagacé, "Grid-side converter control of DFIG wind turbines to enhance power quality of distribution network," in *Power Engineering Society General Meeting*, 2006, p. 6 pp.: IEEE.

[66] K. Okedu, "A study of wind farm stabilization using dfig or statcom considering grid requirements," *Journal of Engineering Science and Technology Review,* vol. 3, no. 1, pp. 200-209, 2010.

[67] V. Akhmatov, H. Knudsen, and A. H. Nielsen, "Advanced simulation of windmills in the electric power supply," *International Journal of Electrical Power & Energy Systems,* vol. 22, no. 6, pp. 421-434, 2000.

[68] L. Fernández, F. Jurado, and J. Saenz, "Aggregated dynamic model for wind farms with doubly fed induction generator wind turbines," *Renewable energy,* vol. 33, no. 1, pp. 129-140, 2008.

[69] J. M. Carrasco *et al.*, "Power-electronic systems for the grid integration of renewable energy sources: A survey," *IEEE Transactions on industrial electronics,* vol. 53, no. 4, pp. 1002-1016, 2006.

[70] R. Billinton and Y. Gao, "Multistate wind energy conversion system models for adequacy assessment of generating systems incorporating wind energy," *IEEE Transactions on Energy Conversion,* vol. 23, no. 1, pp. 163-170, 2008.

[71] V. Akhmatov, H. Knudsen, M. Bruntt, A. H. Nielsen, J. K. Pedersen, and N. K. Poulsen, "A dynamic stability limit of grid connected induction generators," in *IASTED International Conference on Power and Energy Systems*, 2000, pp. 235-244.

[72] S. Megh, K. D. Lalit, and N. K. G, "FACTS Devices in Renewable Energy Plants to solve Power System issues," *SSRG International Journal of Electrical and Electronics Engineering (SSRG-IJEEE),* vol. 3, no. 5, p. 6, 2016.

[73] F. Shewarega, I. Erlich, and J. L. Rueda, "Impact of large offshore wind farms on power system transient stability," in *Power Systems Conference and Exposition (PSCE)*, 2009, pp. 1-8: IEEE.

[74] N. Dizdarevic and M. Majstrovic, "FACTS-based reactive power compensation of wind energy conversion system," in *IEEE Power Tech Conference Proceedings*, Bologna, 2003, vol. 2, p. 8 pp. Vol. 2: IEEE.

[75] M. Pratibha and R. K. Nava, "Impact Analysis of Wind Power System Installation in Kathmandu Valley Network," *Proceedings of IOE Graduate Conference,* pp. 180–185, 2015.

[76] "Grid connection code for renewable power plants (RPPs) connected to the electricity transmission system or the distribution system in South Africa " South Africa, 2014.

[77] P. Sorensen *et al.*, "Power quality issues on wind power installations in Denmark," in *Power Engineering Society General Meeting*, 2007, pp. 1-6: IEEE.

[78] J. Matevosyan, T. Ackermann, and S. M. Bolik, "Technical regulations for the interconnection of wind farms to the power system," *Wind power in power systems,* pp. 115-142, 2005.

[79] T. de Assis, E. H. Watanabe, L. A. S. Pilotto, and R. B. Sollero, "A new technique to control reactive power oscillations using STATCOM," in *10th International Conference on Harmonics and Quality of Power*, 2002, vol. 2, pp. 607-613: IEEE.

[80] J. J. Gutierrez, J. Ruiz, P. Saiz, I. Azcarate, L. Leturiondo, and A. Lazkano, "Power Quality in Grid-Connected Wind Turbines, Wind Turbines," I. Al-Bahadly, Ed.: INTECH, 2011.

[81] Y. Alharbi, A. S. Yunus, and A. Abu-Siada, "Application of STATCOM to improve the high-voltage-ride-through capability of wind turbine generator," in *Innovative Smart Grid Technologies Asia (ISGT) IEEE PES*, 2011, pp. 1-5.

[82] F. Zhou, G. Joos, and C. Abbey, "Voltage stability in weak connection wind farms," in *Power Engineering Society General Meeting*, 2005, pp. 1483-1488: IEEE.

[83] J. Gutierrez, J. Ruiz, L. Leturiondo, and A. Lazkano, "Flicker measurement system for wind turbine certification," *IEEE Transactions on Instrumentation and Measurement,* vol. 57, no. 12, pp. 375-382, 2008.

[84] V. Yuvaraj and S. Deepa, "Improving grid power quality with FACTS device on integration of wind energy system," in *Fifth Asia Modelling Symposium (AMS)*, 2011, pp. 157-162: IEEE.

[85] E. Rodrigues, A. Bizuayehu, and J. P. Catalao, "Analysis of requirements in insular grid codes for large-scale integration of renewable generation," in *T&D Conference and Exposition, PES*, 2014, pp. 1-5: IEEE.

[86] M. H. J. Bollen, "Understanding power quality problems," *Piscataway, NJ, USA: IEEE,* vol. 1, pp. 1-35, 2000.

[87] S. Sewchurran and I. Davidson, "Introduction to the South African Renewable Energy Grid Code version 2.9 requirements (Part I—Introduction)," in *AFRICON*, 2017, pp. 1220-1224: IEEE.

[88] T. García-Sánchez, E. Gómez-Lázaro, and A. Molina-García, "A review and discussion of the grid-code requirements for renewable energy sources in Spain," in *International Conference on Renewable Energies and Power Quality (ICREPQ'14)*, 2014, no. 12, pp. 565-570.

[89] E. Troester, "New German grid codes for connecting PV systems to the medium voltage power grid," in *2nd International workshop on*

concentrating photovoltaic power plants: optical design, production, grid connection, 2009, pp. 9-10.

[90] I. Arias, "Grid Code Comparision," Masters Thesis, Department of Electrical Engineering, Chalmers University of Technology, Sweden, 2006.

[91] S. Sewchurran and I. Davidson, "Introduction to the South African Renewable Energy Grid Code version 2.9 requirements (Part II—Grid code technical requirements)," in *AFRICON*, 2017, pp. 1225-1230: IEEE.

[92] S. Sewchurran and I. Davidson, "Introduction to the South African Renewable Energy Grid Code version 2.9 requirements (Part III—Discussions and conclusions)," in *AFRICON*, 2017, pp. 1231-1235: IEEE.

[93] S. Sewchurran and I. Davidson, "Guiding Principles for Grid Code Compliance of Medium-High Voltage Renewable Power Plant Distributed Generation Integration onto South Africa's Transmission and Distribution Networks," in *Proceedings of the 24th South African Universities Power Engineering Conference*, 2016, pp. 26-28.

[94] *Grid connection code for renewable power plants (RPPs) connected to the electricity transmission system (TS) or the distribution system (DS) in South Africa*, 2014.

[95] M. Tsili and S. Papathanassiou, "A review of grid code technical requirements for wind farms," *IET Renewable Power Generation,* vol. 3, no. 3, pp. 308-332, 2009.

[96] H. K. Tyll, "FACTS technology for reactive power compensation and system control," in *Transmission and Distribution Conference and Exposition: Latin America*, 2004, pp. 976-980: IEEE.

[97] N. G. Hingorani and L. Gyugyi, *Understanding FACTS*. IEEE press, 2000.

[98] X. Zhang, C. Rehtanz, and B. Pal, "Power Systems," 1998.

[99] J. Chen, S. Song, and Z. Wang, "Analysis and Implement of Thyristor-based STATCOM," in *International Conference on Power System Technology, IEEE*, 2006, pp. 1-5: IEEE.

[100] R. Grünbaum, B. Halvarsson, and A. Wilk-Wilczynski, "FACTS and HVDC light for power system interconnections," in *Power Delivery Conference, Madrid, Spain*, 1999, pp. 1-18.

[101] J. Olamaei, J. Javan, A. Yavartalab, and M. Khederzadeh, "Advanced control of FACTS devices for improving power quality regarding to wind farms," *Energy Procedia,* vol. 14, pp. 298-303, 2012.

[102] A. Cetin, "Design and implementation of voltage source converter based STATCOM for reactive power compensation and harmonic filtering," Ph.D, Electrical and electronics engineering, Middle East Technical University, Turkey, 2007.

[103] H. Klaus and O. L. D, "FACTS-For Cost Effective and Reliable Transmission of Electrical Energy."

[104] A. A. Nikolaev, G. P. Kornilov, T. R. Khramshin, I. Akcay, and Y. Gok, "Application of static Var compensator of ultra-high power electric arc furnace for voltage drops compensation in factory power supply system of metallurgical enterprise," in *Electrical Power and Energy Conference (EPEC), 2014 IEEE*, 2014, pp. 235-241: IEEE.

[105] A. Adebiyi and K. Akindeji, "Investigating the effect of Static Synchronous Compensator (STATCOM) for voltage enhancement and transmission line losses mitigation," in *PowerAfrica, 2017 IEEE PES*, 2017, pp. 462-467: IEEE.

[106] E. Uzunovic, C. A. Canizares, and J. Reeve, "Fundamental frequency model of static synchronous compensator," in *Proc. North American Power Symposium (NAPS)*, 1997, pp. 49-54.

[107] M. A. Mannan, M. H. Ali, R. Takahashi, T. Murata, and J. Tamura, "Stabilization of wind turbine generator system by STATCOM," *IEEE Transactions on Power and Energy,* vol. 126, no. 10, pp. 1073-1082, 2006.

[108] M. Molinas, S. Vazquez, T. Takaku, J. Carrasco, R. Shimada, and T. Undeland, "Improvement of transient stability margin in power systems with integrated wind generation using a STATCOM: an

experimental verification," in *International Conference on Future Power Systems*, 2005, pp. 6 pp.-6: IEEE.

[109] J. A. Barrado, R. Grino, and H. Valderrama-Blavi, "Power-quality improvement of a stand-alone induction generator using a STATCOM with battery energy storage system," in *IEEE transactions on power delivery*, 2010, vol. 25, no. 4, pp. 2734-2741.

[110] V. Jon-Inge, S.-N. D. Martin, and H. Anders, "Reactive power control for wind parks with STATCOM," 2012.

[111] M. Molinas, J. A. Suul, and T. Undeland, "Low voltage ride through of wind farms with cage generators: STATCOM versus SVC," *IEEE Transactions on power electronics,* vol. 23, no. 3, pp. 1104-1117, 2008.

[112] A. N. Pathan, R. Ali, and A. Ahad, "Improvement Of Power Quality For Grid Connected STATCOM Based Inverter With Local Load," *International Journal of Advance Research In Science And Engineering (IJARSE),* vol. 3, no. 9, p. 7, **2009**.

[113] W. Qiao and R. G. Harley, "Power quality and dynamic performance improvement of wind farms using a STATCOM," in *Power Electronics Specialists Conference (PESC)*, 2007, pp. 1832-1838: IEEE.

[114] K. R. Suja and I. J. Raglend, "Power quality improvement in grid connected wind energy system using STATCOM," in *International Conference on Computing, Electronics and Electrical Technologies (ICCEET)*, 2012, pp. 259-266: IEEE.

[115] N. Rana and S. Aggarwal, "Reactive Power Compensation using STATCOM," *International Journal of Computer Applications,* 2015.

[116] P. Sharma, N. K. Saxena, K. S. S. Ramakrishna, and T. S. Bhatti, "Reactive Power Compensation of isolated wind-diesel hybrid power systems with STATCOM and SVC," *International Journal on Electrical Engineering and Informatics,* vol. 2, no. 3, p. 192, 2010.

[117] S. Abd-Elazim and E. Ali, "Optimal location of STATCOM in multimachine power system for increasing loadability by Cuckoo Search algorithm," *International Journal of Electrical Power & Energy Systems,* vol. 80, pp. 240-251, 2016.

[118] G. Choudhary, N. Singhal, and K. S. Sajan, "Optimal placement of STATCOM for improving voltage profile and reducing losses using crow search algorithm," in *International Conference on Control, Computing, Communication and Materials (ICCCCM)*, 2016, pp. 1-6: IEEE.

[119] A. Karami, M. Rashidinejad, and A. Gharaveisi, "Optimal location of STATCOM for voltage security enhancement via artificial intelligent," in *International Conference on Industrial Technology*, 2006, pp. 2704-2708: IEEE.

[120] G. N. Kumar, M. S. Kalavathi, and R. H. Krishna, "Optimal placement of SVC and STATCOM for voltage stability enhancement under contingency using cat swarm optimization," 2012.

[121] S. Mallick, S. Sarkar, A. Chakrabarti, and A. Mitra, "A Study of Exploring Optimal Location for Installing STATCOM in IEEE 14-Bus System."

[122] P. Pourbeik, R. J. Koessler, W. Quaintance, and W. Wong, "Performing comprehensive voltage stability studies for the determination of optimal location, size and type of reactive compensation," in *Power Engineering Society General Meeting, 2006. IEEE*, 2006, p. 6 pp.: IEEE.

[123] M. Taleb, A. Salem, A. Ayman, and M. Azma, "Optimal allocation of TCSC using adaptive cuckoo search algorithm," in *Eighteenth International Middle East Power Systems Conference (MEPCON)*, 2016, pp. 387-391: IEEE.

[124] N. W. Miller, J. J. Sanchez-Gasca, W. W. Price, and R. W. Delmerico, "Dynamic modeling of GE 1.5 and 3.6 MW wind turbine-generators for stability simulations," in *Power Engineering Society General Meeting*, 2003, vol. 3, pp. 1977-1983: IEEE.

[125] X. Jing, *Modeling and control of a doubly-fed induction generator for wind turbine-generator systems*. Marquette University, 2012.

[126] M. Mbukani, "Modelling and Control of Doubly-FedInduction Generator Systems in Wind Turbine Applications," Masters

Dissertation, Department of Electrical Engineering, Stellenbosch University, South Africa, 2017.

[127] V. Peter, *Vector control of AC Machines*. United States: Oxford University press, 1990.

[128] T. Sun, "Power Quality of grid-connected wind turbines with DFIG and their interaction with the grid," Ph.D, Institute of Energy Tecnology, Aalborg University, 2004.

[129] H. Hofmann, S. Sanders, and C. Sullivan, "Stator-flux-based vector control of induction machines in magnetic saturation," *IEEE Transactions on Industry Applications,* vol. 33, no. 4, pp. 935-942, 1997.

[130] Ntsadu N, Folly K, and K. A, "Impact Assessment of Large Scale Penetration of Wind Energy Conversion Systems on Transient Stability of the Grid " presented at the WindAC, Capetown, South Africa, 2017.

[131] A. A. Aduragba, "Investigating the application of Static Synchronous Compensator (STATCOM) for mitigating power transmission line losses," 2017.

[132] D. PowerFactory, "Nine-bus system," ed, 2017.

[133] *NRS 048: Voltage characteristics, compatibility levels, limits and assessment methods: Part 2*, 2003.

Appendix A: Induction Machine Equation in ABC Reference Frame

$$\begin{bmatrix} v_A \\ v_B \\ v_C \\ \cdots \\ v_a \\ v_b \\ v_c \end{bmatrix} = \left\{ \begin{bmatrix} r_s & 0 & 0 & \vdots & 0 & 0 & 0 \\ 0 & r_s & 0 & \vdots & 0 & 0 & 0 \\ 0 & 0 & r_s & \vdots & 0 & 0 & 0 \\ \cdots & \cdots & \cdots & \vdots & \cdots & \cdots & \cdots \\ 0 & 0 & 0 & \vdots & r_r & 0 & 0 \\ 0 & 0 & 0 & \vdots & 0 & r_r & 0 \\ 0 & 0 & 0 & \vdots & 0 & 0 & r_r \end{bmatrix} \begin{bmatrix} i_A \\ i_B \\ i_C \\ \cdots \\ i_a \\ i_b \\ i_c \end{bmatrix} + \right.$$

$$\left. \frac{d}{dt} \left\{ \begin{bmatrix} L_{ss} & L_{ms} & L_{ms} & \vdots & L_m\cos(\sigma) & L_m\cos(\sigma - 2\pi/3) & L_m\cos(\sigma + 2\pi/3) \\ L_{ms} & L_{ss} & L_{ms} & \vdots & L_m\cos(\sigma + 2\pi/3) & L_m\cos(\sigma) & L_m\cos(\sigma - 2\pi/3) \\ L_{ms} & L_{ms} & L_{ss} & \vdots & L_m\cos(\sigma - 2\pi/3) & L_m\cos(\sigma + 2\pi/3) & L_m\cos(\sigma) \\ \cdots & \cdots & \cdots & \vdots & \cdots & \cdots & \cdots \\ L_m\cos(\sigma) & L_m\cos(\sigma + 2\pi/3) & L_m\cos(\sigma - 2\pi/3) & \vdots & L_{rr} & L_{mr} & L_{mr} \\ L_m\cos(\sigma - 2\pi/3) & L_m\cos(\sigma) & L_m\cos(\sigma + 2\pi/3) & \vdots & L_{mr} & L_{rr} & L_{mr} \\ L_m\cos(\sigma + 2\pi/3) & L_m\cos(\sigma - 2\pi/3) & L_m\cos(\sigma) & \vdots & L_{mr} & L_{mr} & L_{rr} \end{bmatrix} \begin{bmatrix} i_A \\ i_B \\ i_C \\ \cdots \\ i_a \\ i_b \\ i_c \end{bmatrix} \right\} \right\}$$

Appendix B: Induction Machine Equation in DQO-dqo Reference Frame

$$\begin{bmatrix} v_{Dro} \\ v_{Qro} \\ v_{Oro} \\ \cdots \\ v_{dro} \\ v_{qro} \\ v_{oro} \end{bmatrix} = \left[\begin{array}{ccc:ccc} r_s & 0 & 0 & 0 & 0 & 0 \\ 0 & r_s & 0 & 0 & 0 & 0 \\ 0 & 0 & r_s & 0 & 0 & 0 \\ \cdots & \cdots & \cdots & \cdots & \cdots & \cdots \\ 0 & 0 & 0 & r_r & 0 & 0 \\ 0 & 0 & 0 & 0 & r_r & 0 \\ 0 & 0 & 0 & 0 & 0 & r_r \end{array}\right] \begin{bmatrix} i_{Dro} \\ i_{Qro} \\ i_{Oro} \\ \cdots \\ i_{dro} \\ i_{qro} \\ i_{oro} \end{bmatrix}$$

$$+ \left[\begin{array}{ccc:ccc} L_{ss}-L_{sm} & 0 & 0 & \frac{3}{2}L_m & 0 & 0 \\ 0 & L_{ss}-L_{sm} & 0 & 0 & \frac{3}{2}L_m & 0 \\ 0 & 0 & L_{ss}+2L_{sm} & 0 & 0 & 0 \\ \cdots & \cdots & \cdots & \cdots & \cdots & \cdots \\ \frac{3}{2}L_m & 0 & 0 & L_{rr}-L_{rm} & & \\ 0 & \frac{3}{2}L_m & 0 & & L_{rr}-L_{rm} & \\ 0 & 0 & 0 & & & L_{rr}+2L_{rm} \end{array}\right] \begin{bmatrix} i_{Dro} \\ i_{Qro} \\ i_{Oro} \\ \cdots \\ i_{dro} \\ i_{qro} \\ i_{oro} \end{bmatrix} + \omega_r \left[\begin{array}{ccc:ccc} 0 & -(L_{ss}-L_{sm}) & 0 & 0 & -\frac{3}{2}L_m & 0 \\ L_{ss}-L_{sm} & 0 & 0 & -\frac{3}{2}L_m & 0 & 0 \\ 0 & 0 & 0 & 0 & 0 & 0 \\ \cdots & \cdots & \cdots & \cdots & \cdots & \cdots \\ 0 & 0 & 0 & 0 & 0 & 0 \\ 0 & 0 & 0 & 0 & 0 & 0 \\ 0 & 0 & 0 & 0 & 0 & 0 \end{array}\right] \begin{bmatrix} i_{Dro} \\ i_{Qro} \\ i_{Oro} \\ \cdots \\ i_{dro} \\ i_{qro} \\ i_{oro} \end{bmatrix}$$

Appendix C: Induction Machine Equation in DQO-dqo Stationary Stator Reference Frame

$$\begin{bmatrix} v_{Dst} \\ v_{Qst} \\ v_{Ost} \\ \cdots \\ v_{dst} \\ v_{qst} \\ v_{ost} \end{bmatrix} = \left[\begin{array}{ccc:ccc} r_s & 0 & 0 & 0 & 0 & 0 \\ 0 & r_s & 0 & 0 & 0 & 0 \\ 0 & 0 & r_s & 0 & 0 & 0 \\ \cdots & \cdots & \cdots & \cdots & \cdots & \cdots \\ 0 & 0 & 0 & r_r & 0 & 0 \\ 0 & 0 & 0 & 0 & r_r & 0 \\ 0 & 0 & 0 & 0 & 0 & r_r \end{array}\right] \begin{bmatrix} i_{Dst} \\ i_{Qst} \\ i_{Ost} \\ \cdots \\ i_{dst} \\ i_{qst} \\ i_{ost} \end{bmatrix}$$

$$+ \left[\begin{array}{ccc:ccc} L_{ss}-L_{sm} & 0 & 0 & \frac{3}{2}L_m & 0 & 0 \\ 0 & L_{ss}-L_{sm} & 0 & 0 & \frac{3}{2}L_m & 0 \\ 0 & 0 & L_{ss}+2L_{sm} & 0 & 0 & 0 \\ \cdots & \cdots & \cdots & \cdots & \cdots & \cdots \\ \frac{3}{2}L_m & 0 & 0 & L_{rr}-L_{rm} & & \\ 0 & \frac{3}{2}L_m & 0 & & L_{rr}-L_{rm} & \\ 0 & 0 & 0 & & & L_{rr}+2L_{rm} \end{array}\right] \begin{bmatrix} i_{Dst} \\ i_{Qst} \\ i_{Ost} \\ \cdots \\ i_{dst} \\ i_{qst} \\ i_{ost} \end{bmatrix} + \omega_r \left[\begin{array}{ccc:ccc} 0 & 0 & 0 & 0 & 0 & 0 \\ 0 & 0 & 0 & 0 & 0 & 0 \\ 0 & 0 & 0 & 0 & 0 & 0 \\ \cdots & \cdots & \cdots & \cdots & \cdots & \cdots \\ 0 & -\frac{3}{2}L_m & 0 & 0 & (L_{rr}-L_{sm}) & 0 \\ -\frac{3}{2}L_m & 0 & 0 & -(L_{rr}-L_{sm}) & 0 & 0 \\ 0 & 0 & 0 & 0 & 0 & 0 \end{array}\right] \begin{bmatrix} i_{Dst} \\ i_{Qst} \\ i_{Ost} \\ \cdots \\ i_{dst} \\ i_{qst} \\ i_{ost} \end{bmatrix}$$

Appendix D: Induction Machine Equation in DQO-dqo Synchronously Rotating Reference Frame

$$
\begin{bmatrix} v_D \\ v_Q \\ v_O \\ \cdots \\ v_d \\ v_q \\ v_o \end{bmatrix} = \left[\begin{array}{ccc:ccc:c} r_s & 0 & 0 & 0 & 0 & 0 & \\ 0 & r_s & 0 & 0 & 0 & 0 & \\ 0 & 0 & r_s & 0 & 0 & 0 & \\ \cdots & \cdots & \cdots & \cdots & \cdots & \cdots & \cdots \\ 0 & 0 & 0 & r_r & 0 & 0 & \\ 0 & 0 & 0 & 0 & r_r & 0 & \\ 0 & 0 & 0 & 0 & 0 & r_r & \end{array}\right] \begin{bmatrix} i_D \\ i_Q \\ i_O \\ \cdots \\ i_d \\ i_q \\ i_o \end{bmatrix}
$$

$$
+ \left[\begin{array}{ccc:ccc:c} L_{ss}-L_{sm} & 0 & 0 & \frac{3}{2}L_m & 0 & 0 & \\ 0 & L_{ss}-L_{sm} & 0 & 0 & \frac{3}{2}L_m & 0 & \\ 0 & 0 & L_{ss}+2L_{sm} & 0 & 0 & 0 & \\ \cdots & \cdots & \cdots & \cdots & \cdots & \cdots & \cdots \\ \frac{3}{2}L_m & 0 & 0 & L_{rr}-L_{rm} & & & \\ 0 & \frac{3}{2}L_m & 0 & & L_{rr}-L_{rm} & & \\ 0 & 0 & 0 & & & L_{rr}+2L_{rm} & \end{array}\right] \begin{bmatrix} i_D \\ i_Q \\ i_O \\ \cdots \\ i_d \\ i_q \\ i_o \end{bmatrix} + \omega_s \left[\begin{array}{ccc:ccc:c} 0 & -\omega_s(L_{ss}-L_{sm}) & 0 & 0 & -\frac{3}{2}\omega_s L_m & 0 & \\ \omega_s(L_{ss}-L_{sm}) & 0 & 0 & \frac{3}{2}\omega_s L_m & 0 & 0 & \\ 0 & 0 & 0 & 0 & 0 & 0 & \\ \cdots & \cdots & \cdots & \cdots & \cdots & \cdots & \cdots \\ 0 & -\frac{3}{2}(\omega_s-\omega_r)L_m & 0 & 0 & -(\omega_s-\omega_r)(L_{rr}-L_{sm}) & 0 & \\ -\frac{3}{2}(\omega_s-\omega_r)L_m & 0 & 0 & (\omega_s-\omega_r)(L_{rr}-L_{sm}) & 0 & 0 & \\ 0 & 0 & 0 & 0 & 0 & 0 & \end{array}\right] \begin{bmatrix} i_D \\ i_Q \\ i_O \\ \cdots \\ i_d \\ i_q \\ i_o \end{bmatrix}
$$

Appendix E: DSL Graphical Implementation of STATCOM Controller

Controller Block Diagram:

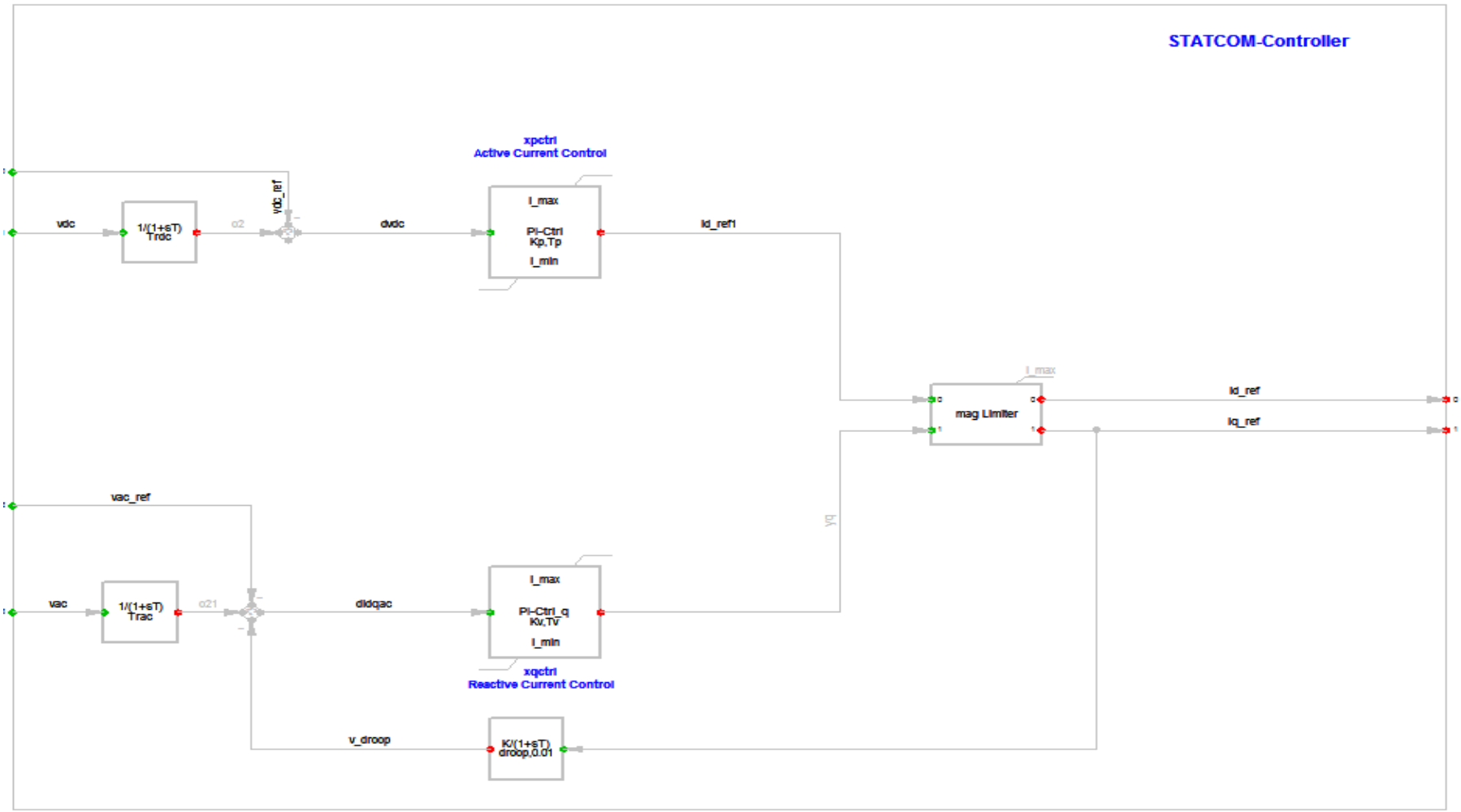

Appendix F: IEEE 9 Bus System Data

F1: Generator data

Quantity	**G1**	**G2**	**G3**
Nominal apparent Voltage (MVA)	247.5	192.0	128.0
Dispatch active power (MW)	-	163.0	85
Nominal Voltage (kV)	16.5	18.0	13.8
Voltage setpoint (p.u)	1.040	1.025	1.025
Nominal Power factor	1.00	0.85	0.85
Plant Category	Hydro	Coal	Coal
Rotor Type	Salient pole	Round rotor	Round rotor
X_d (p.u)	0.3614	1.7199	1.6800
X'_d (p.u)	0.1505	0.2300	0.2321
X_q (p.u)	0.2328	1.6598	1.6100
X'_q (p.u)	-	0.3780	0.3200
X leakage (p.u)	0.0832	0.1000	0.0950
R'_{d0} (s)	8.960	6.000	5.890
R'_{q0} (s)	-	5.35	0.600
Inertia Constant (s)	9.5515	3.9216	2.7665

F2: Bus Data

Line	From	To	R (Ω)	X (Ω)	B (μs)
Line 4-5	Bus 4	Bus 5	5.2900	44.9650	332.70
Line 4-6	Bus 4	Bus 6	8.9930	48.6680	298.69
Line 5-7	Bus 5	Bus 7	16.928	85.1690	578.45
Line 6-9	Bus 6	Bus 9	20.631	89.9300	676.75
Line 7-8	Bus 7	Bus 8	4.4965	38.0880	281.66
Line 8-9	Bus 8	Bus 9	6.2951	53.3232	395.08

F3: Transformer Data

Transformer	From	To	Rated Power (MVA)	HV side (kV)	LV side (kV)	X1 (p.u)
T1	Bus 1	Bus 4	250	230	16.5	0.1440
T2	Bus 2	Bus 7	250	230	18.0	0.1250
T3	Bus 3	Bus 9	150	230	13.8	0.0879

F4: Load Data

Load	Bus	P (MW)	Q (MVAr)
Load A	Bus 5	125	50
Load B	Bus 6	90	30
Load C	Bus 8	100	35

Appendix G: DFIG Data

Quantity	Magnitude
Active Power (MW)	2.5
Nominal Voltage (kV)	0.69
Number of poles	2
Frequency (Hz)	60
Stator Resistance (p.u)	0.01
Stator reactance (p.u)	0.1
Magnetising reactance (p.u)	3.5
Rotor resistance (p.u)	0.01
Rotor reactance (p.u)	0.1